JLCX-001
Feb. 2002

JLC X-BAND TECHNICAL NOTE

Main-body bonding of DDS3 and related studies

T. Higo, T. Suzuki, N. Toge, K. Takata
Y. Funahashi, Y. Higashi, N. Hitomi, T. Takatomi, Y. Watanabe
KEK
High Energy Accelerator Research Organization

K. Asano
Akita National College of Technology

H. Tsuchiya, T. Niino, H. Endo,
M. Yamamoto, A. Yamamoto, T. Watanabe, N. Kaneko
H. Sakae, S. Mandai
Ishikawajima-Harima Heavy Industry

Abstract

The main body of DDS3 structure was successfully fabricated. Two preceding studies with dummy cells were performed before the DDS3 fabrication. Throughout these studies, we obtained many technical experiences and understandings necessary for the fabrication of these structures. The technologies developed here became the base for the following structure fabrications. In this note we try to summarize all the experiences till DDS3 fabrication in order to describe the technological base in detail as a reference to the future design and fabrication of RDDS structures.

The DDS3 structure came out of furnace for diffusion bonding with a vacuum leak tightness but with a fairly big bowing of 230 microns. However, this bow is almost in one plane and in a very smooth manner, which can be easily straightened in the later processes. The cumulative bookshelf phenomenon was observed in DDS3 and it should be avoided because it cannot corrected after bonding.

Main-body bonding of DDS3 and related studies

T. Higo, T. Suzuki, N. Toge, K. Takata
Y. Funahashi, Y. Higashi, N. Hitomi, T. Takatomi, Y. Watanabe
KEK
High Energy Accelerator Research Organization

K. Asano
Akita National College of Technology

H. Tsuchiya, T. Niino, H. Endo,
M. Yamamoto, A. Yamamoto, T. Watanabe, N. Kaneko
H. Sakae, S. Mandai
Ishikawajima-Harima Heavy Industry

Abstract

The main body of DDS3 structure was successfully fabricated. Two preceding studies with dummy cells were performed before the DDS3 fabrication. Throughout these studies, we obtained many technical experiences and understandings necessary for the fabrication of these structures. The technologies developed here became the base for the following structure fabrications. In this note we try to summarize all the experiences till DDS3 fabrication in order to describe the technological base in detail as a reference to the future design and fabrication of RDDS structures.

The DDS3 structure came out of furnace for diffusion bonding with a vacuum leak tightness but with a fairly big bowing of 230 microns. However, this bow is almost in one plane and in a very smooth manner, which can be easily straightened in the later processes. The cumulative bookshelf phenomenon was observed in DDS3 and it should be avoided because it cannot corrected after bonding.

Contents

1. Introduction

One of the key characteristics for the accelerating structure for the main linac of the linear collider is the effective reduction of wake field in the structure by two order of magnitude[1,2]. KEK has been pursuing the detuned structure (DS) scheme for several years. In this scheme, the frequencies of higher modes are properly distributed and the wake fields are canceled when seen by following bunches. In order to make this mechanism work, the cell alignment of the structure should be of the order of 5 microns in addition to the frequency tolerance of about 1 MHz for the lowest dipole modes. These requirements were satisfied in the 1.3m structure with diameter of 80 mm[1].

At SLAC the structures with medium damping in addition to the detuning of higher modes have been studied. The structure is called damped detuned structure (DDS)[3]. This medium damping is preferred because it makes the wake field damp well especially at a longer bunch train where the wake field in the DS case recoheres, which is annoying characteristics.

SLAC made two DDS structures, DDS1 and DDS2. These two structure were based on the same design. The cells for these structures were made by KEK. One of the structures was tested at ASSET to confirm the wake field characteristics. However, the manifold running through the structure did not match well towards extracting wave guide outside so that the wake field damping was not very well. There also found a large step of more than several tens of microns between cells so that it did not serve as a critical feasibility study of the DDS scheme.

Another structure, named DDS3, was then programmed[4]. This structure was designed to be well matched at higher mode extraction ports and also the cells were assumed to be much well aligned[5]. The frequency distribution of the lowest dipole mode is designed such that the k(dn/df) follows gaussian distribution instead of (dn/df) does[3,6]. These three points, the proper frequency distribution, reasonable matching for the higher mode frequencies and smooth cell-to-cell alignment with a straightness of less than 10 microns, are the main motive force of the DDS3.

The last characteristics cannot be met reliably with SLAC's previous fabrication technology, where the 38 cells are firstly diffusion bonded to make a blocks of 38 cells and then these blocks are bonded in the later process. The reason of the difficulty is that the end surface of this 38-cell stack is not good after the first bonding so that it is not easy to realize a smooth connection between blocks in the later process. On the other hand, the one-shot bonding technology adopted at KEK serves a tool to realize a smoothness of cells throughout the structure. This scheme was successfully applied to three 1.3m structure, M2, IH1 and IHD1[7] and also one 1.8m structure, MD1[8].

In the last example, MD1, a pre-bonding(PB) technology was also applied for the first time. The technique is supposed to prevent the slippage of the cells during the diffusion bonding process.

Considering the above situation, SLAC and KEK agreed to make the DDS3 structure based on the one-shot bonding technology[4]. All of the cell design was made by SLAC. The cells were made at LLNL. The one-shot bonding of the main body was performed by KEK. All the following processes such as brazing, straightening and

support etc. were done by SLAC. The structure was tested at ASSET to check the wake field characteristics and the beam position information extracted from manifold[9].

The present paper covers from some mechanical quality checking of cells to the diffusion bonding of the main body.

2. Chronological description of DDS3 related activities

A possible collaboration on DDS3 was discussed during the workshop in July 1997 at SLAC. The idea was further discussed and agreed among three laboratories, SLAC, LLNL and KEK, in early September. The responsibility of each laboratory on DDS3 was defined as follows;

SLAC	Basic electrical and mechanical design. Brazing to assemble peripherals such as wave guide, water channel etc. ASSET run.
LLNL	Cell fabrication.
KEK	One-shot bonding of main body.

The schedule as of Sep. 5, 1997, proposed by R. Pope of SLAC was to reach ASSET test in June 1998 as shown below;

LLNL & SLAC	QC	Jan. 98
KEK	Stack and bonding	Mar. 98
SLAC	Brazing etc.	Mar.--May 98
ASSET	Wake field measurement	June 98

KEK proposed to make a test using dummy cells before going to DDS3 to make sure all the technologies are applicable to a long and thin structure. This dummy structure is called DDS3D1. The cells are stacked on a granite V-block. After pressing axially by 24kg, the staked cells are moved to vertical position hanging in a vacuum furnace to be diffusion bonded. This was performed in March 1998. The structure came out with a big bow of the order of 1 centimeter. Some ceramic springs were broken in the furnace and the structure was almost falling down in the furnace.

We analyzed the configuration and found a big mistake in the design of the bonding fixtures. We understood now the mechanism which made this fault fairly well but we discussed the possibility of applying a relatively new method, pre-bonding, as a safest way which we have at our hand. In late April 1998, we finally decided to take the pre-bonding process before going into the diffusion bonding.

We programmed again to make another dummy-cell bonding in early summer to finish DDS3 in summer to be in time for the ASSET run in late 1998. That time, we were very nervous and careful so that the dummy cells were designed as similar as the actual DDS3 cells. The dummy-cell structure, called DDS3D2, was finished in early August. The bow was about 500 microns but the cell-to-cell slippage was fairly small.

Therefore, we could decide to apply the same method for DDS3 even if chasing DDS3D2 so closely in time, actually some processes were overlapping.

Following is the history related to DDS3D2 and DDS3 in the year of 1998.

Item	DDS3D2	DDS3
Cell	June	June
Stacking / IHI, Tokyo	July/End	Aug./Beg.
Bonding / IHI. Kure	Aug./Beg.	Aug./Mid.
Checking / IHI, Tokyo		Aug./End
Shipping to SLAC		Sep. 1

3. Description of fabrication flow

Here is described the essential stream of DDS3 fabrication processes focusing on cell stacking till shipping to SLAC. That of DDS3D2 is the same as DDS3 while that of DDS3D1 is the same except for the lack of process related to pre-bonding.

Following list shows briefly the actual processes in the fabrication stream.

1. Receiving cells from SLAC.
2. Inspection of cells at IHI, Tokyo, by eye.
3. Rinsing cells.
4. Stacking cells on V-block.
5. Measurement of cell alignment on V-block.
6. Put viton constraint.
7. Application of axial pressure by 600 kg or more.
8. Measurement of cell alignment on V-block.
9. Reduce axial pressure to 100 kg.
10. Transportation from Tokyo to Kure.
11. Apply 600 kg again.
12. Measurement of cell alignment on V-block.
13. Pre-bonding at 150 °C.
14. Measurement of cell alignment on V-block.
15. Measurement of cell alignment in vertical situation with wire.
16. Diffusion bonding at 890 °C.
17. Measurement of cell alignment in vertical situation with wire.
18. Measurement of cell alignment on V-block.
19. Transportation from Kure to Tokyo.
20. Measurement of cell alignment on V-block.
21. Set on shipping girder.

In the following sections, we describe various characteristics we observed during two test bondings preceding DDS3 in addition to the actual fabrication of DDS3.

4. Cells of present studies

4.1 DDS3 cell description

The main body of the DDS3 structure is composed of 206 parts which are listed in Table 4.1. The peripheral parts were to be bonded at SLAC after diffusion bonding of the main body in Japan. All of the parts to be bonded in this diffusion bonding were with their diameter 60.9565 mm. Some typical shape of those cells are shown in Fig. 4.1. Some of the characteristics to be noted are the following;

1. Numbering is located around +160° on the smaller-diameter part of OD of every cell. This was scribed by hand at LLNL.
2. Tuning holes are located at various angles for some special cells.
3. Holes for inserting thermocouple wire are 3.2 mm in diameter and 5 mm in depth and located at +20° designed at cells #11, #26, #64, #102, #140, #178 and #193.
4. Scribed line for rotational alignment was made on all of the cells at 45° on the smaller-diameter part of OD.
5. Non uniform OD is adopted for the design of the diamond turning operation[4]. Bigger size for defining radial position for alignment with 60.9565 in diameter and 3.44 mm in length while the other part with less diameter by 100 microns and 4 mm in length is for setting of the cell on lathe concentric with respect to the already cut parts.
6. Brazing groove of 1.3mm X 1.3mm is located at the one of the edge of the OD of every cell.

In the above description, the angle to describe the rotational position is measured from the X axis, the horizontal position defined in the Fig. 8.1 towards the Y axis, the vertical top side.

Table 4.1 Description of cells for DDS3.

cell number	type	comments
#-1	input end cell	
#0	input cavity cell	four tuning holes at +-22.5° and 180°+-22.5°
#1	cell #1	two tuning holes at +20° and -160°
#2	cell #2	two tuning holes at -45° and +135°
#3	cell #3	
#4	standard cell	
#5--#9	vacuum pumping	
#10--#68	standard cell	
#69--#73	vacuum pumping	
#74--#132	standard cell	
#133--#137	vacuum pumping	
#138--#194	standard cell	
#195--#199	vacuum pumping	
#200	standard cell	
#201	cell #201	
#202	cell #202	
#203	cell #203	two tuning holes at -45° and +135°
#204	cell #204	two tuning holes at +20° and -160°
#205	Output coupler cell	four tuning holes at +-22.5° and 180°+-22.5°

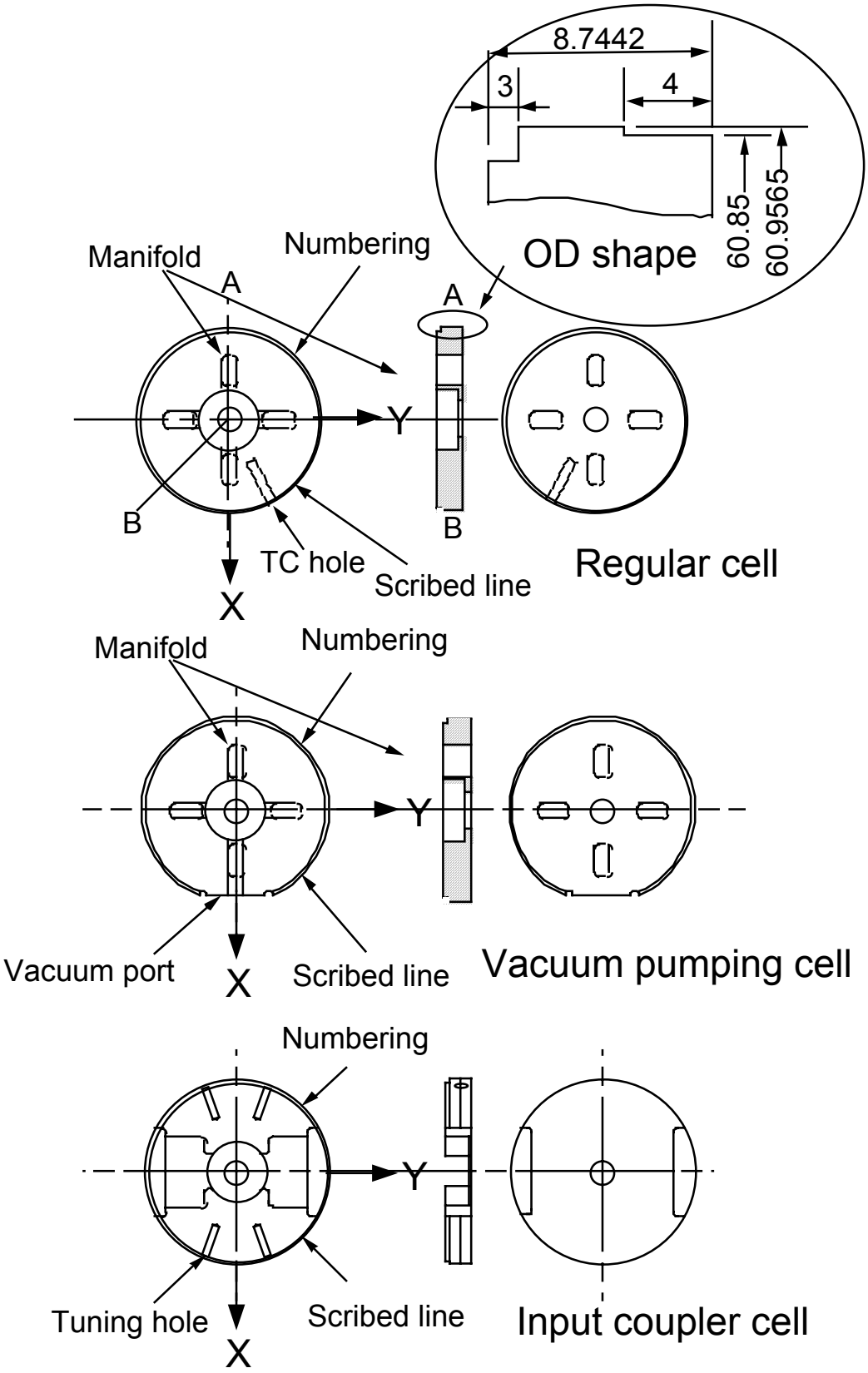

Fig. 4.1 Schematic drawings of typical cells for DDS3. The outside diameter of all of the cells is 60.9565mm and the thickness is 8.7442mm.

4.2 Methods of quality checking of cells

4.2.1 Inspection by eye

The cells as received or as machined and just before rinsing were firstly checked by eye and stocked in a container with nitrogen gas purged.

4.2.2 Measurements using capacitive sensor, Microsense

OD measurement:

A cell to be measured were placed on a linear guide together with a reference cell, where these two cells were fairly well aligned with respect to linear guide axis by the help of two guide pins. Two Microsenses [10] were set to face both sides of a cell at the same time and the sum of both Microsense readings gives us the value a fixed offset - OD of the cell. By moving the two cells and comparing the measurements between that of the reference cell and that of the cell under measurement, we obtain a relative OD difference with respect to the reference cell. Microsense reading error was estimated to be about +-0.2 micron. The temperature of the cells were checked during the measurement. If it is large, thermal expansion correction was applied, though we tried to make the temperature of the two cells almost the same by waiting enough.

Thickness measurement:

Another two Microsenses were set head on with each other with a separation a little larger than the cell thickness. By inserting the cell under measurement and the reference cell in turn, we obtain a relative thickness of the cell with respect to the reference cell. The reading error is the same as that of OD.

4.2.3 Measurements using interferometer

The ZYGO interferometer system type MARK-IV was used for measurements of surface flatness and parallelism. The ZYGO interferometer system type MAXIM-3D was used for surface roughness of the cells and inspection of various microstructures on the surface. The actual methods are described below in detail.

Surface flatness:

The cell was set vertically with the three finger supplied by ZYGO. This setup was on a granite precision base where the interferometer was also sitting. Usual interferometry pattern was checked on the monitor screen and the video output was printed. Also the value calculated automatically by the interferometry system was recorded as a nominal number of the flatness of the cell. Both sides were measured in the same way.

Parallelism:

Two interferometer systems were faced to each other with a separation of about several tens of centi-meters. These were sitting on a precision granite base. An optical flat was inserted in between to adjust the axis of the two interferometers' optics. Then,

the optical flat was replaced by the cell under measurement. The inclination of one side was observed by setting the other side to be vertical with respect to the optics. This inclination is equal to the parallelism of the cell.

Surface roughness:

Magnification of ZYGO interferometer system was set typically X20 to see the area of 100 microns in height and 200 microns in width.

4.3 DDS3D1 cells

Before the present program, the IHI company has made a few structures based on the diffusion bonding. However, those structures were all 1.3m in length and comprising of cells with the diameter of 80mm. So, one of the main aims of the DDS3D1 preceding DDS3 was to have an experience of stacking and bonding by essentially using the same technology for the cells up to 1.8m with cells of 61mm in diameter.

The number of cells prepared for it was about 230 in total but the adopted shape was simplified as schematically shown in Fig. 4.2.

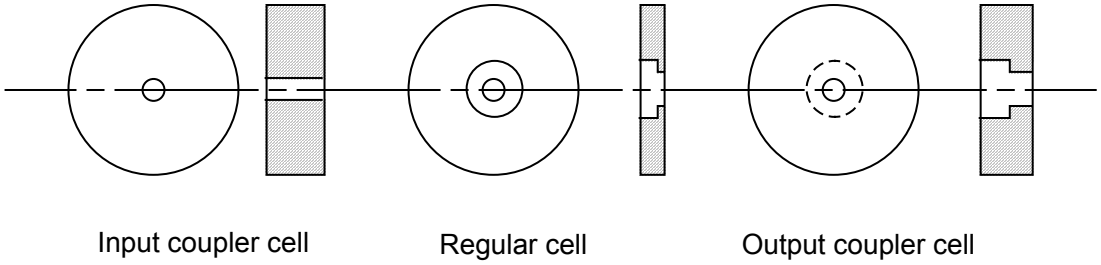

Fig. 4.2 Schematic drawing of cells for DDS3D1. The structure comprises of an input coupler cell, 204 regular cells and an output coupler cell. Completely cylindrically symmetric shape was adopted. The beam hole diameters of all of the cells were set to 8 mm and those of cell diameter to 21 mm.

Cell fabrication:

The OFHC copper material of Class 1 was used. It was 62 mm in diameter and supplied by Hitachi Cable, Ltd. The rough machining and stress release by annealing at 500°C for an hour were processed as IHI's usual way, which is the same to that of KEK. The final diamond turning was made by 'N1' [11] which was moved from KEK to IHI to make cells at IHI with the same quality as those of KEK.

In order to confirm the technology as for the alignment of those cells, it is essential to measure their dimensions better than the alignment requirements. Therefore, the outside diameter of all of the machined cells were measured. The result is shown in Fig. 4.3. The measurement error was about +-0.2 micron so that the alignment raw data could, for the purpose of alignment study, easily be corrected by better than 1 micron based on these measured values. The thickness of the cells were also measured to make it possible to analyze a shrinkage due to the bonding in addition to check the machining performance. The result is shown in Fig. 4.4. The flatness of the mating surface is very

important to make a reliable diffusion bonding. The flatness of all of the cells at both sides were measured using ZYGO interferometer. Results are shown in Fig. 4.5. It was found that large amount of cells were better than 0.4 micron flatness, which was probably within the safe region for the diffusion bonding judged from our experience.

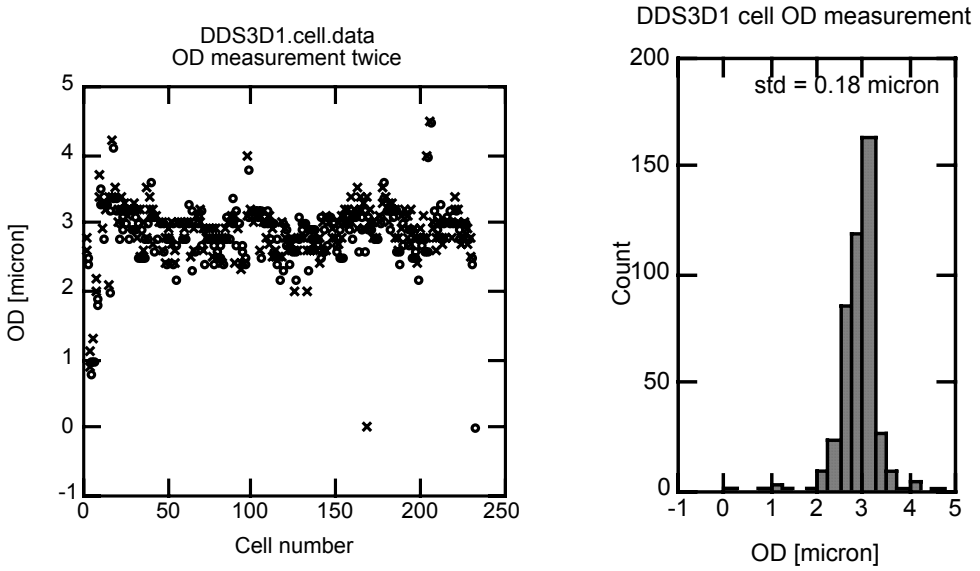

Fig. 4.3 Outside diameter of DDS3D1 cells. The measurements were done twice. The difference between the two measurements is within +-0.5 μm. Standard deviation was 0.18μm.

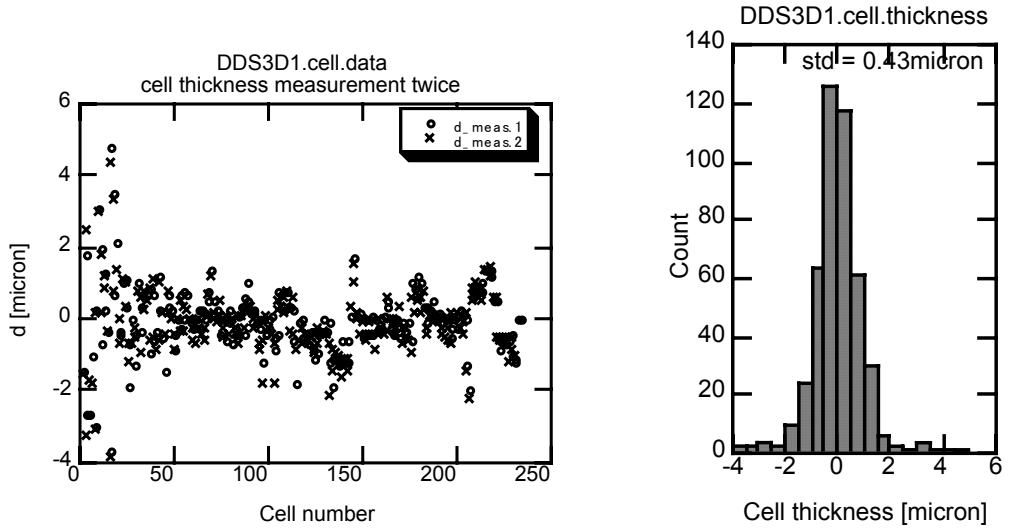

Fig. 4.4 Thickness of DDS3D1 cells. The measurements were done twice. The difference between the two is within +-1μm. Standard deviation was 0.43μm.

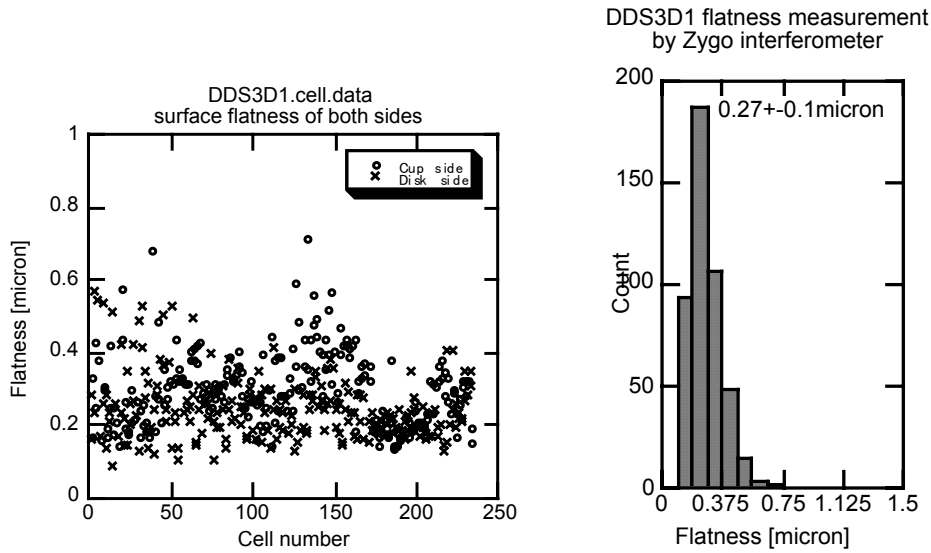

Fig. 4.5 Flatness of DDS3D1 cells. The average value was 0.27μm with a standard deviation of 0.1μm.

4.4 DDS3D2 cells

The cells made for the dummy structure DDS3D2 were almost the same as those of DDS3 cells except the inner cell shape. Such features as the position and size of the manifold, the shape for vacuum pumping port and HOM port, some irregular cell shapes near coupler cells, etc. were determined by following those of DDS3. However, very small amounts of differences in dimensions were neglected and those cells were replaced by some standard cells.

Scribed line

The original DDS3 cell design is equipped with a large groove (of the order of 5mm in width and in depth) on the outer surface of each cell. This groove requires an interrupted cutting in a final diamond cutting process which might be better to be escaped from. In addition, we do not know very well how much we can rotationally align the cells based on the mechanism when we think about the procedure for the cell stacking.

On the other hand, we have already a mechanism which runs along the reference line, V-block, and carries a microscope so that it can check the rotational position of any cell by seeing some mark on the OD. We put the scribed line for this aim.

Cell dimension measurement

Key dimensions, OD and thickness, of all of the cells were measured by comparing with those of the reference cell. The result was shown in Figs. 4.6 adn 4.7.

The OD's of cells #171 and #202 deviated more than 7 microns from the other cells. Such large differences were to be corrected to analyze the fitness of the cells to the V-block.

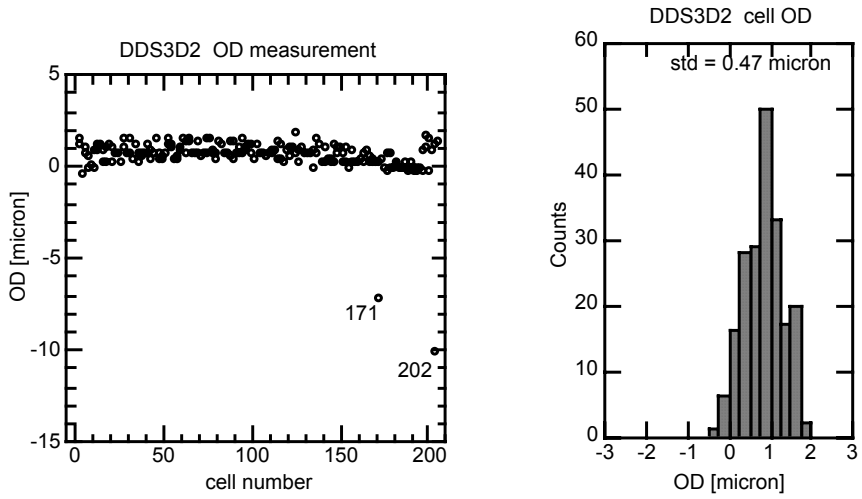

Fig. 4.6 Outside diameter of DDS3D2 cells. The distribution for the cells excluding cells #171 and #202 are plotted in the right figure. The standard deviation of such cells was 0.47 micron.

The results of flatness measurement are shown in Fig. 4.8. Cells for vacuum pumping showed poor flatness. This was due to non-symmetrical 3D shape. This time we did nor seriously try to improve assuming that this was not fatal to judge the bonding results.

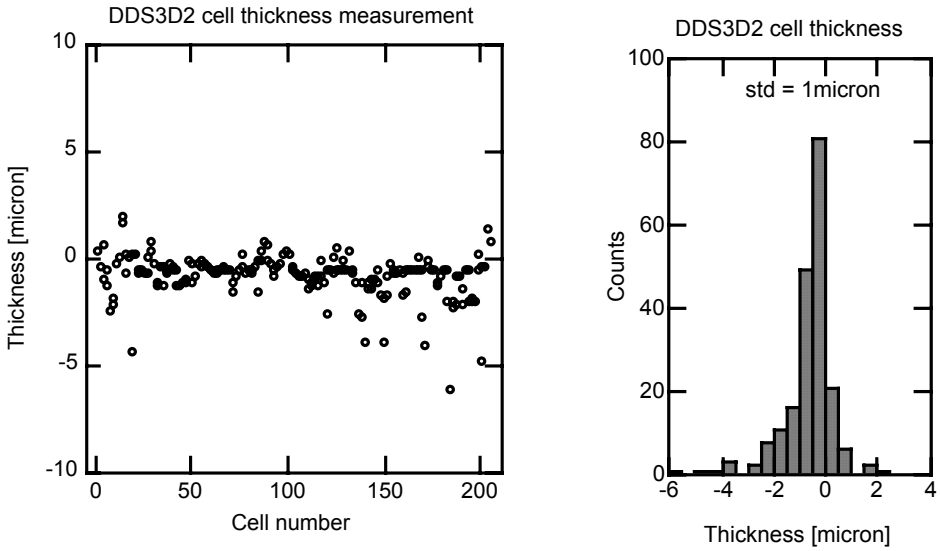

Fig. 4.7 Thickness of DDS3D2 cells relative to a reference cell. That of cell #202 was -78 microns which was the result of many-times cuttings for obtaining a good surface flatness. The standard deviation of the other cells was 1 micron.

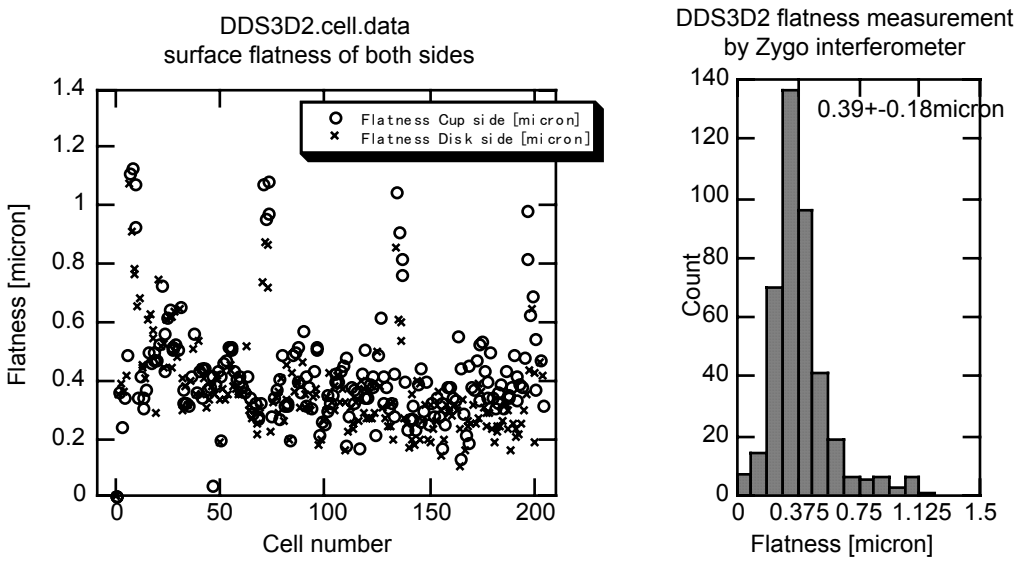

Fig. 4.8 Flatness of DDS3D2 cells. Average value and standard deviation are 0.4 and 0.2 micron, respectively. Flatness of the disk was measured with a mask hiding the disk part where the radius is smaller than cell inner radius.

4.5 DDS3 cells

All of the cells were made by LLNL and measured electrically by SLAC. Then they were shipped directly to IHI.

Cell measurement:

The cell outside diameter and thickness were measured at IHI with two Microsenses [11] sandwiching the cell. It means that the measurement is the relative one comparing to a reference cell. The results are shown in Figs. 4.9 and 4.10.

The flatness was measured by the laser interferometer. The results in Fig. 4.11 shows that most of the cells were better than 0.8μm.

The parallelism was also measured using two interferometer facing each other with the cell in between[11]. The parallelism is better than one micron for almost all of the cell as shown in Fig. 4.12.

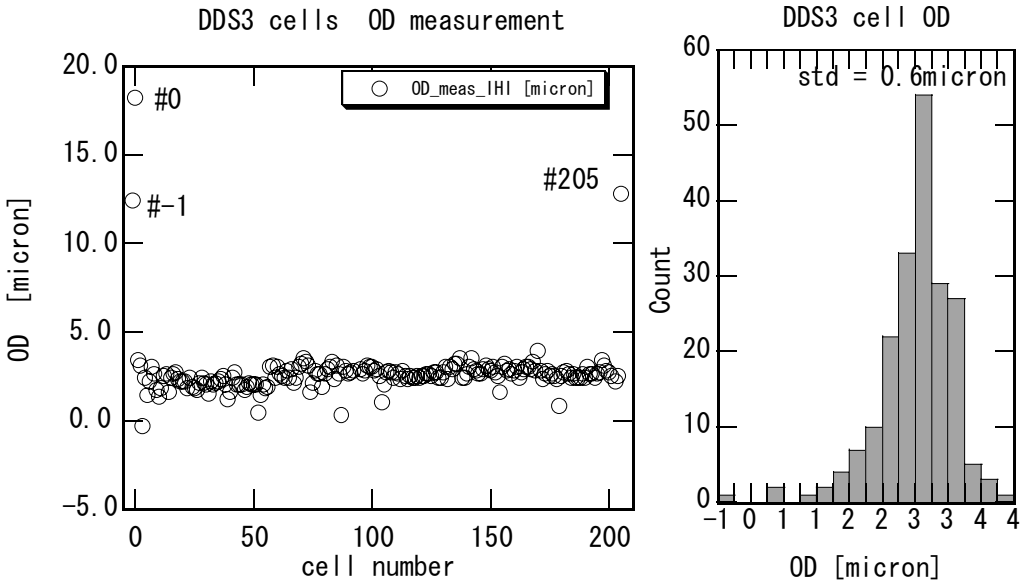

Fig. 4.9 Outside diameter of DDS3 cells. Standard deviation of OD is 0.6μm if excluding three cells near ends.

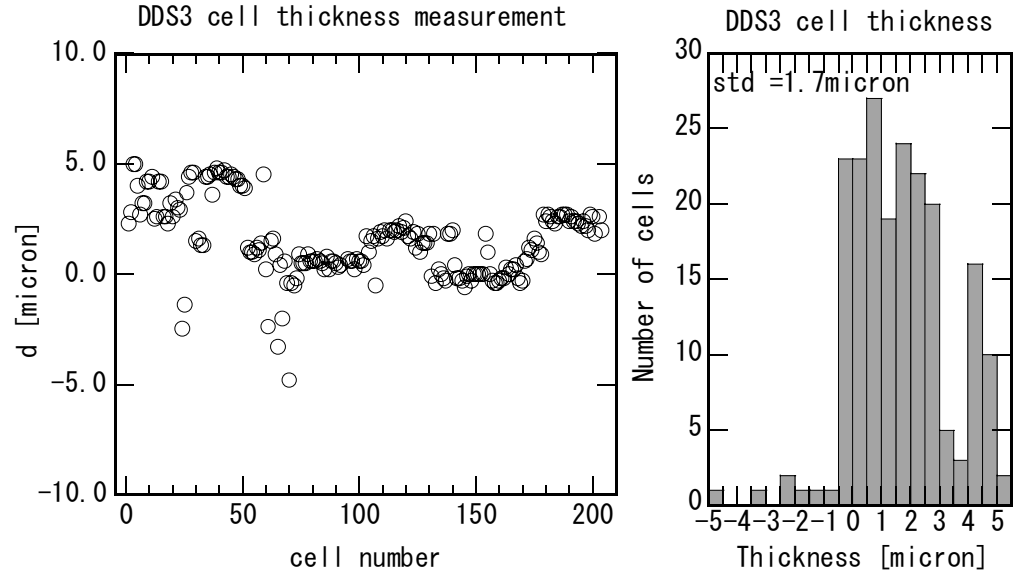

Fig. 4.10 Thickness of DDS3 cells. Standard deviation of cell thickness is 1.7 μm.

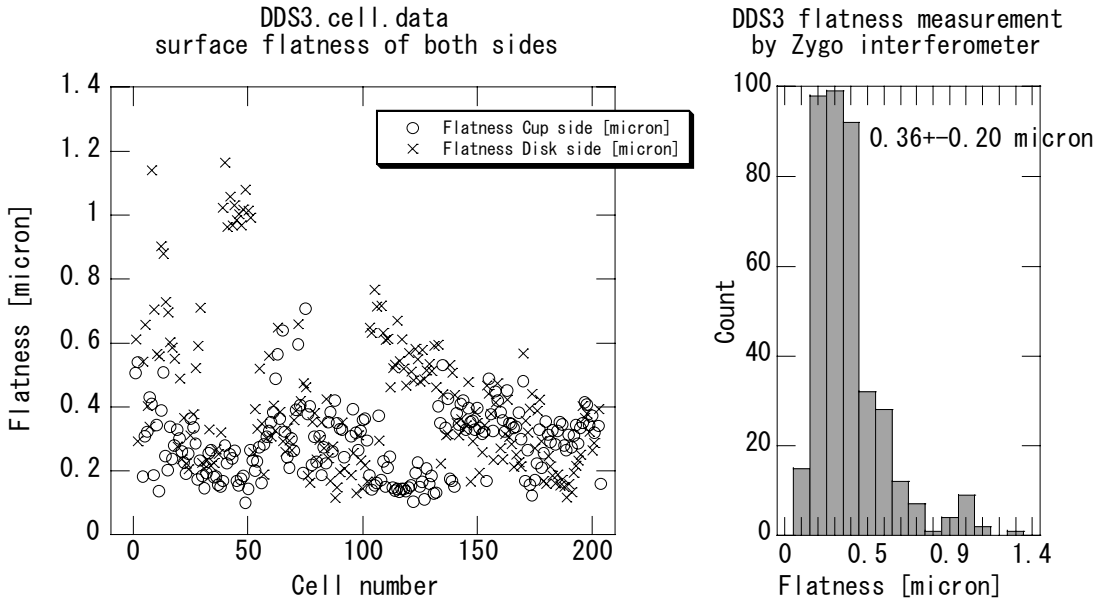

Fig. 4.11 Flatness of the DDS3 cells. Average value and standard deviation of the flatness of cup side, disk side and both sides are (0.29+-0.11), (0.43+-0.24) and (0.36+-0.20) micron, respectively. Flatness of the disk side covers all of the flat surface from OD to beam hole aperture.

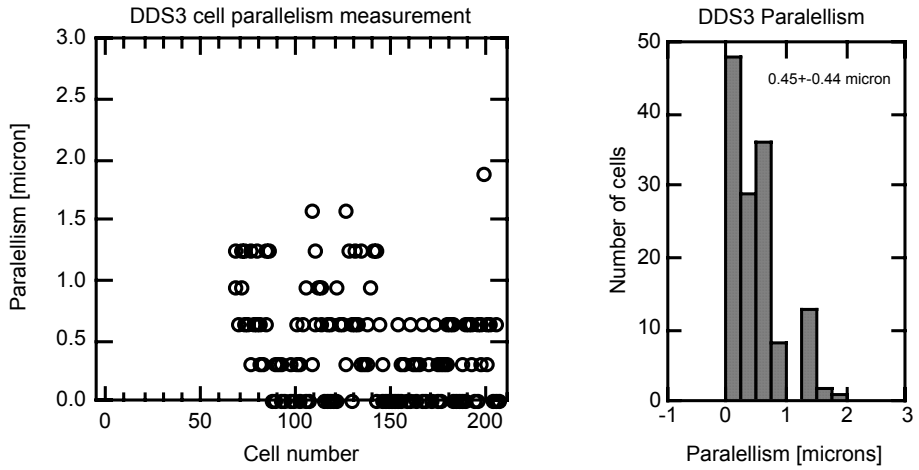

Fig. 4.12 Parallelism of DDS3 cells. Average value and standard deviation are 0.45 and 0.44 μm, respectively. Data of the cells with the number less than 66 happened to be lost.

4.6 Cell recovery

In the early stage of the stacking of DDS3, we found by eye a step between the cells #2 and #3, where those cells should form a HOM port. The step seemed to be of the order of 0.1mm. We tried to evaluate the step quantitatively by specially setting a microscope over the cells. Unfortunately, the setting by utilizing the magnetic chucking tool on an

iron bed running above the cells was not stiff so that the magnetic stand happened to fall down on the stacked cells. It hurts the cell heavily so that we need to recover it if happened.

Before ISG2 we agreed to make a recovery cell by LLNL, where LLNL agreed to make the recovery in two weeks. However, the furnace schedule was found so tight and the dead line for the recovery was in a few days so that we could not wait for two weeks this time. Therefore, we agreed during the ISG2 that IHI would make such recovery cells.

Thus, the recovery of cell #3 was performed at IHI. The cells was roughly machined and annealed. Then the milling was very carefully performed taking for more than several hours. Finally the final diamond turning cutting was performed. Firstly the cutting was done with an undercut of thickness of 10 micrometers.

Then the frequency was measured using the single-cell QC stand used at SLAC. It was found from the data measured by SLAC as shown in Fig. 4.13 that a smooth curve as a function of the cell number down to cell #3 was estimated while a sudden step appeared from cell #3 to cell #2 because of the holes for the RF tuning purpose on cell #2. Therefore it was decided that the frequency difference between that of cell #3 and that of cell #4 should be tuned to the same value, 20MHz, as that measured at SLAC to adjust the frequency of the recovery cell #3.

The additional cutting was performed in the series of measurement points with the order of the cutting as shown in Fig. 4.13. Finally the frequency reached 2MHz higher than the target value, the point with number 4 in the figure, and then we stopped further tuning.

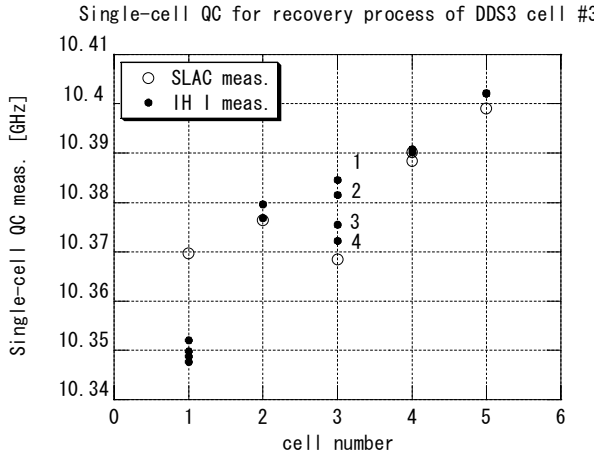

Fig. 4.13 Measured frequencies of the recovery cell #3 through the series of final cutting process were shown in solid circles with the numbering 1 through 4 to indicate the ordering of the additional cutting. Open circles are those measured at SLAC before shipping.

5. Cell cleaning

5.1 Basic ideas behind trial rinsings for DDS3

We have succeeded diffusion bonding of cells which were machined using an ultra-precision lathe with a diamond tool. To prepare the cell surface for bonding, we have rinsed the cells for removing oxygen layer by using weak acid, Hcl, or even rinsing with acetone solution only. It was found that these rinsing gave us a vacuum leak-tight bonding.

The technique of utilizing acid does not seem preferable when considering the post-process of the waste solution, especially in a mass production stage. On the other hand, we are not confident that the rinsing with acetone only would remove all unfavorable materials which may deteriorate a stable high field operation or even a reliable diffusion bonding.

In order to study the feasibility of better rinsing technology, we decided this time to apply an ozone-included pure-water rinsing for some of the cells, in addition to the rinsing with a weak acid for some of the cells and that without any rinsing other than an acetone solution for others. These trial applications are for the purpose of comparing and studying these technologies.

5.2 Some basic studies on copper surface and surface treatment

Various rinsing characteristics were examined up to now by inspecting the surface using Auger Electron Spectroscopy. One of the key materials in our care is the oxygen because it easily corrodes the copper surface and may prevent the surface from diffusion bonding. Another one is carbon or carbon related chemicals. These may be included in cutting process, various handling processes and even from high-temperature furnace operation and may result in possible field emission sites or one of the high-Z materials as a residual gas. Various carbon-related deteriorations especially in super-conducting cavity cases were reported in [12] and we understand that it is better to remove those materials.

Consideting the above background, the rinsing of these two components, O and C, from copper surface has mainly been studied. Fig. 5.1 shows one of the typical examples of the tests. The process of rinsing with H_2SO_4 is described in ref. [1].

It was found that the components of chlorine and sulfer existed. The latter appeared after rinsing with H_2SO_4.

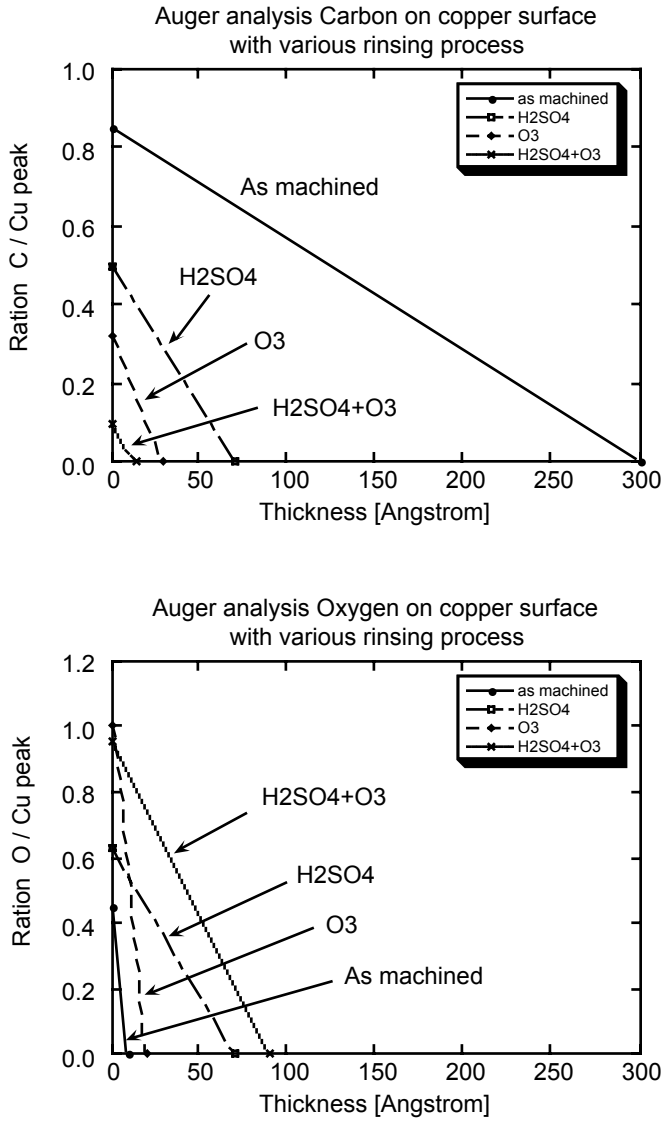

Fig. 5.1 Results of AES spectroscopy on copper surface comparing various rinsing process. Vertical axis is the relative strengths of AES peaks of carbon and oxygen normalized to the copper peak. Horizontal axis is the typical thickness where the clear evidence of the existence disappears.

Another test was performed to evaluate the effect of various rinsing processes. The result is listed in Table 5.1. In all of the cases, the initial process is the acetone rinsing. The oxygen and carbon components on top surface of copper base were measured relative to the AES peak of copper at 920eV.

It was found that the acetone rinsing even creates a big carbon contamination, while the following acid treatment or ozone-included pure-water rinsing (OPWR) process removes those carbon materials. The increase of oxygen components is clear after the OPWR process.

Table 5.1 Relative strength in AES spectroscopy on copper surface with various rinsing processes. Acetone rinsing = the rinsing in an ultra-sonic bath with acetone solution, OPWR = ozone-gas included pure-water rinsing, acid = 3.5% Hcl solution and bonding = high temperature diffusion bonding in a vacuum furnace.

Process	C / Cu	O / Cu
As machined	0.37	0.45
Acetone rinsing only	0.73	0.38
Acid rinsing	0.32	0.49
OPWR	0.11	0.87
Acid + OPWR	0.22	0.88
OPWR + bonding	0.18	0.67

It has been discussed that the OPWR would replace the copper surface by a copper oxide, CuO. Though this oxygen layer is dense and may prevent further oxdization process, we were afraid that it might also prevent it from being diffusion bonded.

However, the bonding of the cells after OPWR rinsing has been proved to be leak tight in many cases. We are now confident that the OPWR process can be as one of the rinsing technologies for copper cells.

5.3 Actual rinsing

For the purpose of clean rinsing, teflon holders were prepared to hold the cell during rinsing and drying process. Essentially three points, bottom, left and right on the outer rim of the cell were touched with the jig. Sixteen cells were processed at once as a batch.

5.3.1 DDS3D1

A procedure list for DS3D1 is shown below. All processes are listed, though actually some of the processes were skipped for some of the cells.

1. Eye inspection of cell surface
2. Acetone ultra-sonic bath — 5 min.
3. Acetone ultra-sonic bath — 5 min.
4. Hcl 3.5% — 30sec or 5sec.
5. Pure water ultra-sonic bath — 3min.
6. Pure water ultra-sonic bath — 3min., use always new solution.
7. OPWR 3--4 ppm — 15 min.
8. Pure water flowing — 1min.
9. Acetone ultra-sonic bath — 5min., use always new solution.
10. Nitrogen gas blow and dry.
11. Eye inspection of cell surface
12. Store on a teflon stocker.

With Hcl without OPWR

Firstly, we checked the rinsing performance by eye for the processes with weak acid for 30 sec. but without OPWR. This gives red traces at the contact area between the cell and the cell holder indicating the existence of Cu_2O. This coloring became weak but were still seen even for the case of reduced period of weak acid rinsing down to 5 sec.

With OPWR without Hcl

Then we studied the case with and without OPWR following acetone Ultra-sonic bath rinsing. The qualities checked by eye for the cell surfaces of the two cases were not very different.

Decision

Therefore, it was decided to make cleaning half of the residual batches by OPWR and another half without OPWR but both without acid rinsing.

Actual rinsing condition

Ozone density in an OPWR was kept between 3 to 4 ppm during the rinsing. The process time was for 15 minutes. Ozone density, conductivity and pH of the solution was frequently checked during the rinsing. It was found that many visible bubbles were formed and attached on the cell surface, most of which were removed by gentle stirring of the solution.

5.3.2 DDS3D2 and DDS3

We decided that this dummy-cell stack should be bonded through two steps, the first, a low-temperature (180°C) pre-bonding step and the second, high-temperature diffusion bonding step. We were not sure whether such process as OPWR is suitable for the first step or not, because the OPWR process makes a dense layer of CuO which might prevent from a good pre-bonding. However, the tests on pre-bonding mechanism proved that the cells rinsed by OPWR are potentially possible to be bonded strongly enough.

Considering the preference of escaping from acid process, we decided to apply the OPWR rinsing for all of the cells of DDS3D2 and DDS3. Typical cleaning procedure is the following.

1. Eye inspection of cell surface
2. N_2 gas blow
3. Acetone ultra-sonic bath 3 min.
4. N_2 gas blow
5. Pure water 1 min.
6. Pure water 1 min.
7. Pure water 1 min.
8. Pure water ultra-sonic bath 3 min.
9. OPWR 3--4 ppm 15 min.

10. Pure water ultra-sonic bath 3 min.
11. N_2 gas blow
12. Sink in an acetone bath 1 min.
13. Sink in an acetone bath 1 min.
14. N_2 gas blow
15. Eye inspection of cell surface
16. Put on a teflon stocker
17. Storage in a desiccator

6. Stacking condition

6.1 Circumference

We estimate that the stacking room for DDS3 is a typical one for all the cases of the present studies. In the following are described that of DDS3. Temperature was 20+-1°C and humidity was about 70%. In this room, the alignment jig was set as shown in Fig. 6.1. Typically five to seven staffs were working around it. The stacking jig was set under one of the HEPA filters of the cleanroom. The filter was 56cm X 56cm wide and located at the ceiling of the room.

Particle counting was performed along the V-block. The result is shown in Fig. 6.2. Upper part of the V-block, indicated by T in the figure, was directly exposed to the air flow from the HEPA filter. Four points along the V-block were picked up for the measurement. Typical value was about 2000 particles / ft^3 for particles larger than 0.5 micron.

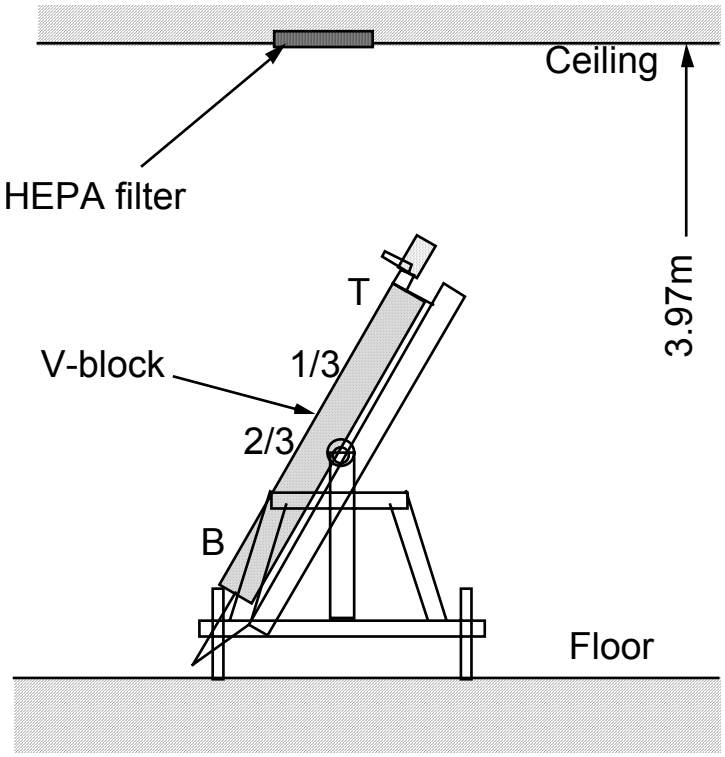

Fig. 6.1 Set up for stacking cells in a clean room.

6.2 Stacking jig

Schematic drawing of the whole jig is already shown in Fig.6.1. Key components are described in the following;

Support structure with rotation mechanism

It was made of steel and the structure was made by welding. Rotation was done manually by rotating a worm gear by hand. A friction plate was equipped for a precise

control of rotation and for being free from an oscillatory swing back associated with the rotation process. The set angle can be set from 0° to over than 90°.

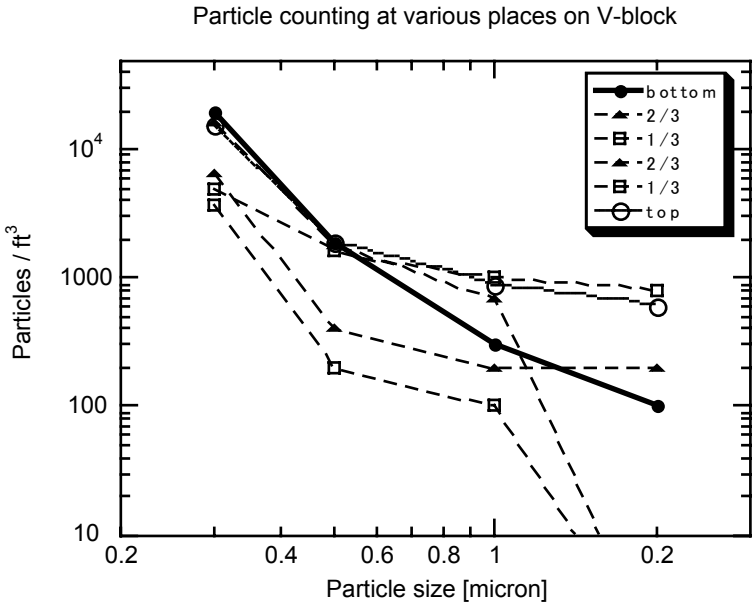

Fig. 6.2 Particles at various places on the V-block set under a HEPA filter for the cleanroom. Mark indicated by top and bottom are those measured at the top and bottom of the V-block, respectively. Those with 1/3 and 2/3 are those at the middle locations of the V-block, while the numbers are the distance from the top in unit of V-block itself.

Rotable table

It is made of steel. Two linear motion guide rails [13] are set on this table running parallel to the V-block. This guide is used for the positioning of the sensor bed. Though the off-axis motion is in principle corrected by utilizing the laser alignment system, this correction term should be small so as to make the system stable. Therefore, the guide should be well resistant against temperature change and also its angle change.

Linear motion mechanism

Case I: for DDS3D1

Two linear motion guides (LMG) were set directly on the V-block as shown in Fig. 6.3. The difference of thermal expansion coefficients between steel and granite made the deformation of the V-block at the different operating temperature than that during setting the LMG. If this happens during the stacking process, it might be a serious difficulties. However, the stacking was performed in a temperature controlled cleanroom so that we did not care much on the thermal deformation.

However, when the structure was measured at Kure work, the temperature could not be controlled. Since the timing for the process was in March, the nominal temperature was

near 20°C while measuring the cells. However, the temperature varied during a day so that we understand that the deformation of the V-block was inevitable.

Case II: for DDS3D2 and DDS3

A ball screw [14] was used for moving the sensor bed which was mounted on the two linear motion guides. Its diameter is 28mm and the pitch is 6mm

Grease was used as a lubricant. As the material is easily put on a wear of the clean wear during stacking process, an oil-less system or some kind of covering seal should be equipped for future cleaner process.

The sensor was set manually at a starting point by judging the position of the sensor by eye. Then the ball screw was driven by a pulse motor. The number of rotation of the pulse motor determined the positioning of the sensor. By this method, we estimate the present position repeatability was about +-0.5mm.

Bed which measurement devices were set

A moving bed was mounted on the two linear motion guide rails and was driven by a pulse motor.

Two Microsense sensors were facing the cell outer surface being set at +-45° from the direction perpendicular to the V-block axis. They were set with micrometer heads so that they could be easily adjusted to the cell surface. Two Wallaston prisms were equipped on the lines extending the Microsense axes.

A microscope was also set on the same bed for measurement of rotational alignment.

Support for autocollimator and laser system

The HP laser alignment system[15] was used for correcting off-axis motion of the sensor bed. Two laser heads and interferometer systems were set on an end of the support. At the other end were equipped with two mirrors.

An autocollimator was set on axis of the V-block. It looked at the lastly stacked cell from the output coupler side. This autocollimator was used to measure the inclination of the cell with respect to the V-block axis.

V-block

Case I: DDS3D1

A granite V-block was used for DDS3D1. These V-blocks are both 2.3m in length and schematically shown in Fig. 6.3. Two linear motion guides, LMG, made of SUS were set on the V-block.

Case II: DDS3D1 and DDS3

The 2.3m long steel V-block was used which was made of S45C steel. The surface was plated with chromium by a thickness of 200μm and the surface was finished with remaining at least 50μm chromium layer. The reason of the V-girders both at top and bottom is to make the structure symmetric to be more rigid against thermal deformation. The top surface of the V-block is though equipped with numerous number of screws for pressing viton plates.

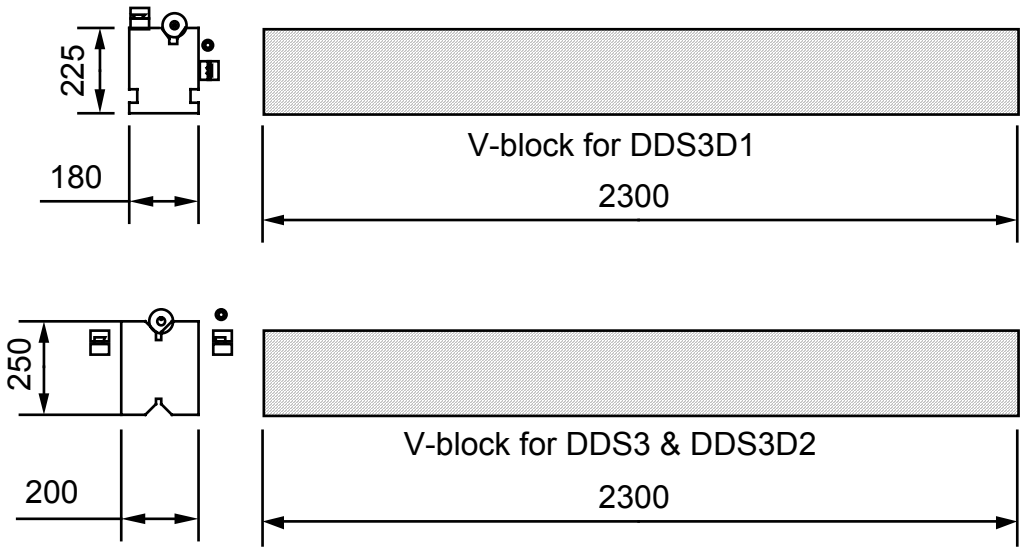

Fig. 6.3 V-blocks used for DDS3D1 (upper figure) and for DDS3 and DDS3D2 (lower figure). The former is made of granite while the latter made of steel. Two linear motion guides are also shown schematically indicating the position of them with respect to the V-block. The ball screw which moves the sensor bed is also shown by a double circle.

Hood for suppressing air turbulence

By covering the V-block top surface, LMG, sensors and mirrors with a hood, the passage of the two laser beams were protected against air turbulence which deteriorates the straightness measurement by using the laser beam.

Working foothold beside V-block

Since the stacking was performed with the V-block rotated from horizontal position by 60°, it was impossible to access the higher part of the V-block without a foothold. Not only stacking but also measurement setting, various pressing processes, setting various items at the top of the stacked cells, etc. were performed standing on this foothold.

6.3 Cell stacking procedure

1. Twenty cells are stocked on a teflon cart for the storage after surface cleaning.

2. The V-block was set at 60° from horizontal position.

3. The front end surface of the bottom SUS block was checked as for the perpendicularity with respect to. the V-block axis by measuring the angle using the autocollimator for three rotational angles of the block each separated by 120 degrees. This checking was only in one (vertical) direction, though. After choosing the best angle out of the three angles, a ceramic block was set on it and made an initial surface for the stacking of the cells.

4. Every staff for stacking wears a one-piece type clean wear from foot to head. He also puts powder-free thin groves of operational purpose on hands.

5. A staff takes one cell out of stocker. Another staff examines the surface by eye and recorded in a logbook. Then, the cell is handed to the stocker.

6. The cell is put on and the rotational alignment is adjusted. Then the cell is pushed by two fingers towards downward and monitors the behavior of the reading of the autocollimator. If the reading becomes stable in several seconds, the last stacking is understood to be reasonably well done. This final reading is recorded. The rotational alignments of the top three cells were checked before going to the next-cell stacking.

6.4 Stacking cycle

DDS3D1 case

Just keep stacking till end with intermittent alignment measurements. Finally an axial pressure of 24kg was applied by three ceramic springs.

DDS3D2 case

After every 35-cells stacking an axial pressure of 15kg was applied on the top of the stacked cells to stabilize the stacked-cell pillar. The pressure was applied by a steel spring, the backing of which was set on the V-block. After stacking more than 70 cells, a viton plate of 5mm in thickness and 50mm in width was pressed with a SUS backing plate. This plate was pushed toward V-block in every 80mm unless any inconvenient interference occurred. Alignment measurements were performed by removing the jigs for this pressing.

After stacking all of the cells, ceramic block was set on the top followed by SUS blocks which were pressed to V-block via in-vacuum-use ball bearing. These SUS blocks were set to transfer the pressure of 600kg by spring as parallel to the axis of V-block as possible.

Firstly 600kg was applied by an oil pressure jack to push the SUS block from the back of the spring. After reaching the nominal pressure, i.e. a required shrinkage of the spring was realized, the SUS back plate pushing the spring was fixed by three stud bolts and nuts. Finally the pressure applied by oil pressure jack was released.

The transportation process was performed with keeping this 600kg pressure.

DDS3 case

The stacking procedure was essentially the same as DDS3D2. Typical measurement procedure were proceeded by removing 3 jigs at once, which push the viton and SUS backing plate at an interval of 80mm. This made the alignment measurement over 30 cells at once. To measure the next position, the next pressing jig was removed with a jig in the other side being reset. This method is called 'measuring worm method' in this note.

The axial pressure during the transportation from Tokyo to Kure was determined to be 100kg, contrary to the parameter of 600kg for the case of DDS3D2. This decision was made intuitively based on the idea that the deformation or stress due to this pressure in the stacked-cell pillar should be small enough not to lead to a large bending but it should also be large enough to keep a friction force to restrict the cell-to-cell motion.

6.5 Rotational alignment

A scratch mark was put on the outer surface of each cell. This was designed to be at 45° from vertical position. Its position was checked by a microscope which was set at an angle 20° from horizontal. The scratch mark on a monitor screen was seen by eye and compared with each other.

7. Long distance transportation and cleanness near furnace

7.1 From Tokyo to Kure

Cell situation on V-block

DDS3D1: The cells were pressed axially by 3 ceramic springs which were basically equipped for bonding at a pressure of 24kg, which was equivalent to that of the bonding. Then the cells on a horizontal V-block were pushed against the V-block via teflon plates of 5mm in thickness and of a few centi-meter in width, which were pressed towards V-block with number of rubber bands wrapping around them.

DDS3D2 and DDS3: Since the cells were pushed to V-block in a configuration of pre-bonding with viton plates being pressed by SUS plates, no more constraint was necessary. Only a stopper in axial direction was set on the V-block. The axial pressure being applied during the transportation was 600kg for DDS3D2 but 100kg for DDS3.

Packing configuration

A device[16] measuring the acceleration in three directions during the transportation was set on an L-shaped support which was fastened to an end surface of the V-block.

Upper part of the V-block and the cells were wrapped by a vinyl sheet and purged by dry nitrogen gas. Though the humidity inside this sheet became less than 10% soon after starting nitrogen gas purge, it became back to a few tens of percents in a few hours or less. The reason why so quickly it becomes humid is not well understood yet.

In the case of DDS3D1, the V-block was packed in a wooden box with cushion materials[17] inserted between them.

In the case of DDS3D2 and DDS3, the V-block was firstly fastened on a metallic plate and covered with a metallic box. Inside this box it was purged by a nitrogen gas. This box was packed on a wooden box with cushion material with the thickness of 20cm in between.

The long side of the wooden box was set in the same direction the truck's direction. The box was fixed by fixing bands with self-pulling mechanism which is usually used for truck loading purpose.

Trucks

Air suspended and air-conditioned trucks was used. The maximum acceleration was 1.8G which was in up/down direction in the DDS3 case. The temperature was set 20 ° C for the case of DDS3D1 in March. The temperature for the case of DDS3D2 and DDS3 in July and August was at 26°C. The latter setting of temperature is for easily adjusting the material temperature after reaching Kure where the nominal temperature in the morning was estimated to be nearly 30°C.

7.2 From Kure to Tokyo:

The bonded structure was set on a V-block and packed in the same way as from Tokyo to Kure except the transverse constraint for the cells which was not necessary any more. Usual trucks were used.

Table 7.1 Vibration and temperature setting and measurement during the transportation process.

Structure	DDS3D1	DDS3D2	DDS3
Tokyo ---> Kure (before bonding)			
Truck			
air suspended	Yes	Yes	Yes
air conditioned	20°C	26°C	26°C
Max acceleration			
up/down	*	1.2	1.2
front/back	*	0.2	0.2
left/right	*	0.9	0.9
Tokyo ---> Kure (after bonding)			
Truck			
air suspended	No	No	No
air conditioned	No	No	No
Max acceleration			
up/down	2.7	Not meas.	2.1
front/back	0.9	Not meas.	0.3
left/right	0.6	Not meas.	0.9

* No data due to paper jam.

7.3 From Tokyo to SLAC

Such effects as dust inclusion, oxidization and reactions with water were considered. The structure was firstly covered by a double-layer sheet consisting of a vinyl sheet with backing of an aluminum sheet. Inside the wrapping sheet were set several packages of materials one for absorbing humidity and another for absorbing oxygen[18]. Finally the wrapping bag was evacuated by a rotary pump and then sealed by a thermal sealing method. Teflon plates were set on a V-shaped support made for the transportation. The wrapped structure was set on it. Rubber bands were used for fixing the structure on the support.

The structure on this support was put on an aluminum box which was that for the Tokyo-Kure transportation. It was nitrogen purged for ten minutes. The box was set in a wooded crate with cushion materials of about 20cm in thickness between the metallic box and the wooden crate.

For the route of Tokyo-Tsukuba-Narita, an air-suspended truck was used.

7.4 Handling tools

The careful movement of the structure, especially that in a vertical motion, was done with the aid of chain block of 1ton.

Loading and unloading of structure to and from a truck was done by a fork lift.

7.5 Things we encountered and learned for future cares

Nut falling in DDS3D1

After transporting the DDS3D1 structure from Tokyo to Kure, we found that one of the three nuts which were fixing the compressing jig for applying an axial force of 24kg was fallen down. The reason is not clear. Since the blocks were sitting on the V-block but also pressed by an axial pressure transferred by the three stud bolts and nuts, the nut might be looser than the other two. Even that, it seems difficult to explain the complete falling under vibrations during the transportation. So we cannot exclude the possibility of forgetting about the fastening of the nut from the beginning by some reason. In future activities, some checking procedure should be established to clarify such a situation and be free from such failures.

Dewfall in DDS3D2

The stacking room was in 20°C and relative humidity was about 70% but the place for packing and loading to the truck was 28°C with a similar humidity. Therefore, the V-block surface became wet as soon as it went out of the stacking room. After we learned this, the temperature of the V-block and cells were adjusted near to that at the packing place. In future such behavior as becoming wet surface should be avoided by this kind of temperature equalization and possibly a better sealing method for them with keeping an atmosphere without moisture, such as keeping with dry nitrogen. In the latter case, however, such mechanism should be taken care of as the removal of water content from the surface inside the seal.

7.6 Cleanness near furnace

The working place at Kure was a normal place without extensive cares on cleanness such as preparing a closed area with filtered air supply. Particle counting was performed near the furnace to estimate the typical circumference. The result is shown in Fig. 7.1. As anticipated, the measured value was huge comparing to those measured in a clean room of class 10000. A typical value for the particles larger than 0.5μm was 2 million/ft^3.

Therefore, a tentative clean hut was made even if we do not make any assembly process .i.e., cell-to-cell gap is not exposed to the open air. The hut was about 3m high, 3m long and 2m wide and equipped with three HEPA filters each of which was 65cmX65cm set at the top frame. The hut was covered with vinyl curtain. Particle counting was performed 50cm above floor level. The particles when staff was working inside was 15000/ft^3 for larger than 0.5μm, while that after finishing inside work and waiting for 5 minutes was 4000/ft^3 to 8000/ft^3. A typical circumference during the wire measurement was measured and shown in Fig. 7.2. The particle circumference was much worse than the value stated above. This worse value might be due to the frequent in/out process of the operators for the wire measurement. On the other hand, it was

found that the particles of smaller size less than 1 micron was reduced a lot by a factor of 5 or so.

Sophisticated operations and precise measurements using Microsenses or vertical wires were performed in it. The transition of the structure from this clean hut to the vacuum furnace was in an open air where no care was taken as for the cleanness. When the structure was outside the hut it was only covered by a vinyl sheet as long as we could.

No temperature control nor humidity control was applied in this hut due to the limited time and money and by considering difficulties estimated for the structure to be wet soon after being out of the hut into a hot and humid circumference, in summer in Japan. A typical temperature and the relative humidity in the hut during the DDS3D2 and DDS3 in July and August were 32°C and 54%, respectively.

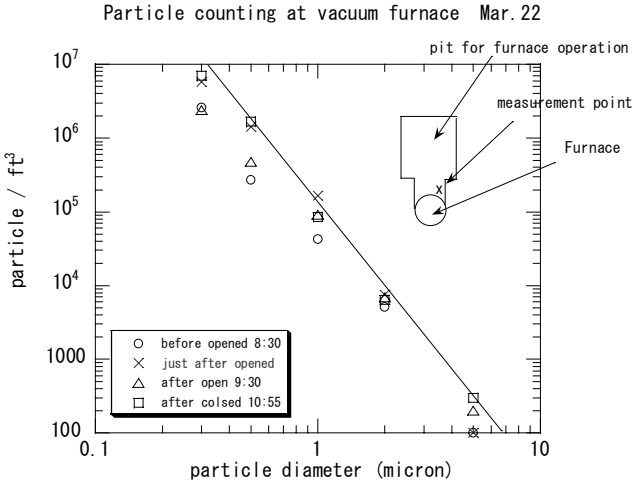

Fig. 7.1 Result of particle counting done near the vacuum furnace as a typical value for the process at Kure outside clean hut.

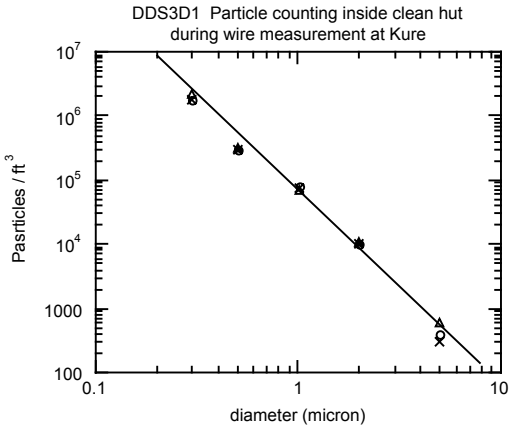

Fig. 7.2 Particle counting done inside clean hut at Kure before, during and after wire measurement.

8. Methods for cell alignment measurement

8.1 Basic description of measurement

Capacitive gap sensors

Two capacitive gap sensors, Microsenses[10], are set at +-45° from the direction removing from V-block as shown in Fig. 8.1(see schematic drawing at upper left). The dynamic range of these sensors is 100+-25 microns and the resolution is 0.01 micron. These sensors are mounted on a bed running parallel to the V-block guided by two linear motion guides. The bed is driven by a stepping motor with 12 microns/pulse. The transverse movement of each sensor, which is determined by the movement of the bed, can be monitored by a laser alignment system[15]. This laser system can correct the spurious movement of the bed due to various mechanisms.

Gap measurement between wire and cell

The cell alignment in a vertical situation is measured by measuring the gap between the cell and one of the two vertically stretched wires, which is running by the structure in a vertical position. The gap is measured by a laser scanning measurement system[19].

8.2 Definition of coordinate system

The coordinate system cited in this note is shown in the lower-left schematic drawing of Fig. 8.1. This coordinate system refers to viewing the structure from input coupler side when stacking on a V-block with the vacuum-pumping side to the right direction. Therefore, the X-axis is downward while the Y-axis is the horizontal right direction when seeing sitting on a beam in an actual setup in the beam line.

The upper-left view shows the configuration of the measurement using two Microsenses, M1 and M2, running through the V-block. The upper-right view shows the configuration for the wire measurement. Here the structure is seen from the output coupler side. The figure shows the setup for the measurement with wire-A. The measurements with wire-B and wire-C are performed by rotating the structure clockwise by 120° and 240°, respectively, from the configuration shown in the figure.

8.3 Relation between measurement by Microsense and that by wire

Sometimes only Microsense measurement or wire measurement was performed due to limited time etc. Therefore, it is worthwhile to relate one of the two measurement with the other. We define a vector (x,y) as the transverse deviation of the cell at a part along the structure, where the coordinate of Fig.8.1(the lower-left) is taken. Then we can express the values of the wire measurement as A, B and C as

-A = (x Sqrt(3)/2, - y / 2)
-B = (-x Sqrt(3)/2, - y / 2)
-C = (0, y).

Therefore,

x = [B-A] / Sqrt(3)
y = -[C] = [A+B]

and the corresponding Microsense reading becomes

M1 = (-x-y) / Sqrt(2)
M2 = (x+y) / Sqrt(2).

Since the transverse offset was measured in three angles in wire measurements, the measurements are redundant and y value becomes a measure for checking the selfconsistency of wire measurement. This is described in the appendix in detail.

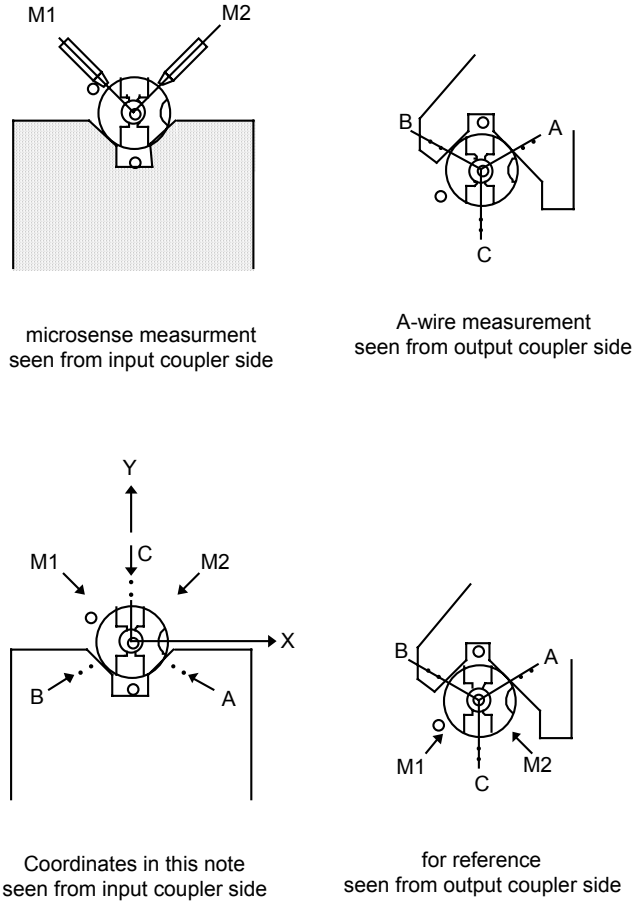

Fig.8.1 Coordinate system in various views.
Lower-left: definition of coordinates in this note.
Lower-right: the coordinate system when seen from output coupler side.
Upper-left: configuration of the alignment measurement using Microsenses and laser correction.
Upper-right: configuration of wire measurement seen from top of the vertically hanged structure, i.e., from output coupler side.

8.4 Vertical straightness measurement system in detail

8.4.1 Set up

We have developed an apparatus for measuring the straightness of the stack in a vertical position. The purpose of this apparatus is to measure the straightness of the stack before and after the bonding process. A schematic view of the apparatus is shown in Fig. 8.2.

The apparatus consists of two vertically tensioned wires and a laser gap meter. The wires are referred as standard straight lines. A stage equipped with a laser gap meter slides along the structure guided by two guide poles and the gap meter measures the distance between the cell outside surface and the wires. The thick rectangular steel post that is fixed on a base plate supports the whole apparatus as a backbone. The stack is suspended by a crane in order to avoid an extra deformation of the apparatus. For a stable installation of the apparatus on the floor, three screws adjust the horizontal level of the base plate.

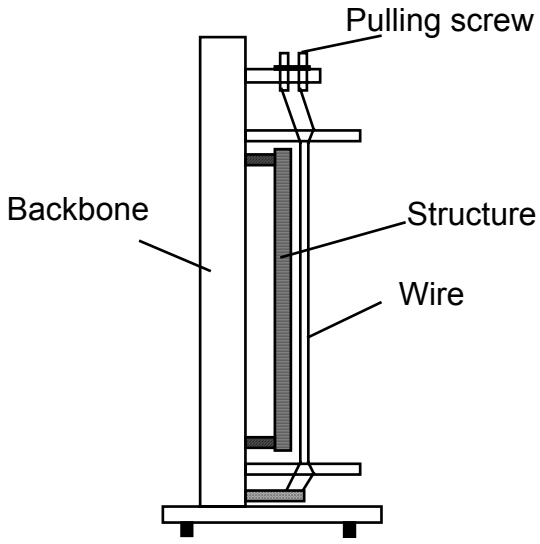

Fig. 8.2 Set up for the wire straightness measurement system.

8.4.2 Laser gap meter

A commercial laser scanning gap meter [19] was used to measure the distance between the stack and two wires. An oblate beam is emitted by a semiconductor laser. The beam is displaced by a rotating polygon mirror and a cylindrical lens. Two lenses focus the beam on a photo detector array. A position of an object is detected as the bright/dark variation which is synchronized to the rotation of the polygon mirror.

According to the specification, the accuracy of measurement of a cylinder with 10mm in diameter placed 80mm apart is given within +-2 microns in the region of 10mm X 20mm. On the other hand, the specification of the resolution with 768 averaging is +-0.3 micron or less while the actual measured performace was much better than the value as 0.7(micron)/Sqrt(N), where N is the number of sampled data to be averaged.

8.4.3 Tensioned wires

We used two piano wires with 0.3mm diameter and 2m in length. Each wire was stretched close to its maximum available strength with a lowest-mode frequency of 126Hz. Here the tension is $\sigma = 2.0$ GPa, which is almost the strength of the piano wire with 0.3mm diameter[20]. Actually we pulled wires with the lowest-mode frequency of about 100Hz.

Two wires were streched in parallel in a mirror symmetric set up with each other as for the direction of the bending. We can check the straightness of wires by measuring the linearity of the distance between the two wires. Typically it shows the non-linearity of at most 10 to 20 microns as described in the appendix.

8.4.4 Possible improvements

In addition to those considerations stated above, we understand further improvements such as the following.

1. Use a wire with guaranteed cross-sectional homogeneity and surface smoothness.
   A gold coated BeCu wire for particle detector may be a candidate.
2. Make the steel post and guide poles more rigid.
3. Make automatic translation mechanism for the sliding stage.
4. Introduce a computer controlled measurement.
5. Use a wire tensioner that makes no local bending on the wire.

8.5 Measurement of rotational alignment

The rotational alignment was measured in the configuration shown in Fig. 8.3. The scratch mark was introduced on the outer surface of each cell at 45° from horizontal angle as shown in the figure. A microscope was set on the same bed for the Microsenses and focused at the scratch mark seen from 20° from horizontal plane. The video image was put on a monitor screen and the relative position of the scratch mark was measured by eye.

The width of the scratch mark was about 5 mm in the screen. As the shift on the outer surface of the cell by 4 microns corresponded to 1mm on the screen, the scratch mark was seen to be about 20 microns. The edge of the scratch mark was not very sharp and the judging of rotation by eye on the monitor screen was at most a few mm so that the reading resolution was 10 microns. As the straightness of the linear motion guide was better than 10 microns, the system accuracy should be better than 20 microns.

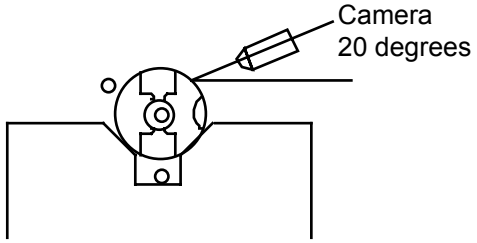

Fig. 8.3 Configuration of the measurement of the rotational alignment by watching the scratch mark.

8.6 V-block straightness

The V-block straightness was measured to check the measurement system. The measurement also serve as obtaining the reference of the cell stacking.

Two V-block were made by the same company. The straightness of the V-blocks itself were measured as a usual inspection process by using an autocollimator. The specification of the V-block was 10 microns and the measured value were well less than the value.

Case I: DDS3D1

The V-block made of granite and the linear motion guides made of stainless steel have different thermal expansion coefficients. Since the linear motion guides were set on the V-block as shown in Fig.6.3, this V-block is weak against temperature change. A calculation was performed to obtain a thermal deformation of the V-block due to the temperature change of 1°C using the following material values.

Table 8.2 Material constant for the analysis of thermal deformation.

Material	Thermal coefficient 10^{-6} / K	Young's modulus kg/mm^2	Poisson's ratio
Granite	8.3	6000	0.3
SUS	11.2	21000	0.3

A finite element analysis [21] gives us an estimation that the V-block is bent by -2.5 and -4 microns to the x and y directions, respectively, where minus sign is defined that the middle part of the V-block sinks with respect to the axis running through the two ends.

The mirror angle changes associated to this deformation. Therefore, for the laser alignment correction purpose, the total change of laser reading amounts -5 microns and -20 microns towards horizontal and vertical direction, respectively, for 1°C change of temperature.

Case II: DDS3D1 and DDS3

There was nothing set on the V-block so that the V-block must be much rigid against temperature change comparing to the one for DDS3D1. The linear motion guide were set on separate support base than V-block.

After installing the present jig, the straightness of the V-block was measured at first by using the measurement system adopted here. However, the laser correction was not fully performed here because of the restriction of time and an inadequate understanding and preparation of the technique.

Fig.8.4 shows the measurement of two Microsenses facing the two surfaces which form the V-surface. Left side surface was measured twice, horizontal position in addition to the nominal angle of 60°, to check the change due to the rotation of the V-block.

Frequent up-downs of a few microns with a period of about 80mm were observed all over the range. This is speculated to be due to the spacing of bolts fixing the linear motion guide to the support structure of the jig. At some places, there also found steps of 5 microns or less. These deviations from the straightness should be corrected in the future activities by utilizing some means such as the laser correction technology.

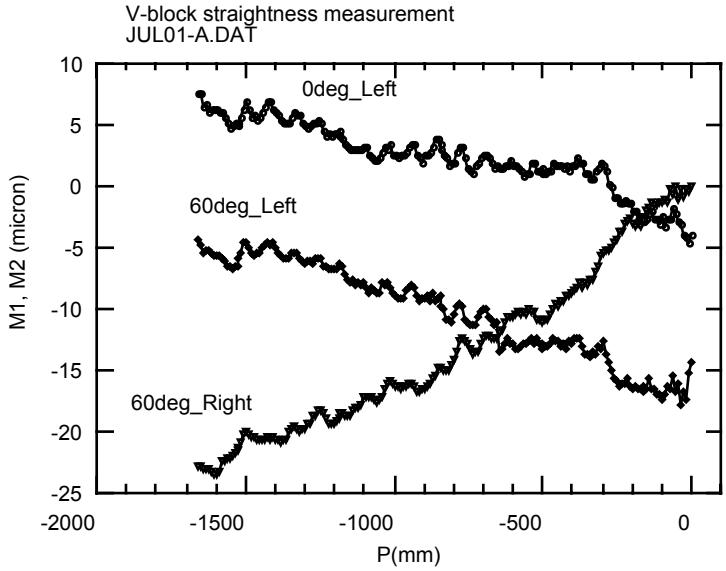

Fig. 8.4 Reading of the Microsenses facing at the two planes of the V-block. Microsense readings are plotted without laser correction. Microsenses are set on the running bed with magnetic chucking tools.

9. Pre-bonding technology

9.1 Background

We experienced that the stacked-cell pillar was not stiff enough so that the bowing pattern changed drastically due to various processes such as axial compression, change of V-block angle, vertical hanging process, etc. However, these changes are not fatal because the bowing can be corrected after bonding. On the other hand, the fatal mechanism is the slippage between the cells because it cannot be corrected after bonding. Therefore, it is necessary to keep the cell-to-cell alignment frozen through the processes after stacking to the completion of bonding.

One of the possible ways to realize the above need is to make a bonding between cells which prevents the cells from moving with each other in the later process. This type of bonding is realized by applying an axial pressure of 600kg over a surface of 61mm in diameter while keeping the temperature over 150°C for 24 hours. The technique is called as "pre-bonding". It was first applied [8] to an 1.8m-long dummy-cell stack. The result is very encouraging; the stack was completed with a cell-to-cell slippage less than a few microns and also with a very small and slow bowing of the structure, about 20 microns.

Based on the above successful case, the parameters and requirements for the reliable pre-bonding were evaluated before practical application by making a series of pre-bonding tests. The experiments and the results are described in section 9.3.

9.2 Nominal parameters

Pressure

We explored the parameters based on the present capability of the ultra-precision machining of cells. It was found that the vacuum leakage through the junction between the stacked cells becomes very small if an axial pressure of 175g/mm^2 is applied[8]. This situation is independent of the surface roughness Ra, from 10nm to 100nm. This characteristics probably means that many high points on the mating surfaces of cells are depressed and the gap between the cells shrinks. Another experiment showed the application of the pressure of 1kg/mm^2 on cylindrically symmetric cells made the vacuum leakage less than the detectable level, 1X10^{-9} Toll liter / sec. It was also found that even after removing the pressure, the junction between the cells were vacuum sealed with a leakage rate of 1X10^{-4} Torr liter / sec level, indicating that some bumps are depressed and partly joined.

Considering these experiences, we set the pressure of the pre-bonding at 600kg over an area with diameter of 61mm, equivalent to about 250g/mm^2.

Heat treatment

The bonding temperature of 150°C for a period of 24 hours was cited based on the experience as of today[14]. Since it is difficult to make the precise temperature control at such a low-temperature in the vacuum furnace of high-temperature use, the temperature is allowed to be a little higher. However, we try to keep the relevant

temperature monitoring values less than 200°C because vacuum-bearings are specified to be up to about 200°C and the viton sheet is specified to use below 250°C.

9.3 Experimental studies

Fout test configurations

In order to evaluate the pre-bonding performance on parameters, four cases with ten-cell stacks were tested as listed in Table 9.1. The actual tested cells are listed in Table 9.2 showing the order of cells in each stack.

The reduction of the pressure from 600kg by 120kg in case 2 and 3 is to study the case of temperature difference of 100°C between the structure and the stud bolts. This difference makes the coil spring length different from nominal one and makes the pressure change. The reduction is actually calculated by the following formula,

$$120\text{kg} = k * \alpha * L_0 * \delta T,$$

where

k=37 kg/mm	spring coefficient of the coil applying the axial pressure,
$\alpha = 1.7*10^{-5}$	assumed thermal expansion coefficients,
$L_0 = 2000$mm	nominal length of the stack,
$\delta T = 100$ °C	assumed maximum temperature difference.

Mechanical strength measurment

The mechanical strength of the test stacks was measured as shown in Fig. 9.1. The maximum stress applied were as follows.

Shearing force between cells	20kg
Bending force	100kg over 10 cells

The shearing force of 20kg in the test is equivalent to a half of the self weight. On the other hand, the bending force in the test is equivalent to a tenth of self weight of the 1.8m-long stack suspended at both ends. The results are summarized in Table 9.3.

Table 9.1 Description of four test cases.

Case	Applied pressure	Nominal temperature	Period	Temperature ramping	Cell shape	Cell cleaning
	kg	°C		°C / hour		
1	600	150	22	10	Cylinder	acid or O_3
2	480	150	10*	10	Cylinder	O_3
3	480	150	22	10	DDS type	O_3
4	600	150	22	10	DDS type	O_3

\# Rinsing in a weak acid bath; H_2SO_4 3%.
O_3 Rinsing in a bath of ozone-gas included pure-water.
* The vacuum furnace had a failure and stopped 10 hours after reaching maximum temperature.

Table 9.2 Configuration of ten cell stack of the pre-bonding tests.

Case	<<---Spring side			Cell stack order				Fixed plate side --->>		
1	29*	28*	27*	24*	23*	2	16	14	13	12
2	36	9	35	8	32	7	31	5	30	4
3	011	015	021	018	003	001	017	022	026	019
4	23#	67#	20#	18#	16#	14#	11#	10#	4#	010

* Rinsed with weak acid bath. Others are rinsed in ozone-included water.
\# Cells made by LLNL. All others were made by IHI co. Ltd.

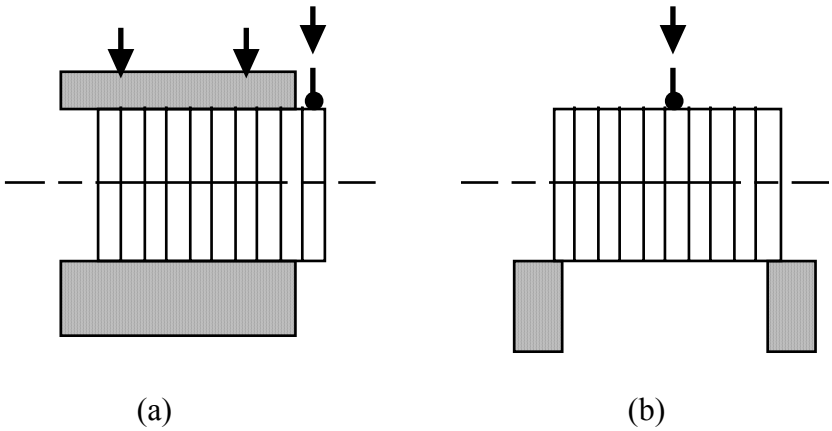

(a) (b)

Fig.9.1 Set up for measuring mechanical strength of pre-bonded ten-cell stack.
(a): test for shearing force and (b) test for bending force.

Table 9.3 Mechanical properties of the pre-bonding tests.

	Shearing force	Bending force
Case 1	12-13, 13-14, 29-28, 28-27 all > 200N	middle of ten cells > 1000N
Case 2	4--30 broken during handling 30--5 < 180N 5--31 > 200N	
Case 3	19--26 , 26--22 ,11--15 ,15--21 ALL > 200N	3--1 < 444N 22--17 < 675N 21 >1000N
Case 4	23 droped when pressure released 67--20 < 174N 20--18 > 200N 10--11 and 16--18 separated during above tests	

It was proved from case 1 that the pre-bonding process with nominal parameters makes a bonding strength above those criteria. This case also indicate that the surfaces treated either with weak acid or with ozone-included water is OK for the pre-bonding.

Case 3 shows that the less pressure by even 20% deteriorates the mechanical characteristics of the pre-bonding. Therefore, keeping the pressure along the structure is important to make the pre-bonding well.

The period at highest temperature in the case 2 is half of that in the case 3. (This parameter we got by accidental failure of furnace operation.) The mechanical performance is miserable indicating that the period of high temperature plays a very important role to make the pre-bonding successful.

The case 4 is the model case with nominal parameters and with using the cells supplied by LLNL, which were the same way as that for DDS3. This case showed the bonding which was mechanically very weak even if under the nominal parameters. Therefore, the present pre-bonding technique might be on a very critical point in the parameter space. Especially the cells in this case were the same as those for DDS3 and there were many holes and slits on the mating surfaces. This complex geometry might have made the pre-bonding difficult.

Vacuum leakage performance

It is to be noted that the vacuum leakage rate of these test stacks show some correlationto the mechanical properties. The results are listed in table. 9.4.

Table 9.4. Vacuum leakage rate measured in the test stacks. Unit is (mb liter / sec).

Case	Leakage / junction	Total leakage
1	$6 X10^{-7} / 2$	$5 X10^{-7}$
3	$2X10^{-7}$ --- $1X10^{-6}$	$1 X10^{-5}$
4	$1X10^{-6}$ --- $3X10^{-5}$	

Inspection of surfaces of separated junctions

Taking these test results in mind, we treated the pre-bonded structure very carefully until diffusion bonding, namely we kept an axial pressure of some amount through all the processes till diffusion bonding.

Finally, some notes on the inspection of the broken surfaces by a SEM device. The broken surfaces at cell 3--1 and cell 17--22 in case 2 shows scattered spots with their diameter of several tens of microns where the characteristic appearance of separation of bonded junction is seen, showing the starting of bonding process. On the contrary, that in the case 3 does not show any typical breaking pattern of bonded junction. In turn, the broken surface between cell 16--18 in case 4 shows many scattered straight lines with their width of one to several microns. These straight spurs are speculated to be due to the original surface quality and they might have prevented the mating surfaces from the good bonding. These phenomena presented important issues but to study these issues were considered to be beyond the scope of the present activity.

Conclusion

From the above tests, the following practical understandings and requirements are concluded for the successful pre-bonding of DDS3.

1. The rinsing of cells with the ozone-included water for the surface treatment is OK for pre-bonding.
2. It is necessary to keep the pressure more than or equal to 600kg during pre-bonding.
3. Heat treatment at 150 °C for 24 hours is required.
4. It is important to handle the pre-bonded stack with as small perturbation as possible.

Taking these conclusions in mind, we treated the pre-bonded structure very carefully until the completion of diffusion bonding, i.e. we kept an axial pressure of some amount through all the processes till finishing diffusion bonding.

9.4 Actual pre-bonding set up

The actual set up of the pre-bonding is shown schematically in Fig. 9.2. The cells are sitting on the V-block. At bottom end they are facing to a ceramic plate which is sitting on a long precise stainless block which is firmly fixed on the V-block. On the other hand, the cell at the top is facing to a ceramic behind which a movable cylinder is set on the V-block pressed toward V-block with a vacuum-use bearing. We design the pressure towards V-block to be 40kg for each block but actually we did push more with

over-compressing the springs. An axial pressure of 600kg or more is then applied through a coil spring made of steel. Here, the axial expansion is sustained by three stainless rods running parallel to the stacked cells. Through the preparation stage to the end of the pre-bonding, a transverse constraint is applied through three viton stripes of thickness about 1cm which are backed by stainless steel plates covering the same area. The transverse pressure is distributed along the structure with an average pressure of 2kg/cm.

It should be noted that the bottom cells sense some extra force due to the weight of the above cells but with less applied pressure due to the friction between the cells and the V-block.

The stacked cells on the V-block was now moved in a horizontal situation towards the support for pre-bonding sitting on the furnace grating base. The movement was performed by the usual crane installed there. Then it is rotated to 60° from flat position.

After bonding, exactly the reverse sequence is taken to set the structure on the V-block back to the alignment/stacking jig.

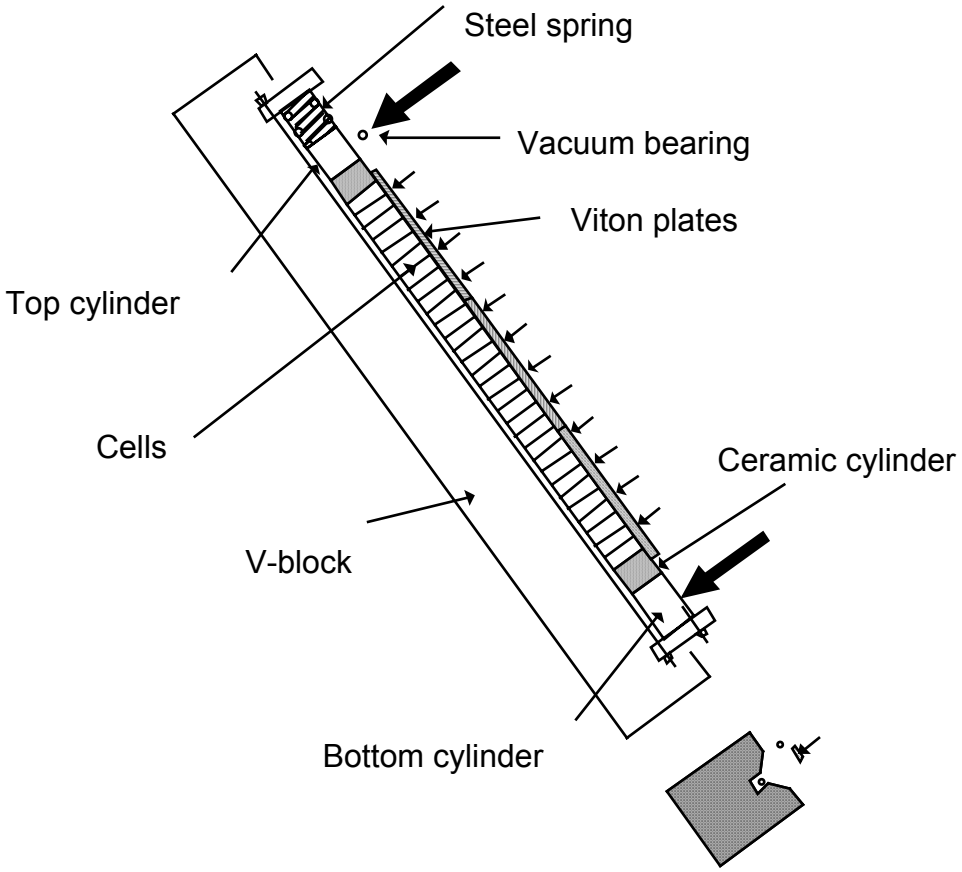

Fig. 9.2. Schematic view of actual pre-bonding setup.

9.5 Temperature control

Temperatures at a few points on the V-block and the structure were monitored by Ni-based thermo couples.

Since the temperature for the pre-bonding is much lower than the usual temperature range for the furnace, no established way of controlling temperature existed. Therefore, the furnace temperature was controlled manually by seeing those monitor temperatures. Rising temperature is performed by setting the target temperature high so that the heater power supplies (divided into three groups) are controlled independently to make the relevant temperature to reach the value. Lowering the temperature is performed firstly by turning the heater off, called vacuum cooling. Then after relevant temperatures become lower than 120 °C or so, the argon gas is inserted to fill the furnace to about 1 atomic pressure with the argon gas circulating through an heat exchanger. (Though in the case of DDS3D2, the step of vacuum cooling was skipped by an accident.)

10. Diffusion bonding technology

The diffusion bonding applied for the structures here is based on our studies as of today. Even if we know that the technology is not matured for mass production, the technique makes a structure without vacuum leakage. The details of the diffusion bonding technology are described in the JLC Design Study Report[1,8].

The parameters of the diffusion bonding for the structures here are as follows;

1. Top temperature 890 °C.
2. Period to keep top temperature more than 10 min.
3. Period of high temperature 1 hours or more at higher than 850 °C.
4. Pressure at the top $10g/mm^2$.

The actual setup is schematically shown in Fig. 10.1. The cell stack was based on a ceramic cylinder which was sitting on a stainless plate hanged by three rods. In the case of DDS3D1, three ceramic springs were inserted between the top and bottom plates connected by three rods. On the other hand in the other two cases, the weight for the diffusion bonding is located at the bottom and loaded on cells through a steel ball and a ceramic cylinder on the top of the stacked cells.

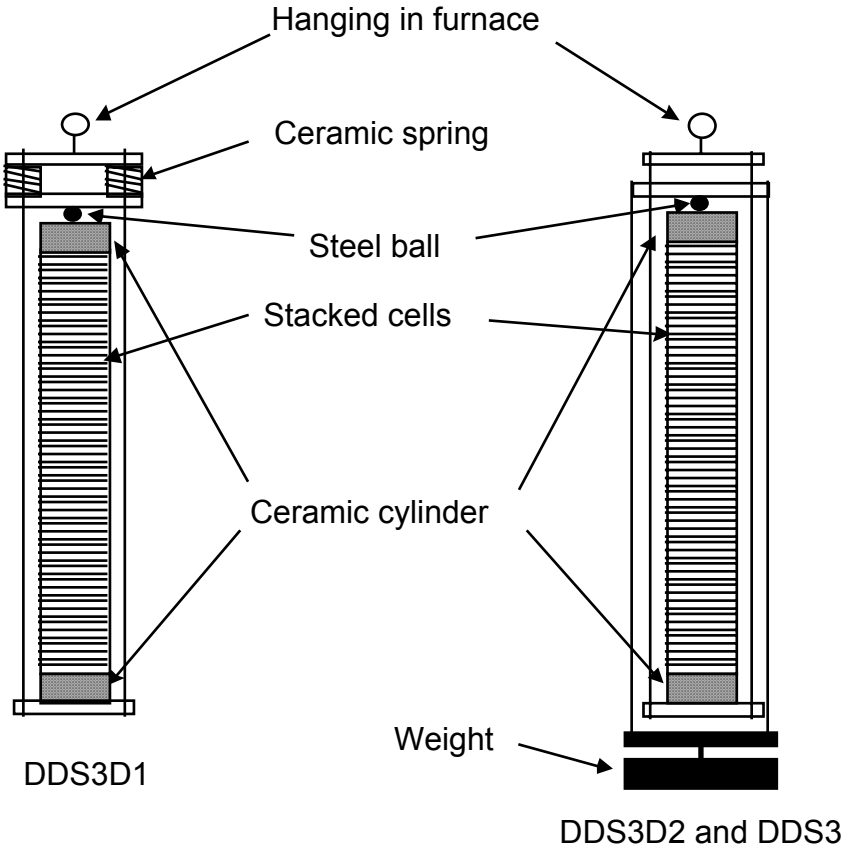

Fig. 10.1 Schematic drawing of the diffusion bonding set up.

11. DDS3D1

11.1 Cell inclinations

The inclinations of the lastly stacked cell surface was measured by an autocollimator [22] during the stacking. The result is shown in Fig. 11.1. The angle was found to vary by +-200 microradian but no cumulative increase was observed.

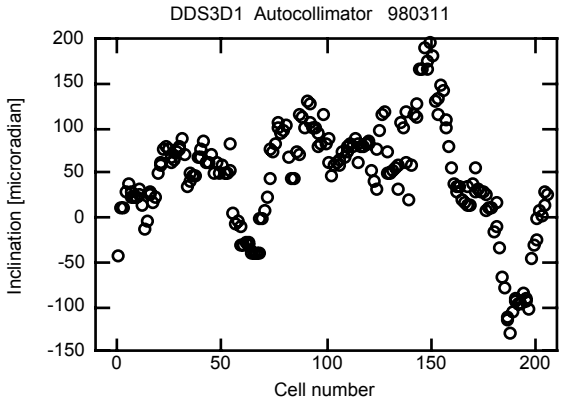

Fig. 11.1 The inclination of the lastly stacked cell during the stacking.

11.2 Cell alignment just after stacking

After stacking studies twice, the cells were rinsed and finally stacked. The alignment of the stacked cells were measured using Microsenses and laser straightness measurement system.

The laser correction method was found feasible with a precision of a few microns level if in the environment where DDS3D1 processes were done in a clean room at Tokyo. Therefore, the data of DDS3D1 were usually analyzed using the laser correction for a better description of the behaviors of stacked cells.

After final stacking at 60° the alignment was measured five times. The result is shown in Fig. 11.2. A smooth bow of about 20 microns was observed in addition to the deviation from this smooth curve by the order of 5 microns over 20 to 40 cells. Moreover, cells near bottom side showed a rapid change in M1 direction, which might be related to the pressure at the bottom through the self-weight on a non-perpendicular base plane for the cell stacking at the bottom.

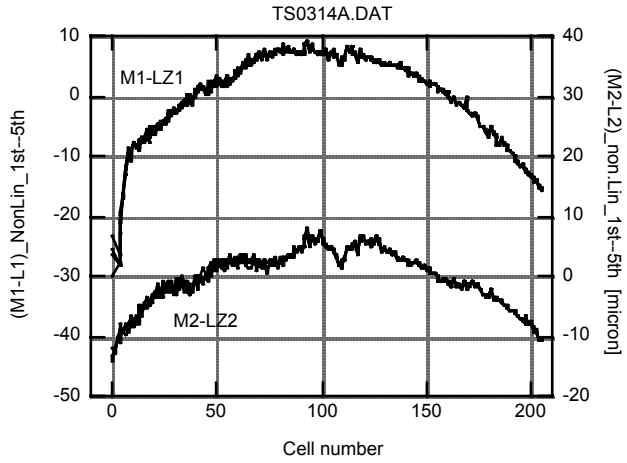

Fig. 11.2 Cell alignment measurement after final stacking at 60°. The measurements were done five times. Each of five traces is the non-linear component for each time and superposed in the figure. Laser correction was performed.

11.3 Stability of stacked-cell pillar against rotation angle

After completing the stacking, the changes of alignment due to various perturbations were measured to study the stability of the stacked-cell pillar. The result is shown in Fig. 11.3.

Keeping the V-block angle at 60°, the stacked cells were axially compressed by four ceramic springs. This pressure application resulted in a floating of 30 to 50 cells near the ends by 20 microns or more which can be seen in the change from bottom trace to the second and third lowest traces in the figure. Then a rotation up to 85° was performed to see how stable the stacked-cell pillar was when reaching a vertical position. The rotation made a bump of the order of ten microns but did not show a drastic change more than that.

Finally it was rotated back to horizontal position for the transportation. Even after rotated to the horizontal position, the bump and floating areas near both ends due to the above process still remained.

It was found from this experiment that the stacked-cell pillar was stable except for 10-20 micron kink or bump among a few tens of cells near end. However, to reach an alignment better than 10 microns, this stability is not enough.

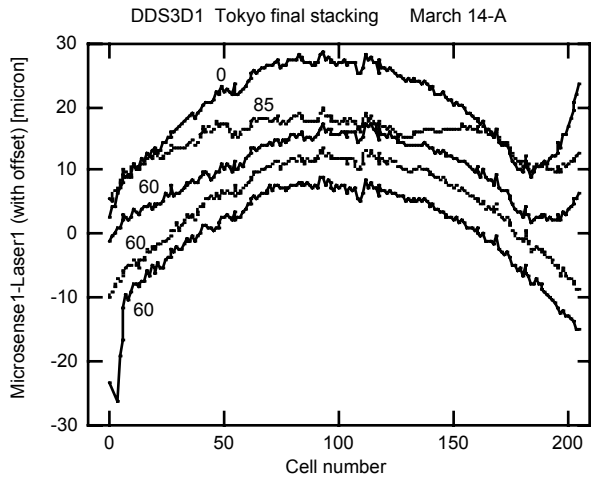

(a) Direction of M1

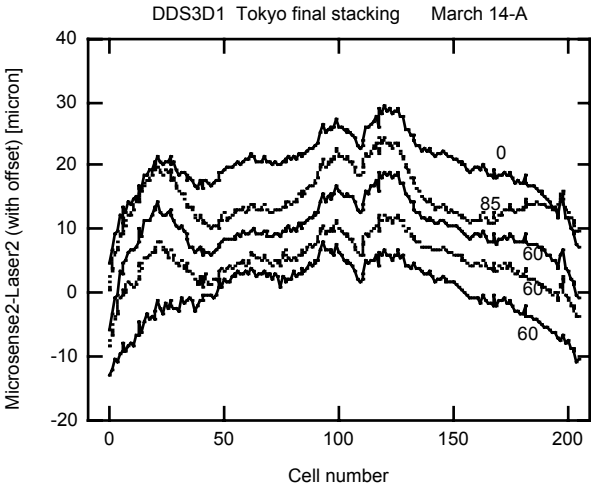

(b) Direction of M2

Fig. 11.3 Stability of stacked-cell pillar.

Cell alignment measurement just before transportation from Tokyo to Kure. Laser correction was performed. Non-linear components were plotted with arbitrary offset to show each line separately. Numbers are the angles of V-block when measurements were performed. The measurement was done in the time sequence shown in the figure from the bottom curve to the top. The conditions were as follows; bottom: just after stacking, second: after axial force applied once and then released, third: re-applying axial force, fourth: rotated to 85° with respect to horizontal plane and finally and top: rotated to horizontal position.

11.4 Cell alignment just before shipping to Kure

The alignment in the last horizontal condition was finally measured carefully before shipping to Kure. The measurements were done twice and the result is shown in Fig. 11.4.

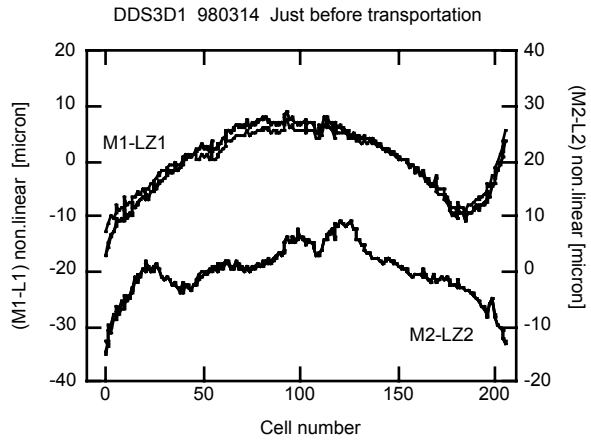

Fig. 11.4 Cell alignment measurement just before shipping to Kure. Measurements were done twice with V-block at horizontal position. The temperature was about 23°C.

11.5 Alignment checking after receiving at Kure

One of the three nuts was found to be fallen after receiving the stacked cells at Kure. Therefore, the nut was re-set and the alignment was measured. The result is shown in Fig. 11.5. A very similar pattern of the misalignment was observed comparing to that before shipping, though the following three points were found in addition,

(1) the amount of the overall bowing was reduced especially in M1 direction,
(2) the deviation from a smooth bowing near the end became small,
(3) the local deviation over a few tens of cells in the middle
from a smooth bow became small,

meaning even a correction to reach a better alignment pattern through the transportation. In the transportation process, a pressing by teflon plate and a long-term vibrational condition during the transport might also contribute to such a change. However, from this change of misalignment, it should also be noted that the pressure of 24kg with teflon constraint could not preserve the alignment of cells through the transportation.

The temperatures during the measurements before shipping and after receiving were 23°C and 19°C, respectively. This different temperature is also be one of the causes of the different shape of the alignment. This kind of consideration was set as a theme for future studies.

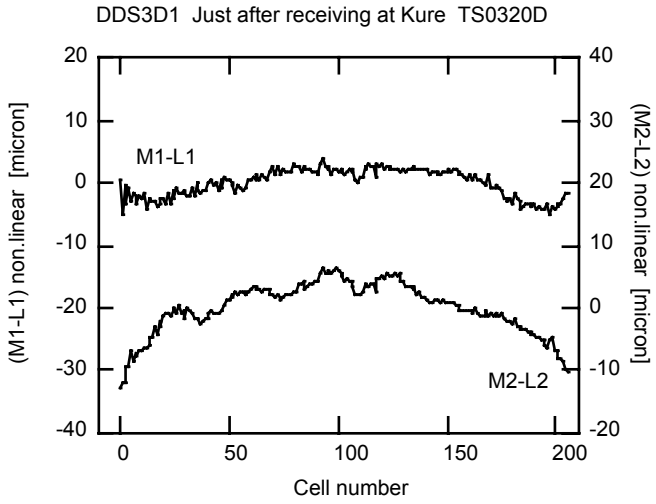

Fig. 11.5 Cell alignment measured after receiving at Kure work and resetting a fallen nut. The V-block is set at the horizontal position. The temperature was about 19°C.

11.6 Stability of stacked-cell pillar against rotation angle measured at Kure

After fallen nut was re-set, the stability against the angle of the V-block was measured. Fig. 11.6 shows the changes with respect to the alignment before resetting the fallen nut. The corresponding angle of V-block are 0°, 60°, 80°, 85° and back to 0° from bottom trace to top. It was found that the alignment was stable within 10 microns.

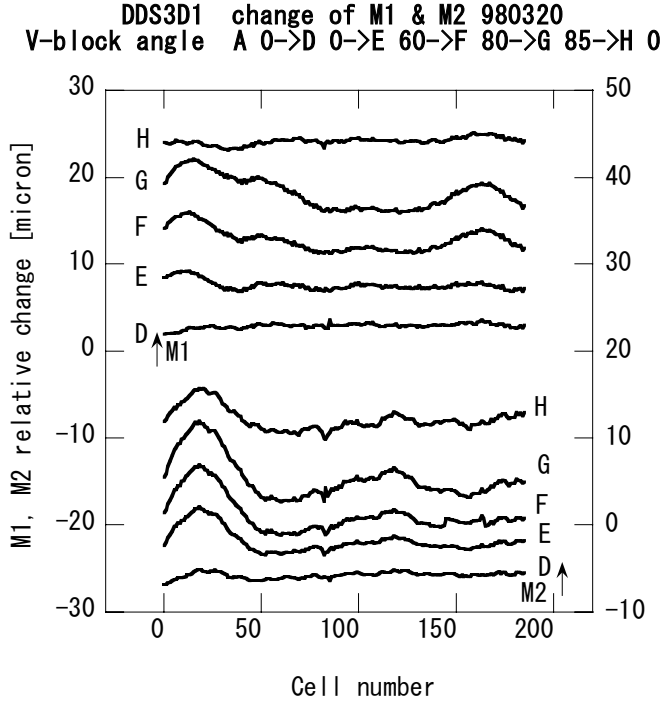

Fig. 11.6 Stability of stacked-cell pillar just before diffusion bonding. The reference is the alignment measurement before re-installing the fallen nut. Then the traces in the figure from bottom to top shows D: after set the fallen nut, E: rotated to 60°, F: to 80°, G: to 85° and H: back to horizontal position. The temperature was about 19°C.

11.7 Wire measurement before diffusion bonding

Before actually setup in a furnace for diffusion bonding, the bowing of the stacked cells was measured in a vertical position. The result is shown in Fig. 11.7. It was found that a bow of more than 0.2mm already appeared in this vertical configuration before bonding. The bowing was much larger than what we measured on the V-block.

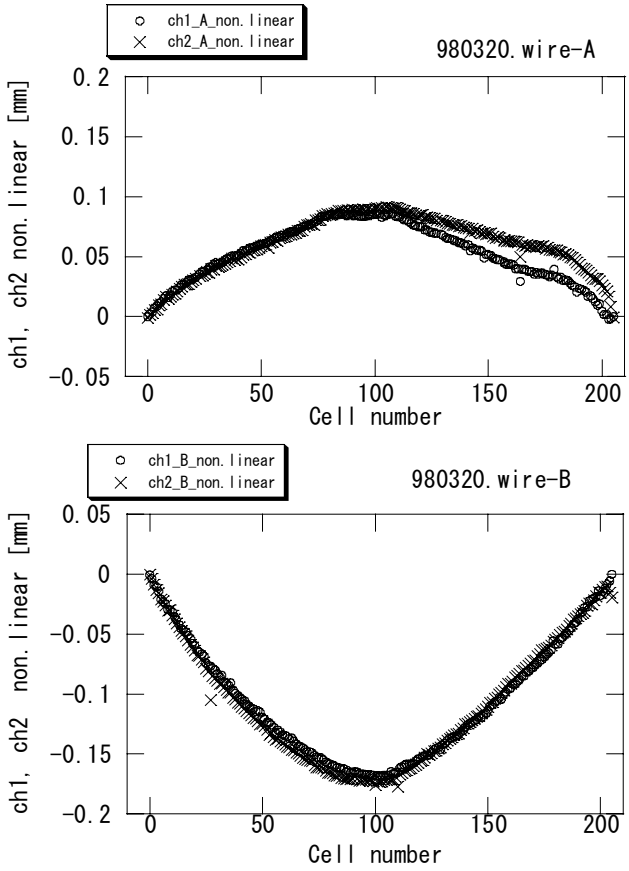

Fig. 11.7 Wire alignment measurement before diffusion bonding. Only non-linear components were plotted. Those with wire A and wire B are in two configuration shown in Fig. 8.1.

11.8 Diffusion bonding temperature

Temperatures monitored at various places of the stacked cells and jigs are shown in Fig. 11.8. Set values are those set in a furnace temperature control program. Furnace temperatures are those measured at the heater position. The points with symbols are those measured by thermo-couples radially inserted to the cells.

We understand that the temperature history was as we designed.

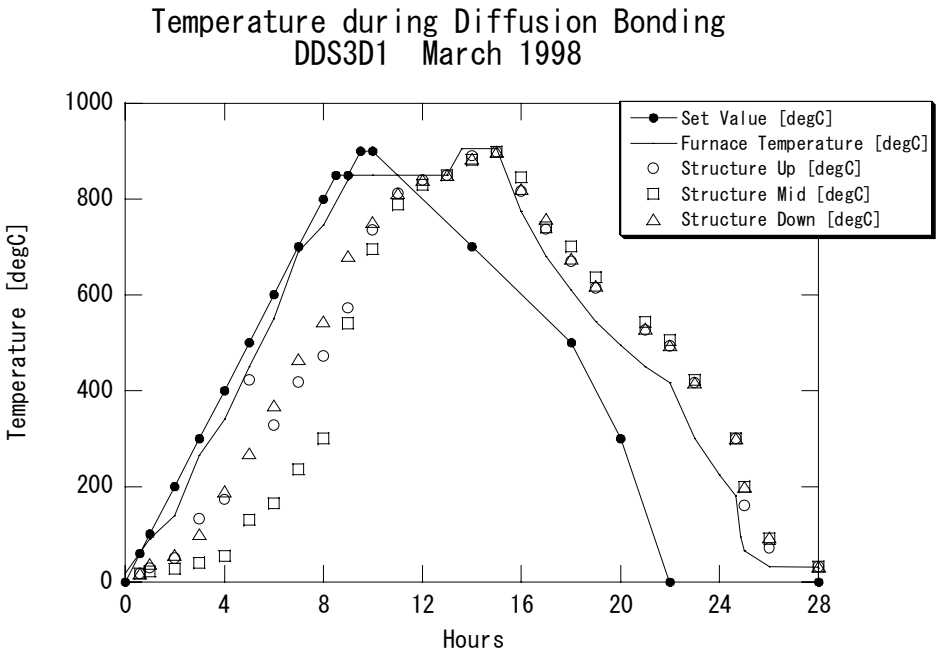

Fig. 11.8 Temperature monitored during diffusion bonding.

11.9 Alignment after diffusion bonding

The structure came out of the furnace in an abnormal situation. Its bow could easily be seen by eye to be a centimeter order. The structure was set on the horizontal V-block and the bending was measured using a scale with respect to the V-block. Fig. 11.9 shows the result showing a bow of about 10mm.

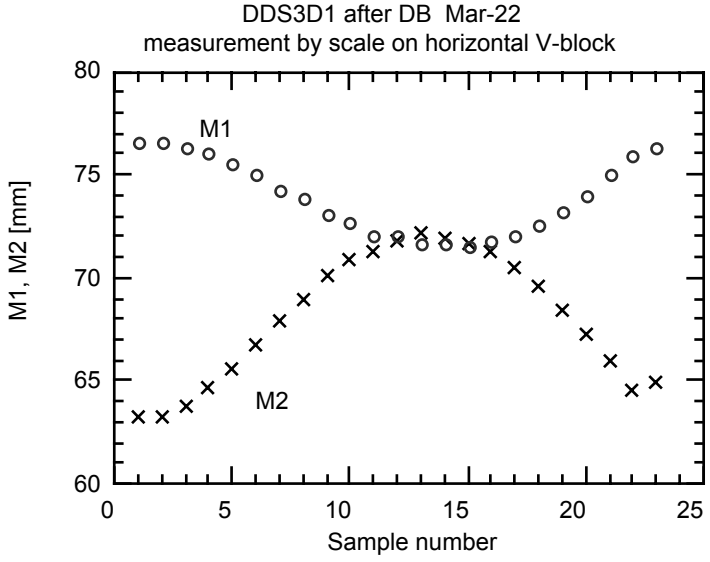

Fig. 11.9 Measurement of the structure bending using a scale. Sampling was approximately every 10th cell. So the data shown extended almost fully along the structure from input end to the output end.

11.10 Analysis of failure

A thermal analysis was performed by IHI[23]. Assuming the emissivity of stud rods made of stainless steel to be 0.4, analysis on temperature history of copper cells was made by varying the emissivity of copper as 0.02, 0.06 and 0.1. The case with emissivity 0.06 best represents the actual temperature history of the cells. Based on the parameters, the whole heat cycle was analyzed.

Rod temperatures are higher than those of copper cells by 350°C at maximum during ramping stage and lower by 200°C at maximum during cooling stage. The corresponding differences of total length of the rod with respect to the structure amounts to be 11mm and -6mm for ramping and cooling stage, respectively.

Since the natural length of ceramic springs are 39.8mm with maximum allowed compression of 5.6mm, the temperature difference in a cooling stage seems too much and resulted in a crush.

Multiple structures with 1.3m length were fabricated successfully before DDS3D1 using the exactly the same mechanism to compress the stacked cells during diffusion bonding. The magic to escape from the same failure was the design of the large cell diameter with water cooling tubes integrated in each cell. The tension rods can run through the holes which are inside the copper stack. In this configuration, the rod temperature is always close to that of copper cell stack and no big difference in length appears.

Though we found a possible mechanism of failure, we designed the diffusion bonding based on a load for the axial pressure with ample free moving space. Further studies based on the compression with ceramic springs should come at least later than DDS3.

11.11 Vacuum leakage checking

The structure was covered by a helium bag and the total leak rate was measured for 10 minutes. The maximum rate measured during the ten minutes was 10^{-8}Torr liter / sec. The background was about 60% of this maximum value which was checked before helium exposure. From this measurement, we conclude that the vacuum leakage rate is less than $5X10^{-9}$Torr liter / sec.

11.12 Summary of DDS3D1

We summarize below what we observed from DDS3D1 fabrication.

1. With stacking simple donut-shaped cells on a granite V-block, the inclination of top cell was within +-200 microradians.

2. Straightness of alignment measuring system could be corrected with a laser alignment measurement system with a precision of a few microns. However, the correction needed a well-behaved air along the laser pass and it was found too

tedious to realize it in a practical measurements outside of a temperature-controlled clean room.

3. Global misalignment of a stacked-cell pillar was a few tens of microns as a whole.

4. Twenty to thirty cells, especially near ends, showed alignment deterioration of at most 10-20 microns in kinks or bumps when rotated between horizontal to vertical.

5. Transportation in a horizontal position with viton plates on top pressing the cells towards V-block made the cell alignment better.

6. It was concluded necessary to re-design the diffusion bonding fixture to cope with the relative movement of jigs at high temperature.

12. DDS3D2

12.1 Setting base for stacking

End block:

The specification of the end block made of SUS is the following. The flatness and perpendicularity are both 1micron / 61mm. The length of the cylinder for the precise fitting to the V-block is 50mm.

Perpendicularity with respect to V-block axis:

A dummy cell was fastened on an end block surface to be a mirror for autocollimator operation. The autocollimator checked the angle only in a plane covering V-block axis and vertical line. The readings varied between +-100μrad when pressing to fix the end block by a bar from top toward V-block.

Ceramics:

The specification of the ceramics was 0.5micron / 61mm in flatness and 3microns / 61mm in perpendicularity and parallelism. The flatness measurement was performed using the Heidenhain depth gauge. The result is shown in Fig. 12.1. The A-ceramic was used at the bottom of the stacking and the B-ceramic was used at the top of the stacking. As shown in the figure, the flatness of the ceramic surface was about 1 micron. The perpendicularity with respect to the cylinder surface was not measured.

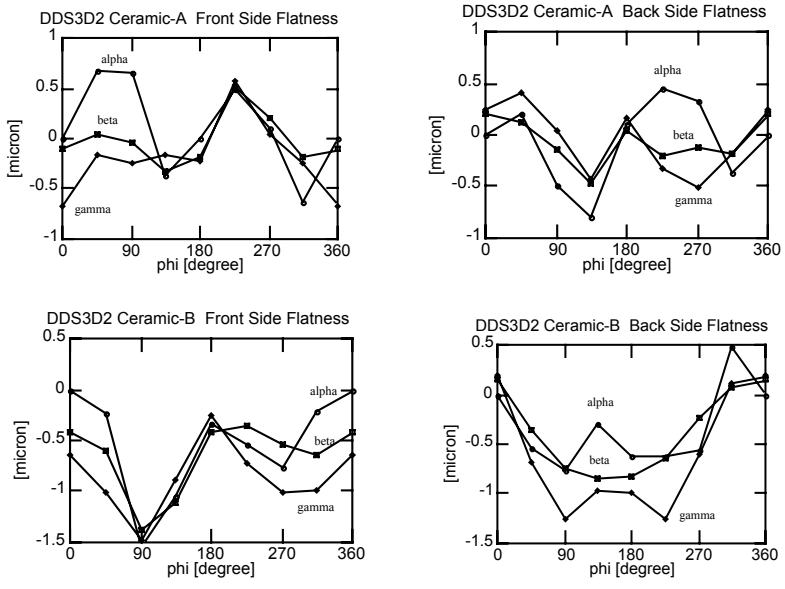

Fig. 12.1 Ceramic surface flatness measurement. Phi is the angle of the measuring points. Data with notation alpha is near outer rim, those with beta in the middle and those with gamma near radius 10mm.

12.2 Stacking studies

First stacking study; with moderate viton constraint use

An alignment measurement after stacking up to cell #93 is shown in Fig. 12.2. The cell #40 was pushed later by hand and found to be squeezed down successfully. Such a floating or migration of the cell should be checked just after each cell stacking if it existed then.

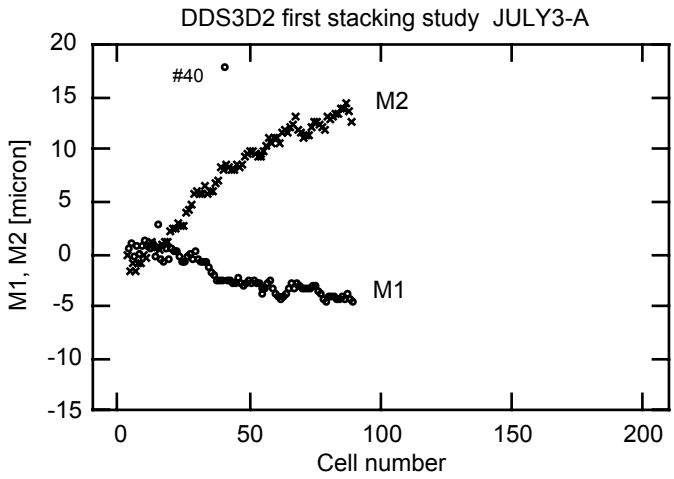

Fig. 12.2 Alignment measurement after initial stacking up to cell #93.

After stacking up to cell #148, an axial pressure of 15kg was applied with a viton plate constraint at the lowest position. Then, the viton plate was removed followed by the pressure release. Then the alignment of cells was measured as shown in Fig. 12.3. Floating of cells by more than 40 microns was observed in the M1 direction.

Some possible reasons for this movement are speculated as follow;

1. transverse component of the applied axial force was large,
2. non-perpendicurarity of ceramic block surface with respect to the V-block axis, which was related to the SUS block surface,
3. torque on the stacked cells was applied when viton was pressed.

The relevant main mechanism should be identified and suppressed for a stable stacking. It should be noted that the bending angle of M1 near cell #50 was 100 microradian, which was much larger than the order of 0.5 to 1 micron / 60mm in the cell flatness or perpendicularity.

By pressing the lower part of the stacking by hand, the floating part could be corrected as shown in Fig. 12.4.

After finishing the stacking of the cells, an axial force of 15kg was applied. The alignment was measured as shown in Fig. 12.5. Fairly large change of the order of 10 microns was observed indicating an unstable situation of the stacked cells.

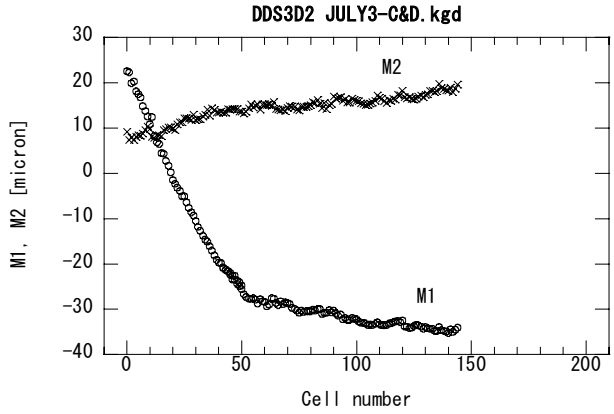

Fig. 12.3 Alignment measurement after pressing by 15kg followed by releasing the pressure and also releasing the viton constraint.

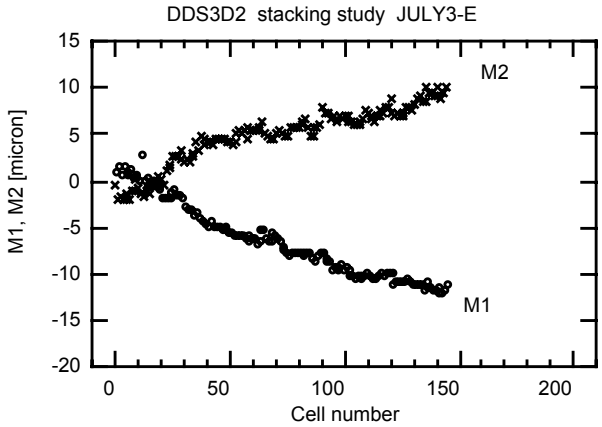

Fig. 12.4 Alignment measurement after the cells of the lower floating part of the stacking was pressed by hand.

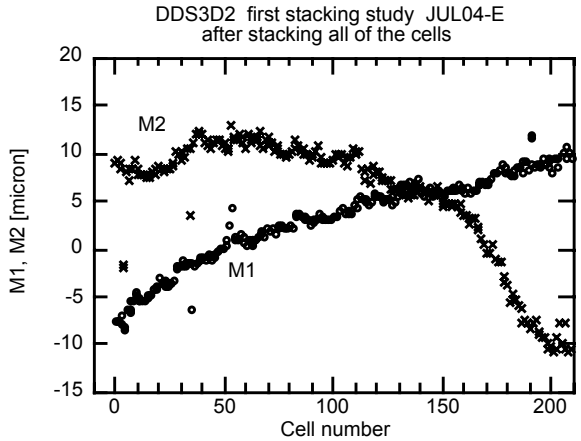

Fig. 12.5 Alignment of cells measured after stacking all of the cells and applying 15kg. A bump of the order of 10 microns appeared.

Finally, an axial force of 600kg was applied. During this process, transverse motion of cells near top was 8 microns or less while at the bottom about 5 microns. The transverse motion of cells in the middle was found smaller.

Following items were found in this first stacking study.

1. Sometimes a single cell floating of the order of 10 microns happens in the stacking process. It can be pushed in by hand but better to be detected as soon as stacking it.

2. An application of an axial force of 15kg introduces a bowing of a few tens of microns or more which remains even after the axial force removal but can be corrected by hand pushing,

3. The application of 600kg axial force gives a moderate change of cell alignment by 10 microns or so.

Since the stacked-cell pillar changes its alignment pattern easily with even an axial pressure of 15 kg or with a hand pushing, we concluded it better to keep the cells constrained transversely always by viton stripes.

Second stacking study; with extensive use of viton constraint

Comparing to the first stacking study, the viton plate constraint was extensively applied this time.

After stacking up to cell #88 in the second stacking study, alignment was measured as shown in Fig. 12.6. It was found that the alignment of cells was very similar to that of the first stacking as shown in Fig. 12.2.

Then the cells up to #148 were stacked and a viton plate was set at the lowest cells up to about cell #70. Alignment before and after pressing by an axial force of 15kg were measured and shown in Fig. 12.7 and Fig. 12.8, respectively. It was found that the lastly stacked cells were stable within a few microns against 15kg axial force if the viton constraint was set below. However, we could not confirm the situation of the lower part of the stacked cells where the constraint by a viton plate was applied.

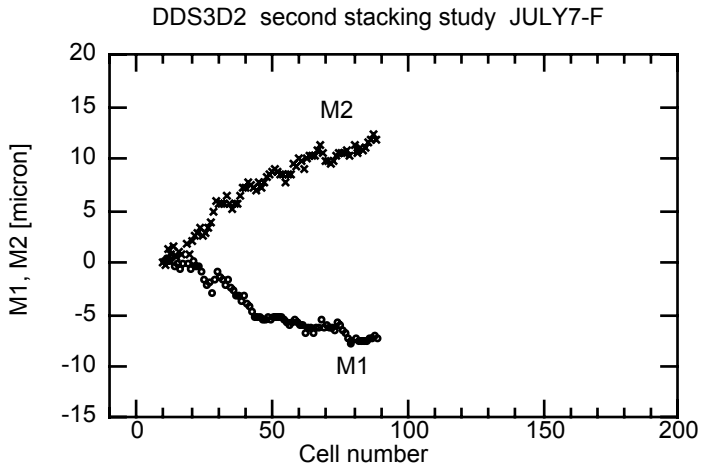

Fig. 12.6 Alignment measurement after stacking up to #88 in the second stacking study.

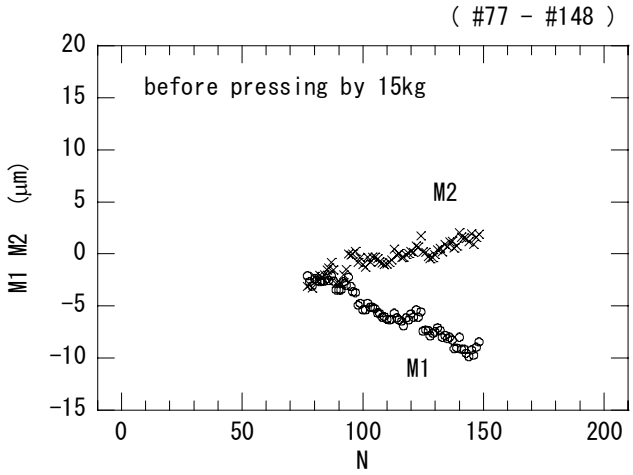

Fig. 12.7 Alignment measurement after stacking up to #148. Lowest viton plate was set but before pressing by 15kg.

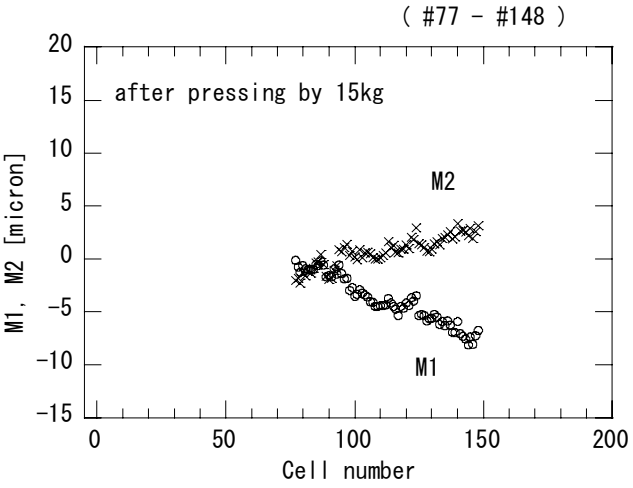

Fig. 12.8 Alignment measurement after applying an axial force of 15kg. No big change was observed comparing to the previous figure.

After stacking all of the cells, alignment was measured before applying an axial force of 15kg while pressing lower 2/3 of the stacked cells with two viton plates. The result is shown in Fig. 12.9. The alignment after applying the 15kg is shown in Fig. 12.10. The cells near the end was also stable now against the axial pressure of 15kg. This phenomenon indicate the stability of the upper part of the stacked-cell pillar established by the transverse constraint by viton plates pressing the lower part of the pillar.

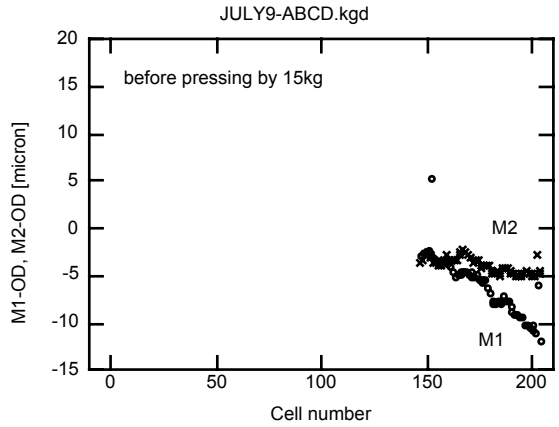

Fig. 12.9 Alignment measurement after stacking all of the cells but before pressing by 15kg. Two viton plates were set at the lower 2/3 of the stack.

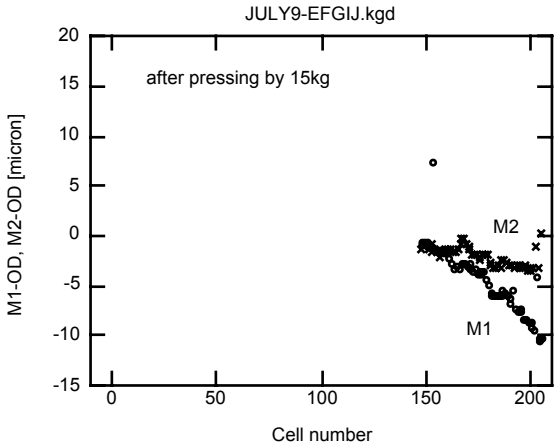

Fig. 12.10 Alignment measurement after pressing by 15kg. Two viton plates were set in the lower 2/3 of the stack.

Finally an axial pressure of 600kg was applied. Contrary to the case of the first stacking study, the cell alignment was measured with keeping the viton transverse constraint. Therefore, it was necessary to do the "measuring-worm" method. Here Microsense are facing the cells in the open region where a few bridges pressing the viton stripe were removed. After measuring the region, the next few jigs were removed and Microsenses were shifted to the next region. Then the jigs in the previous region were set again. The measurement result is shown in Fig. 12.11. In the middle, there was a step due to the drifting of the measurement system which was due to the interval of the rest for an hour.

Fairly abrupt deviation from a smooth curve in the M2 direction was observed over 30 cells near both ends. Comparing to the stability observed in the case of pressure of 15kg application, the application of 600kg affected the alignment more. However, the overall shape of the alignment was similar to that of the first stacking study. As the last three jigs at each end were removed for the measuring-worm method, the transverse constraint for the cells at the end was almost released and the cells moved. On the contrary, the cells in the middle part were pressed via viton plates at both sides even

during the measurements so that the cells could not deviate from a smooth curve even though a large stress was hidden inside.

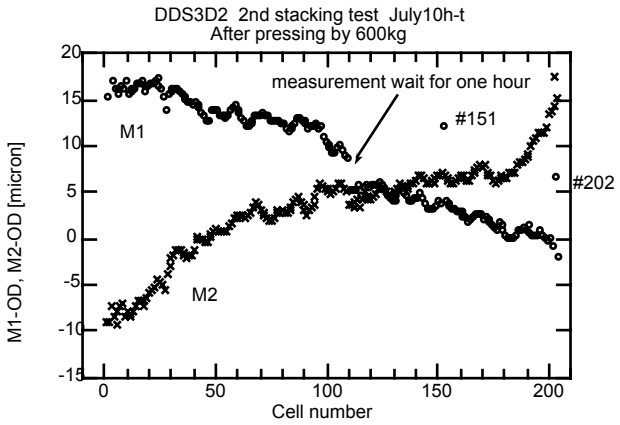

Fig. 12.11 Alignment measurement by measuring-worm method after stacking all of the cells. Cells are pressed by viton plates and an axial pressure of 600kg is applied.

In Fig. 12.12 is shown the alignment measurement after removing all viton plates but keeping the pressure of 600kg. It was to be noted that drastically large transverse movement of 10 microns or more was not observed even under the application of 600kg.

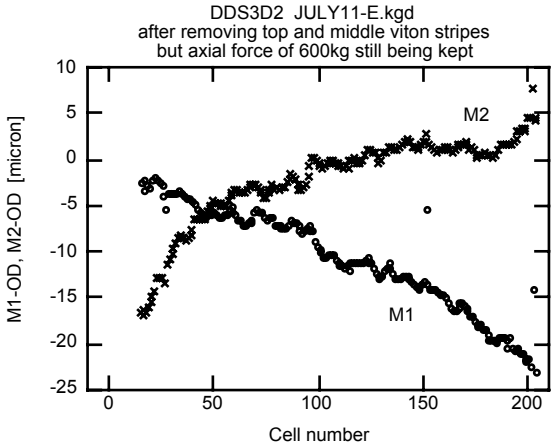

Fig. 12.12 After removing all viton plates but keeping axial force of 600kg.

Finally the alignment of cells was measured after releasing 600kg and the constraints on the top SUS blocks. The result is shown in Fig. 12.13. As shown in the figure, the cells became aligned fairly straight. Considering such a smooth and fairly straight cell alignment after releasing all constraints, we estimate that a significant effect arisen from the axial pressure and the boundary conditions such as a perpendicularity of the end plates play an important role in the stacked-cell pillar. It was also found that the present case shows better cell-to-cell continuity comparing to the restul without extensive viton constraint shown in Fig. 12.5.

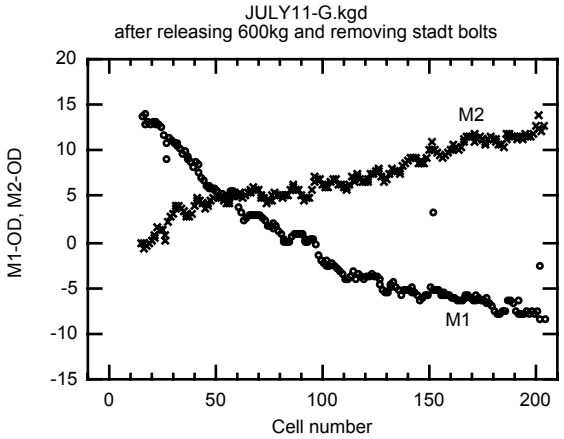

Fig. 12.13 After removing all constraints such as 600kg pressure, vacuum bearings, all viton plates and stud bolts.

What we observed in the second stacking study are the following.

1. Viton pressing was found effective to make the cell-to-cell alignment small.

2. If the transverse constraint via viton stripe was applied to the previously stacked cells, the further stacked cells on top became stable within a few microns against axial force of 15kg.

3. Even with constraint by viton stripes, the misalignment of cells along the structure amounted to about 10 microns or so with a rather steep kinks or bumps under 600kg pressure.

4. After releasing the axial pressure, the cell misalignment recovered to be in a very smooth manner.

12.3 Final stacking

In the same way as the stacking of cells for second stacking study, the cells were finally stacked with measuring the inclination of the top cell. The stacking was performed from the input-side cell towards the output-side one.

The reading of the autocollimator were shown in Fig. 12.15. It was found that the reading is decreased at the rate of -2.4μrad/cell. This behavior of the steady decrease was different from that of the DDS3D1. Whether this is due to the systematic error of the measurement system or actual change of the inclination of the cells should be studied. This study program is being prepared.

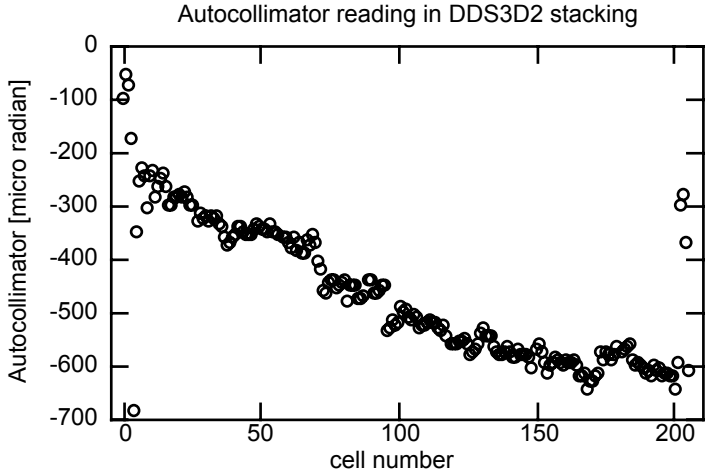

Fig. 12.15 Autocollimator reading as a function of the cell numbering during the stacking. Decreasing value is the direction of removing from the previously stacked cells towards V-block.

After stacking all of the cells, an axial pressure of 680kg was applied. The increase of the pressure than the nominal one was to make sure that the pressure is enough for the pre-bonding even in the case with some unknown perturbations. Then the cell floating of 10 to 15 micron near the output coupler cell was observed but 10-micron shim could not be inserted. Except such an abrupt change near the end, the alignment of cells was fairly stable.

Since we did not observe such a steep rise at the output coupler region in DDS3D1, it may reflect to the shape of the cells which are different to that of regular region or it is related to the big axial pressure application which may derive a transverse component of force.

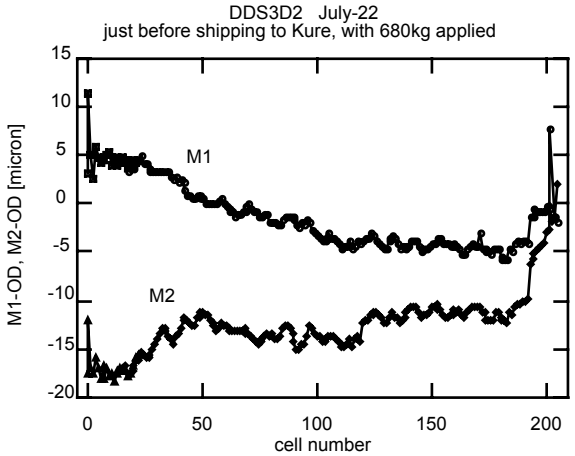

Fig. 12.16 Just before shipping to Kure work. An axial pressure of 680kg was applied. Measuring-worm method was used. Temperature during the measurement was 18 to 19°C.

12.4 Measurements before pre-bonding

After receiving at Kure work, the alignment of cells was measured by measuring worm method. The result is shown in Fig. 12.17. The global pattern and the amount of the misalignment was almost the same as those before transportation.

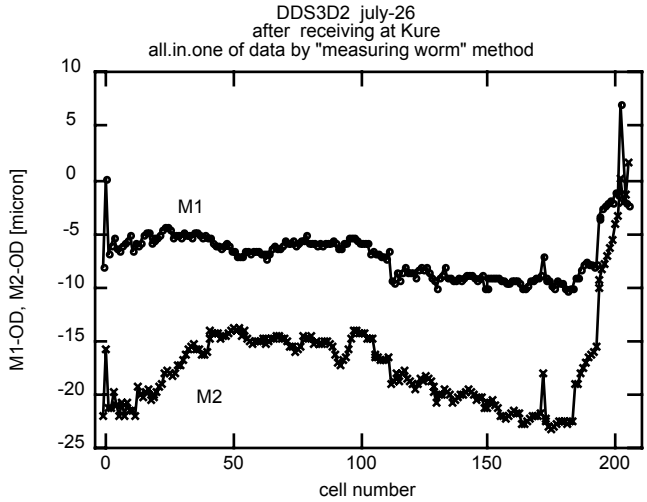

Fig. 12.17 Alignment measurement at Kure just before pre-bonding. Measurement was done by measuring-worm method.

12.5 Pre-bonding

temperature:

Temperature history of pre-bonding is shown in Fig. 12.18. We speculated that one of three monitor points on the structure showed very quick response to the heater control indicating a loose contact to the structure surface. We thought that the temperature of the stacked cells were represented by the other two monitor points. Therefore, the structure was believed to be higher than 150°C for 24 hours.

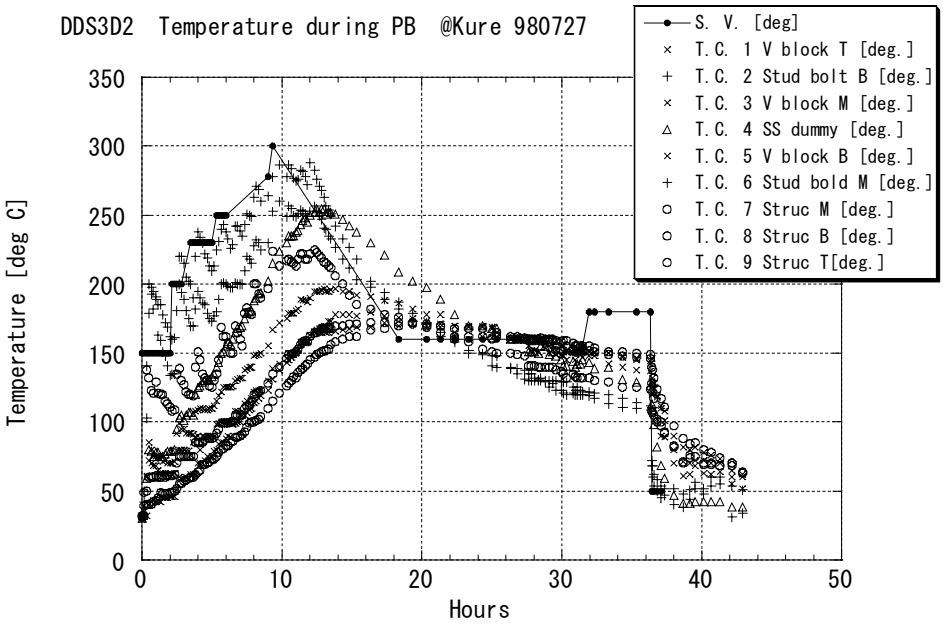

Fig. 12.18 Temperature history during the pre-bonding process. Marks are the temperature defined as follows; solid circles = those of set value for the temperature control program, crosses = temperature of V-block, plus marks = those of stud bolts, open circles = those in structure thermocouple holes and triangles = those at dummy cylinder located at the furnace base.

12.6 Alignment measurement after pre-bonding

After pre-bonding process, the alignment of the cells was measured by measuring worm method with the full pressure kept. It was found that a few tens to fifty cells of the input coupler side show 10 to 20 microns floating while a large floating at the output side disappeared.

On the way to diffusion bonding, the axial pressure was reduced down to 100kg which was intuitively determined as a reasonable value for keeping the stacked-cell pillar stable for various measurement and manipulations and being not far away from the pressure applied for diffusion bonding process, 24kg. The viton constraint was kept and the pressure on the SUS blocks by vacuum-use bearings were kept. The alignment was measured by the measuring-worm method and the result is shown in Fig. 12.20. A smoother bowing was observed comparing to the last measurement with 680kg on.

On the other hand, as soon as the viton plates and the vacuum-type bearings were removed, the alignment of cells became as shown in Fig. 12.21. Very large bow in the M1 plane was observed.

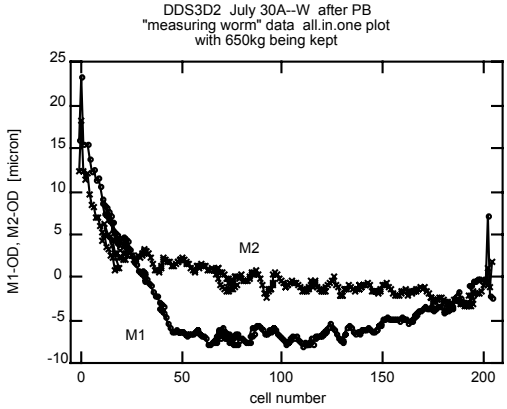

Fig. 12.19 Alignment measurement after pre-bonding. The axial pressure of 680kg was kept. Measuring-worm method was applied.

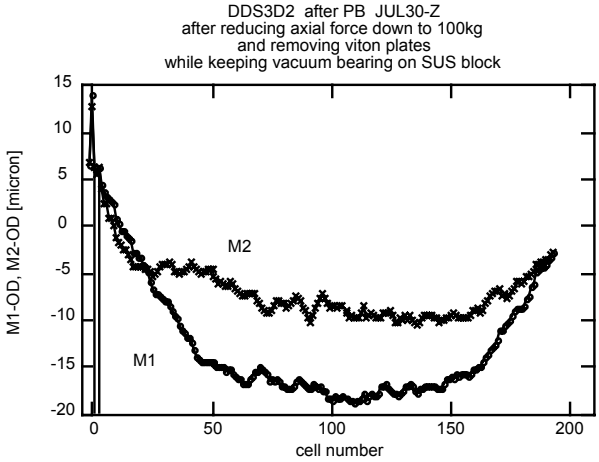

Fig. 12.20 Alignment measurement done after reducing the axial pressure down to 100kg but keeping the vacuum-type bearing pressing the SUS block.

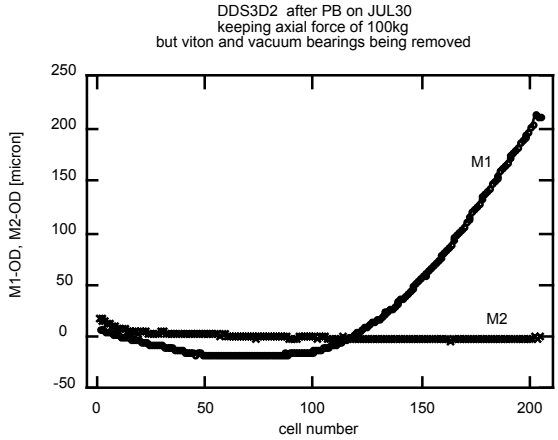

Fig. 12.21 Alignment measurement after pre-bonding with all the constraints removed; axial pressure, viton plates and vacuum-use bearings.

12.7 Wire measurement before diffusion bonding

A wire measurement was performed once between pre-bonding and diffusion bonding. The result is shown in Fig. 12.22. The amount of bow was about 30 microns. This small value is consistent to the last measurement shown in Fig. 12.21. The wire measurement simply happened to be done along the side with very small bow.

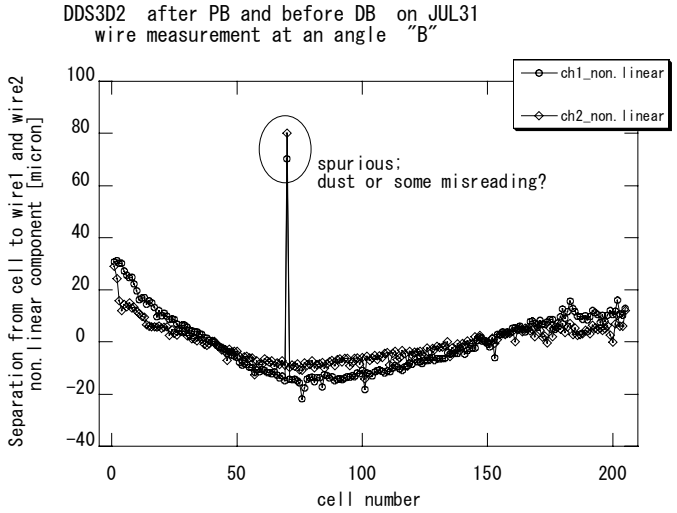

Fig. 12.22 Wire alignment measurement after pre-bonding in a vertical position at an angle "B".

12.8 Diffusion bonding

temperature:

The temperature history of the diffusion bonding process is shown in Fig. 12.23. It was decided to keep the temperature of the structure longer than 4 hours at higher than 850°C.

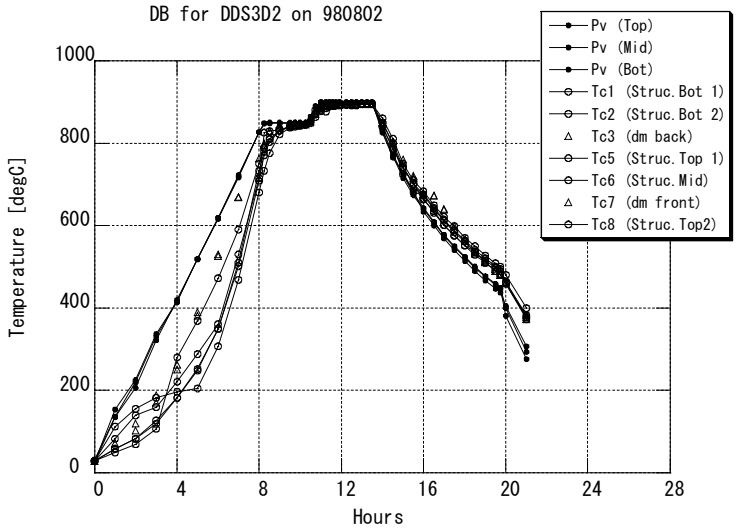

Fig. 12.23 Temperature history during the diffusion bonding process. Marks are the temperature defined as follows; solid circles = heater temperatures, open circles = thermocouples at structure and triangles = those at dummy iron rod, 1.8m long and 61mm in diameter, located at the furnace base.

12.9 Wire measurement after diffusion bonding

Three wire alignment measurements were done after diffusion bonding as shown in Fig. 12.24. A large bow of nearly 500 microns in a horizontal plane was observed. This situation is clearly seen in Fig. 12.25 where three wire measurements are converted to (x,y) coordinates.

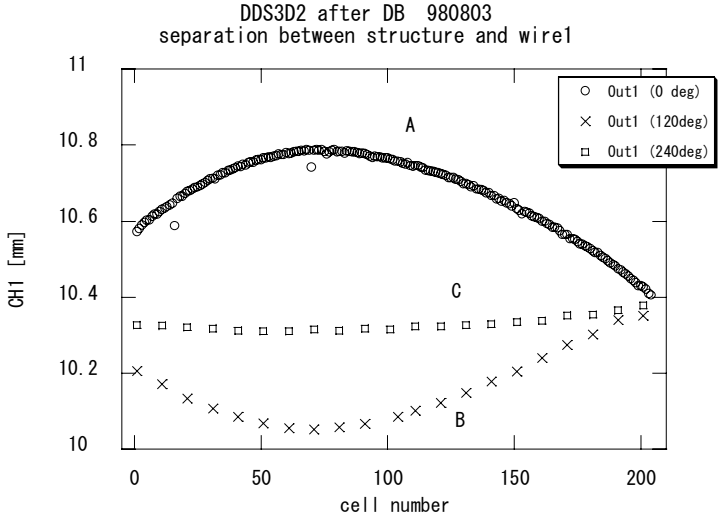

Fig. 12.24 Results of the wire alignment measurements set at three angles.

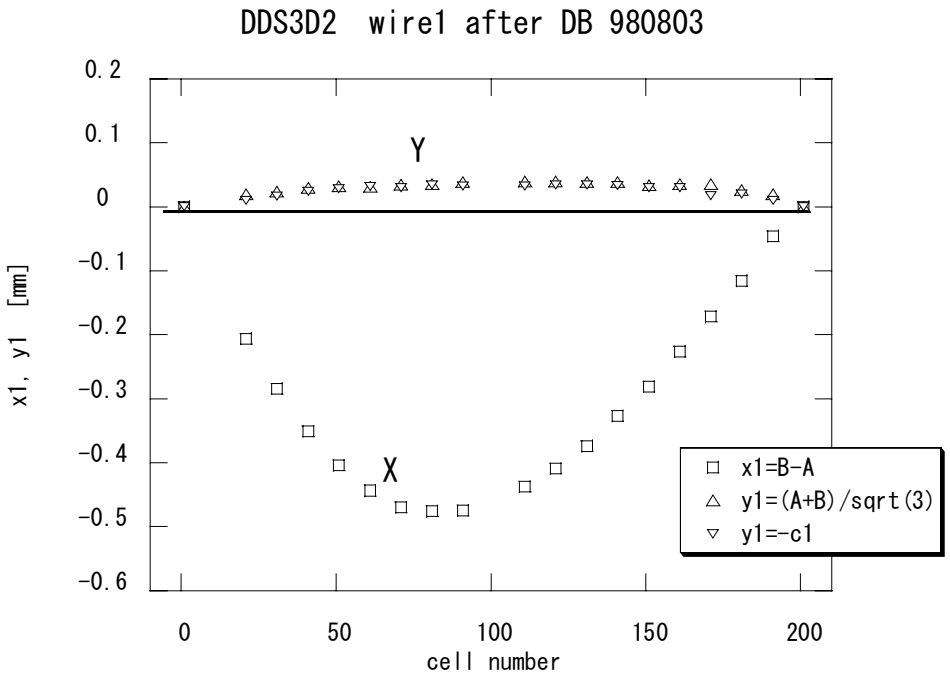

Fig. 12.25 Off-axis values of cells with respect to the axis connecting both ends. The measurements at three wire positions are combined. Squares are offset in the x direction calculated from wire position A and B. Triangles and inverse triangles are offset in the y direction which are calculated from those of wire positions A and B and those from C.

12.10. Summary of DDS3D2

Because DDS3 fabrication work had to be chasing very close to DDS3D2, the alignment measurement using Microsense has not been performed until now.

Following is the summary of what we speculated from DDS3D2 study.

1. Viton constraint is also effective to make cells align well to the V-block so that it is effective to realize a good cell-to-cell alignment.

2. Even with viton constraint, stacked-cell pillar shows unstable situation under a high axial pressure of 600kg or more, especially at top end.

3. Pre-bonding gives a smooth alignment of cells but accompanied by a large bow of hundreds of microns.

4. Diffusion bonding following pre-bonding makes the bowing of cell pillar larger and in a different direction but in a very smooth manner in one plane.

5. Cell-to-cell slippage is kept small through all bonding processes.

13. DDS3

13.1. Stacking

The stacking was performed following the way we did for DDS3D2.

13.2. Cell inclination

The reading of the autocollimator is shown in Fig. 13.1. It was found that the reading decreased at the rate of -4 μrad/cell in average. This situation is the same as that of the DDS3D2 though the rate is a little bigger.

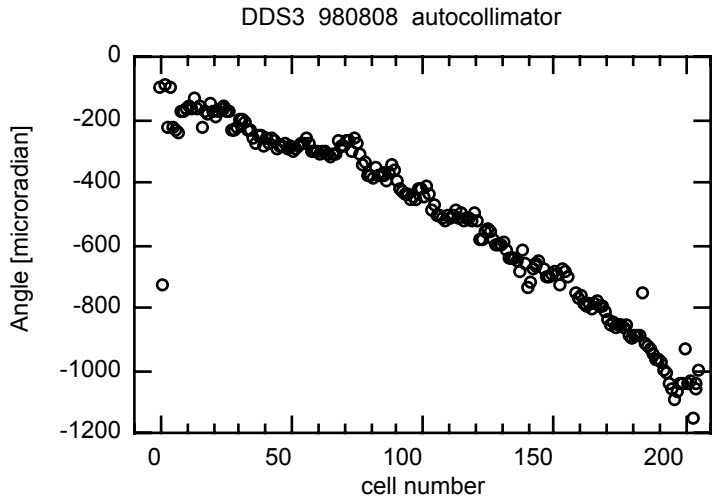

Fig. 13.1 Autocollimator reading as a function of the cell stacking. Decreasing value is the direction of falling from the previously stacked cells towards V-block.

13.3 Rotational alignment

Rotational alignment of each cell after stacking was checked. It was found that all of the scribed lines were aligned within +-50microns.

However, a step between cell #3 and #4 was observed even by eye to be about 0.1mm. We speculate that this kind of rotational misalignment occurred because of the inconsistent marking between the regular cell which has a regular manifold and the special cell without manifold. The marking of the former cell was done by setting one of the manifold on an alignment pin while that for the latter cell by seeing the milling edge at the outer diameter of the cell. This kind of failure should be avoided by careful designing and checking of the scribing process.

13.4 Sticking of cells between #93 and #94

Most cells were stacked and compressed at SLAC for the electrical measurement. After such a measurement, the cells #93 and #94 sticked together. They could not be separated even though various ways were applied such as hand removing, temperature difference between the cells introduced by a thermal shock, etc. Therefore, those two

cells were stacked at once, resulting in a large misalignment between them as shown in Fig. 13.2. In the figure are plotted the results of alignment measurement using measuring worm method after stacking all of the cells.

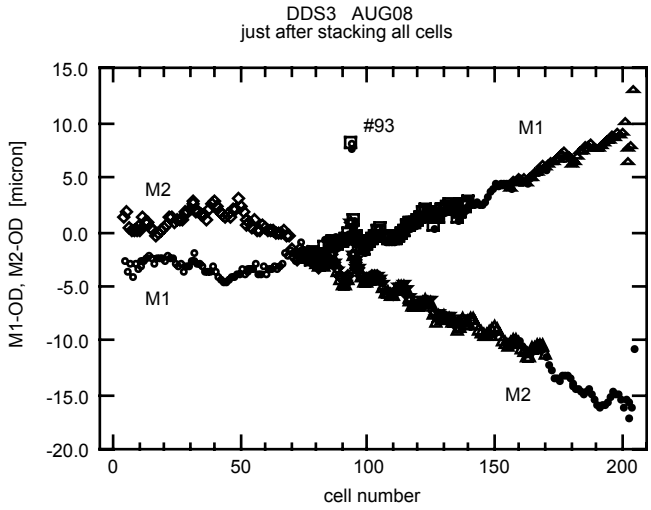

Fig. 13.2 Alignment measurements of DDS3 before shipping from Tokyo to Kure. The measuring worm method was applied while an axial pressure was applied with constraint by viton plates. The different outside diameter s of cells were taken into account to see the degree of alignment with respect to the V-block.

13.5 Microsense measurement before pre-bonding

An axial pressure of 650kg was applied to prepare pre-bonding. About 30 cells near both ends showed movements of about 20 microns.

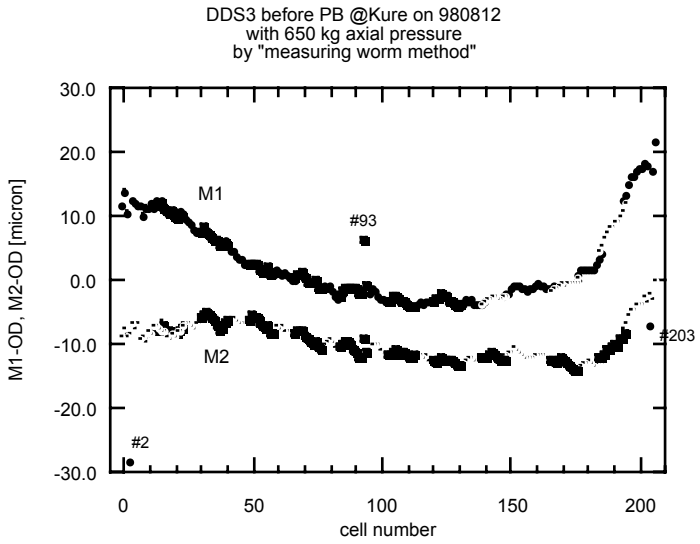

Fig. 13.3 Cell alignment measurement as received at Kure. An axial pressure of 650kg was applied and measuring-worm method was used for measurement.

13.6 Pre-bonding

It was found that the structure temperature was higher than the previous structure, DDS3D2. It was at highest period about 180°C over 20 hours, but kept lower than 200°C.

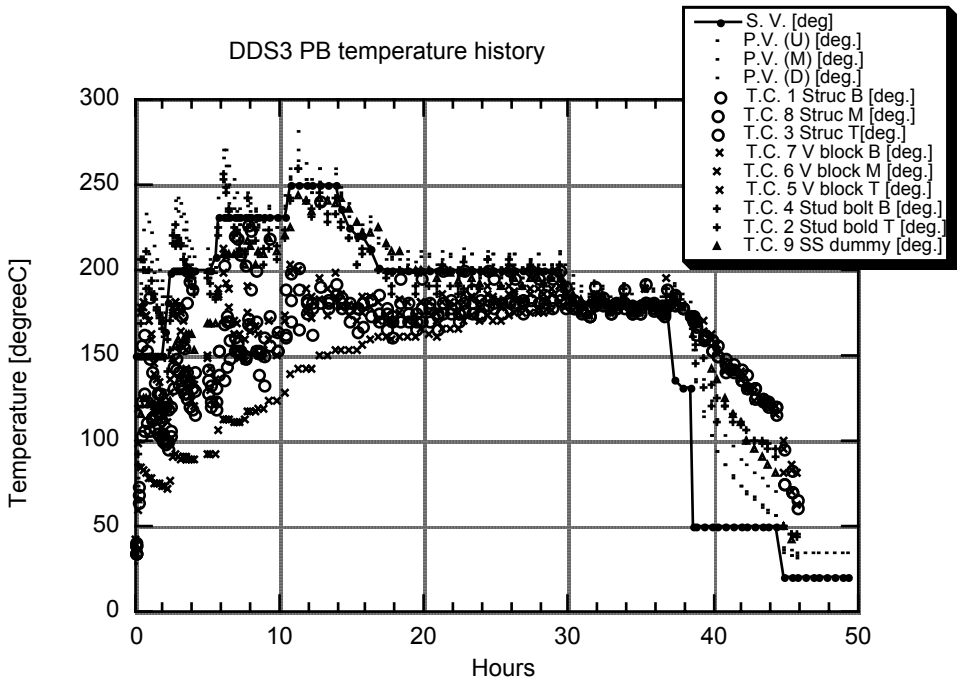

Fig. 13.4 Temperature history during the pre-bonding process. Marks are the temperature defined as follows; solid circles = those of set value for the temperature control program., dots = furnace temperature, crosses = temperature of V-block, plus marks = those of stud bolts, open circles = those in structure thermocouple holes and triangles = those at dummy cylinder located at the furnace base.

13.7 Alignment measurement after pre-bonding

Alignment was measured just after pre-bonding with keeping 650kg pressure and viton constraint. The general pattern of the alignment was very similar to that measured after applying 650kg after receiving at Kure. Some sort of kink was observed neat cell #20, #50 and #180.

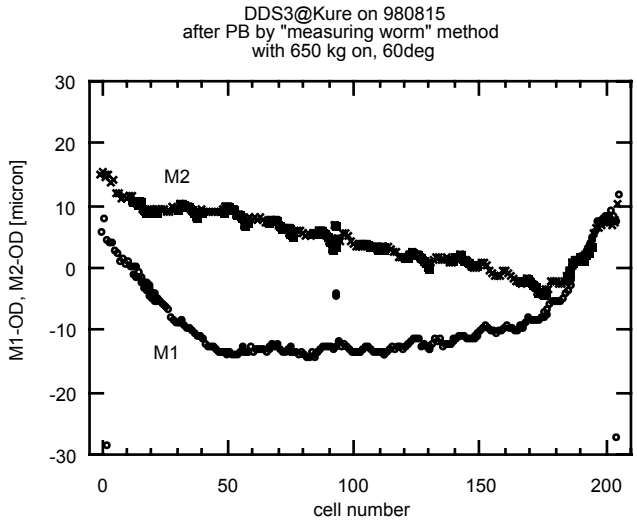

Fig. 13.5 Cell alignment measurement of DDS3 after pre-bonding. Measuring-worm method was applied.

The axial pressure was reduced down to 100kg in a horizontal position. Then the viton plates pressing cells to V-block were removed. Then the cell alignment was measured as shown in Fig. 13.6. Comparing to the middle part, smooth floating of a few tens of microns over a few tens of cells near both ends was observed, that is, kink-type of bending disappeared by releasing from 650kg to 100kg.

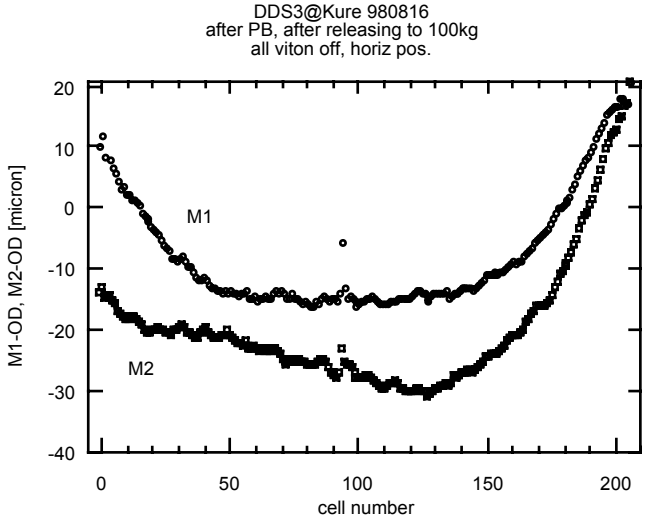

Fig. 13.6 Cell alignment of DDS3 after pre-bonding but before diffusion bonding. Axial force of 100kg was applied but no transverse constraint was applied. The V-block is in a horizontal position.

13.8 Wire measurement before diffusion bonding

On the way to go to the furnace for diffusion bonding, the structure was hanged vertically. The cell alignment was measured in this situation using wires. The results are shown in Fig. 13.7.

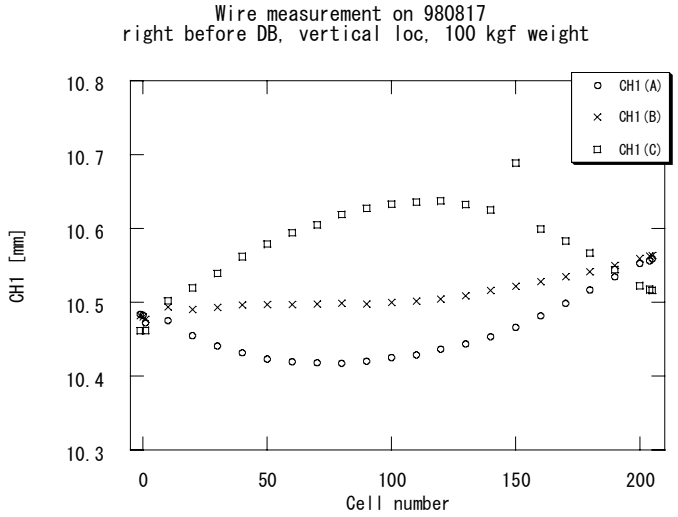

Fig. 13.7 Cell alignment measurement with wire for DDS3 before diffusion bonding but after pre-bonding. We believe that the big deviation at cell #150 was due to some error coming from measurement, in such as a noise in reading, big dust, etc.

13.9 Diffusion bonding

Temperature history during the diffusion bonding process is shown in Fig. 13.8. We kept the temperature monitor points attaching the structure over 850°C for four hours in a process to reach a temperature of 890°C.

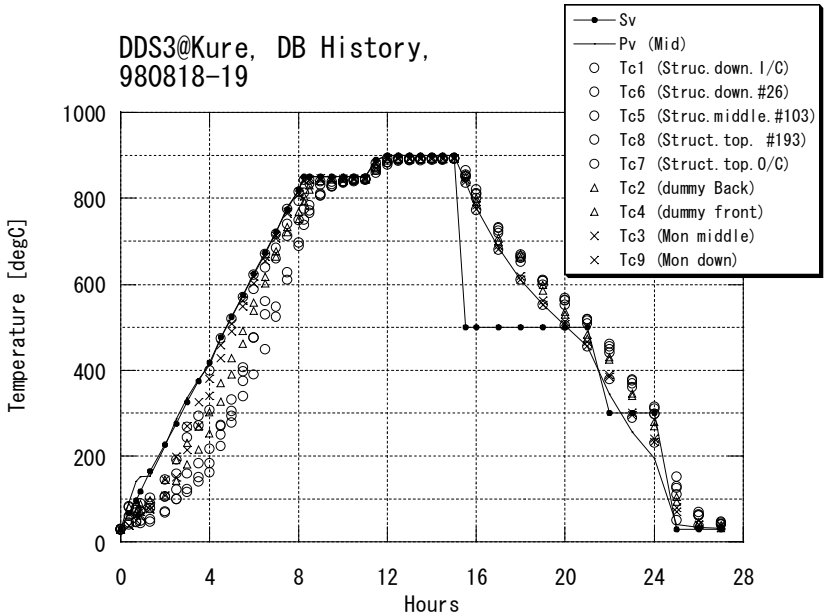

Fig. 13.8 Temperature history during the diffusion bonding process. Marks are the temperature defined as follows; solid circles = the values for the heater temperatures, dots = furnace temperature, open circles = those in structure thermocouple holes, triangles = those at dummy cylinder located at the furnace base and crosses = those at the gate-type support.

13.10 Wire measurement after diffusion bonding

The cell alignment measurement with using the wire was again applied after diffusion bonding and on the way to come back to sit on the V-block. The results are shown in Fig. 13.9.

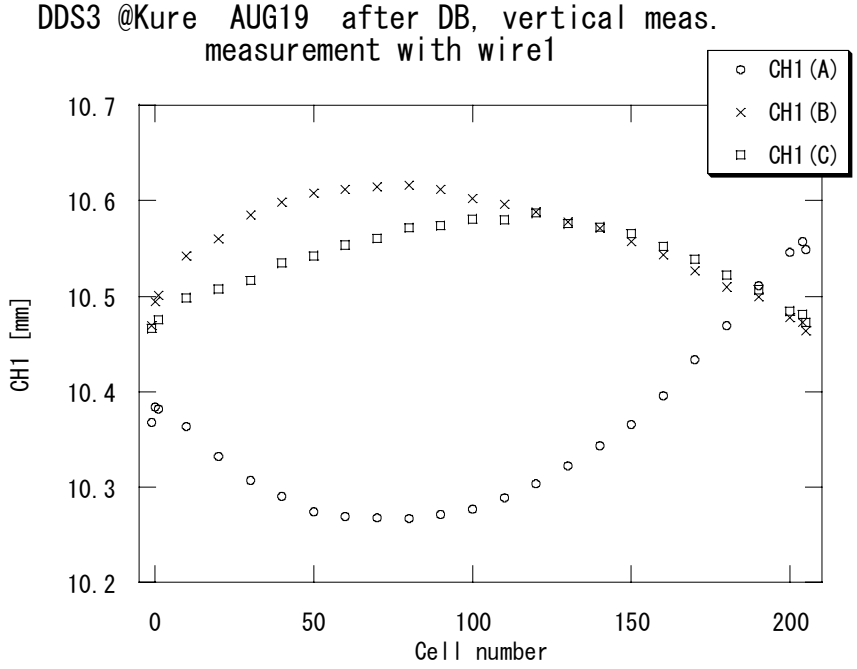

Fig. 13.9 Wire measurement of DDS3 after diffusion bonding.

13.11 Alignment measurement by Microsense after diffusion bonding

The cell alignment was measured at Kure where the structure is set on the horizontal V-block. Fig. 13.10 shows the result where the structure is set on the V-block in a nominal rotational position which is equal to that of the stacking and pre-bonding. The bending of the order of 200 microns was observed.

The alignment measurement with rotating the structure by 120 degrees than the nominal rotational position was performed and the result is shown in Fig. 13.11. The rotational position was chosen to make the two ends to be pressed on the V-block which was speculated from the vertical wire measurement. As speculated, the alignment became much straight. The four regions of missing M1 values are the position where the sensor saw the vacuum pumping ports.

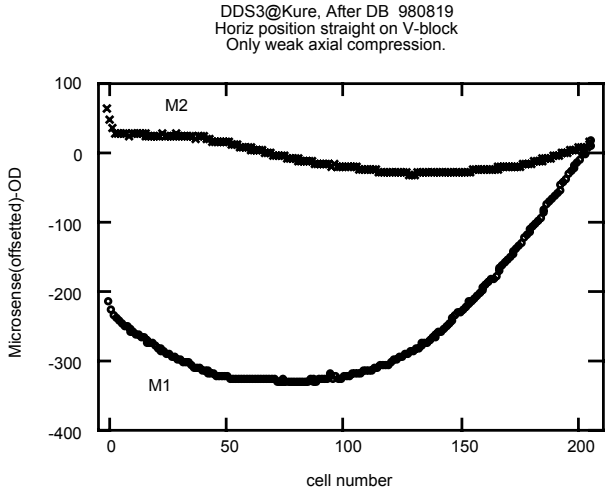

Fig. 13.10 Alignment measurement on a horizontal V-block in a nominal rotational position. The structure was set directly on the V-block.

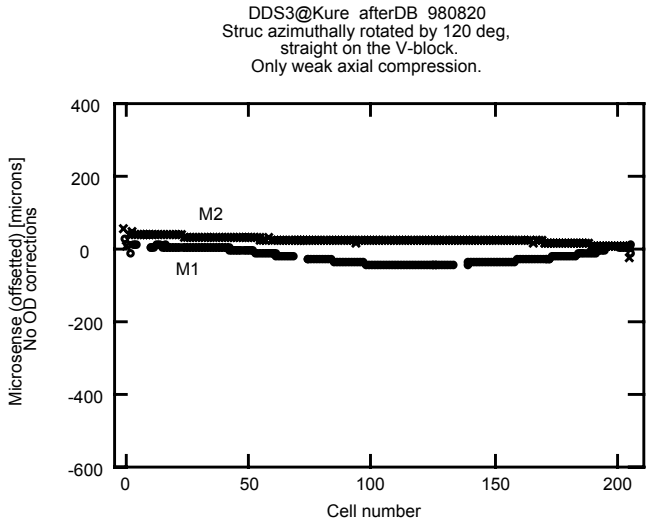

Fig. 13.11 Alignment measurement on the horizontal V-block. The structure was rotated by 60 degrees from the nominal position. Four regions where no data existed are those where the sensor looked at the vacuum pumping ports.

13.12 Alignment measurement at Tokyo

Circumference

The cell alignment was measured finally at IHI, Tokyo, in an air-conditioned clean room environment. Since the schedule was tight, a temperature stabilization process was performed only over a night. Fig. 13.12 shows the temperature variation through a night before starting the measurement on a next day.

Points, T1 and T3, are measurement of air and those of T2, T4 and T6 are those measuring a surface temperature of the alignment jig and V-block. It is to be estimated from this figure that the temperature of the measurement system varied by a degree or so during the final measurement.

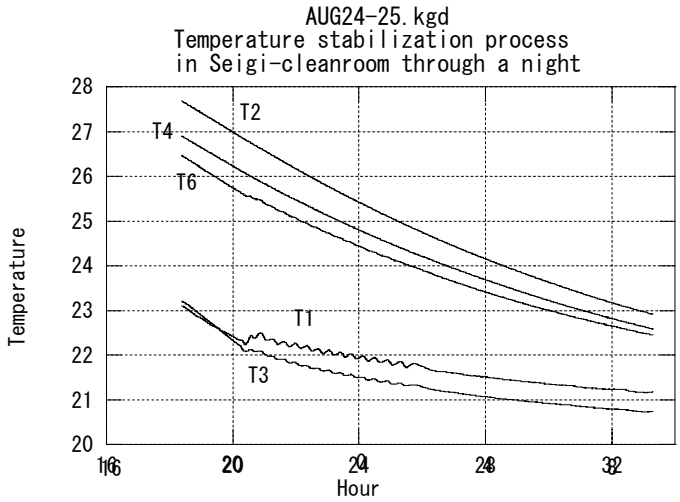

Fig. 13.12 Temperature stabilization record over a night.

Alignment measurement supported at positions to make a minimum sag

The DDS3 structure was supported at cells #48 and #158, where the sag due to self weight was estimated to be minimum, about 9 microns. The result is shown in Fig. 13.13.

If the deviation from an axis running through two ends is seen from the input coupler side, it was found that the deviation is almost in a plane, -17 degrees from X-axis, shown in Fig. 13.14. The maximum deviation is about 230 microns.

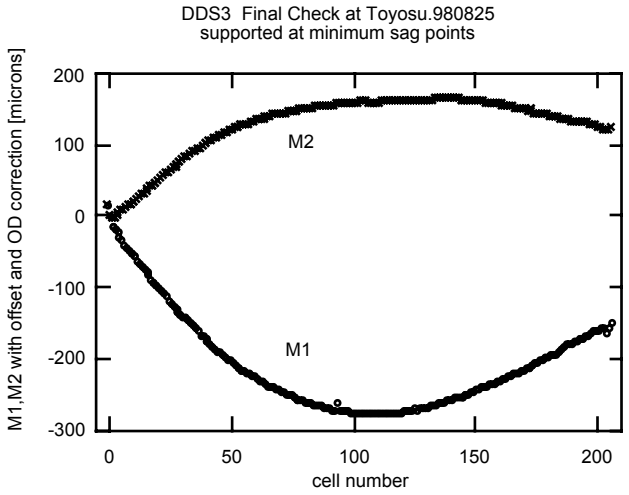

Fig. 13.13 Cell alignment measurement of DDS3 supported at minimum sag points.

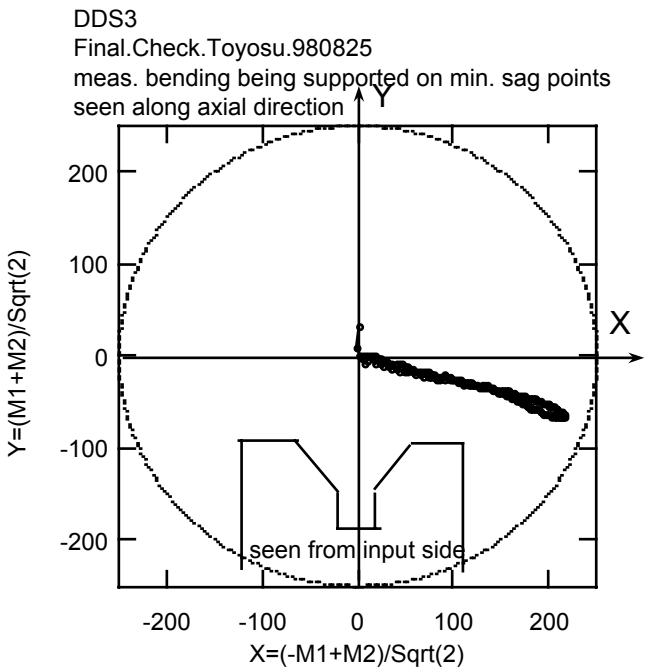

Fig. 13.14 Deviation of cell alignment from an axis running through two ends.

In order to clarify the behavior near end cells, the end-cell regions were studied in detail by measuring in a 0.2mm step as shown in Fig. 13.15. The data showing bumps are those measuring the proper position of outer surface, while those at -25 microns are under ranged where the sensors are facing the position of reduced OD.

The result shows a larger outside diameter of the coupler cells or their floating but also indicate a possible taper of input coupler cell or the big inclination of its angle. To distinguish whether it is due to taper or not can be done by measuring the outer surface of the cell but measuring from both sides, that is two sensors are facing each located at +-90 degrees.

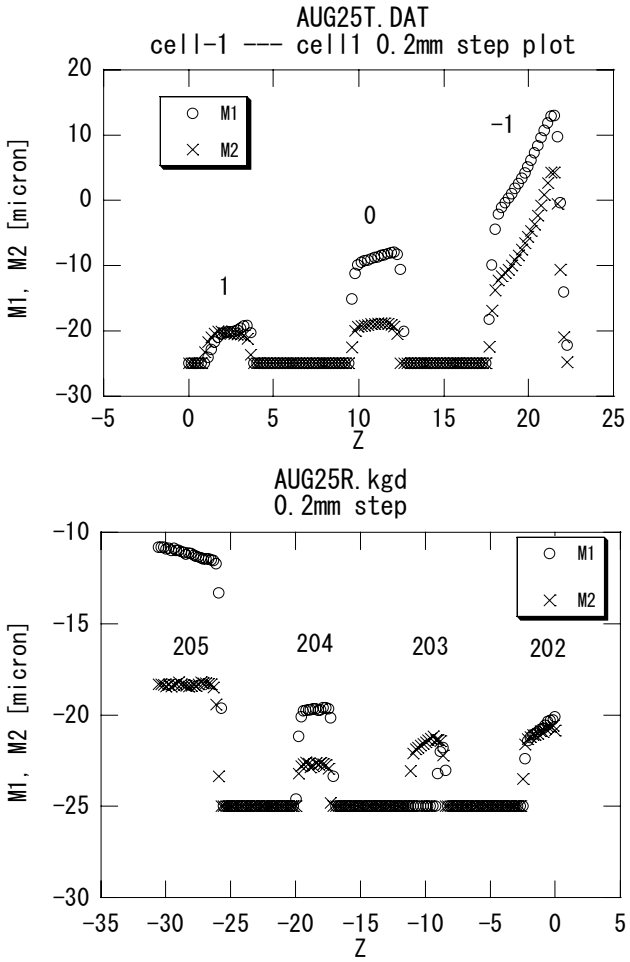

Fig. 13.15 Measurement of cell alignment near coupler cells.

Now let's estimate the situation of cell-to-cell alignment.

The residual after fitting the measured alignment data of Fig. 13.13 by a third order of polynomial is plotted to evaluate a cell-to-cell rapid change of cell misalignment. The residual is shown in Fig. 13.16. The distribution of the amount of the misalignment between adjacent cells except for a few huge ones is shown in Fig. 13.17. It was found that the cell-to-cell steps at more than 190 cell junctions were within 1.5 micron, showing most cells are well aligned with respect to the next.

The large cell-to-cell misalignment at input and output region is speculated to be spurious because in these regions the diameter of the cells increase towards the end surfaces. The large deviation in the middle is that of cell #93 and the situation is almost the same as that before bonding. It proves again the slippage to be very little.

In order to conclude this confirmation, a third order polynomial component which makes a large bowing of 230 microns should be studied to identify whether this is due to bending and not due to cell slippage. In the process for DDS3, the direct checking of whether the step between cells are due to bending or slippage was found difficult. It should be studied in the test of the future structure fabrication.

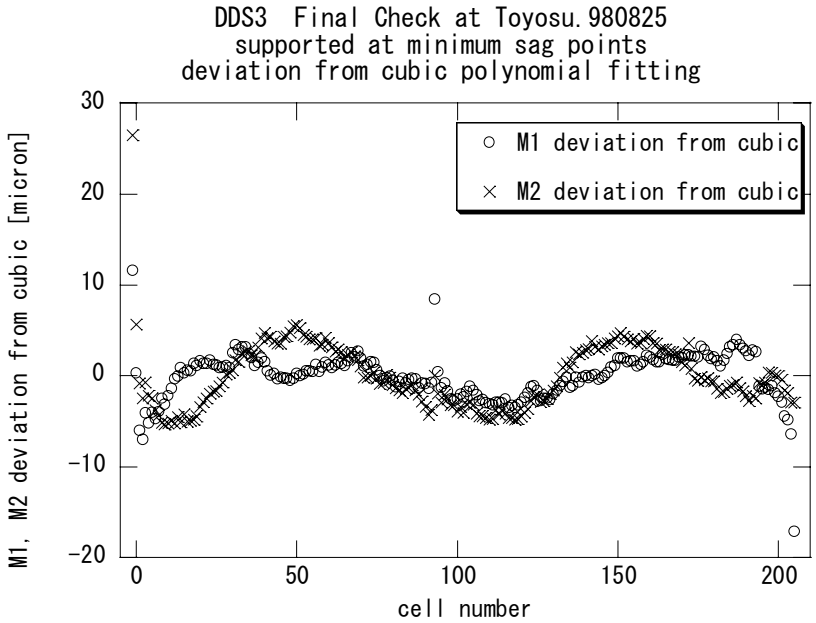

Fig. 13.16 Residual of misalignment of cells after subtracting a polynomial up to a third order.

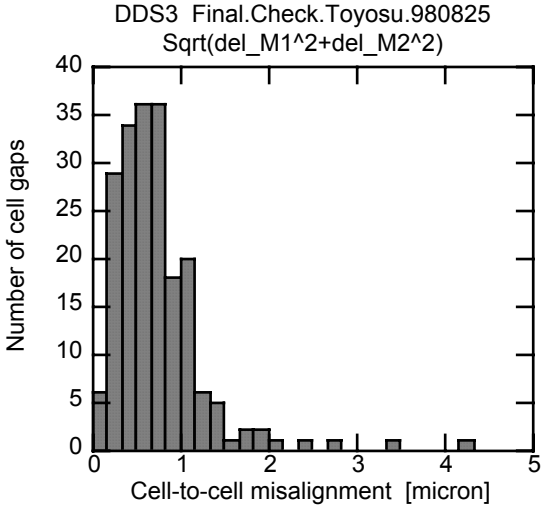

Fig. 13.17 Amount of misalignment between cells.

13.13 Rotational alignment measurement

Rotational alignment of DDS3 was measured after diffusion bonding and transported back to Tokyo. The measurement method is the same as that during stacking. The results is shown in Fig. 13.18. The main cause of the reading of about 160 microns is estimated to be the effect from the bending of the structure of the order of 230 microns in a plane with -17 degrees as shown in Fig. 13.19. A simple geometric calculation from these value gives a maximum reading of

$$230 \times \mathrm{Sin}(20+17) \sim 138 \text{ microns},$$

which is downward and roughly consistent to the measured position change of scratches. Whether the rotational alignment is really kept and simply the structure body

is bent or large rotational misalignments exist should be checked after straightening process.

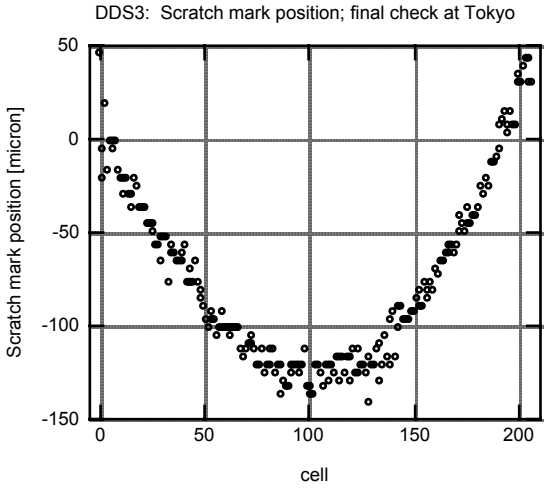

Fig. 13.18 Reading of the rotational alignment scratch seen on a monitor screen.

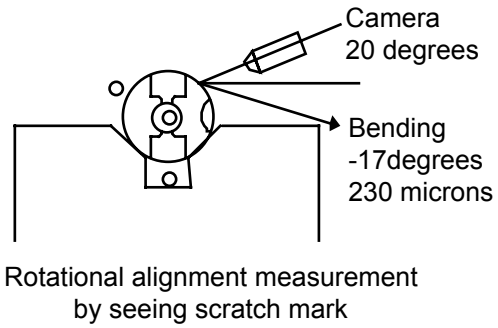

Fig. 13.19 Configuration of the measurement of scratch mark and the bending of the DDS3 structure.

13.14 Vacuum leakage checking

Vacuum leakage for the regular sections were checked by a Helium leak detector. Such open ports as coupler cells, vacuum pumping cells and HOM port cells are sealed using a teflon jig to form a triangular space for an O-ring to be fit to the outer surface of the cell. The configuration is shown in Fig. 13.20. The helium gas was introduced to each junction line between cells by surrounding it using a teflon ring running over the line with a gap of 0.5mm so that it runs easily from a junction to the next. There is a hole 180 degree apart from the inlet of the helium and the inner side of teflon jig was evacuated through the hole.

It was found that this type of sealing and helium exposure technique is not completely effective to specify the checking position so that we encountered a leakage of the order of 10^{-9} mbar liter/sec level or larger in some cases through the seal especially when approaching near the sealed-cell region by several cells.

We measured that the vacuum seal by diffusion bonding of DDS3 is better than 10^{-8} mbar liter/sec.

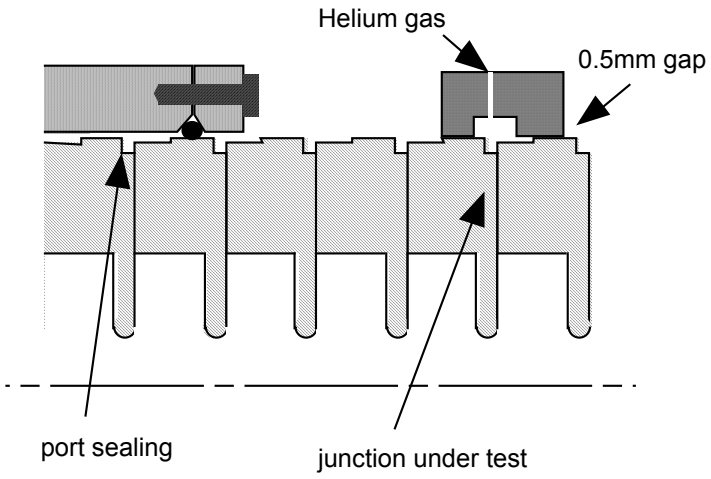

Fig. 13.20 Schematic drawing for the vacuum leak checking configuration. Various ports such as vacuum pumping ports, wave guides and HOM ports were shielded as shown in the left side of the drawing. Each junction was separately exposed to the helium gas as shown in the right side of the figure.

13.15 Summary of DDS3

Following items are summary of important features of DDS3 which were observed from stacking through pre-bonding to diffusion bonding.

1. Cells were stacked with a small cell-to-cell misalignment.
2. Inclination of top cell cumulatively increased reaching finally one milliradian.
3. Cell global alignment as of stacking is within 10 microns with viton constraint and with an moderate axial pressure of 100kg.
4. Stacked-cell pillar shows unstable transverse movement under an axial pressure of 650kg even if with viton constraint. This unstable situation is evident at the top region.
5. Pre-bonding made the cell pillar bow by about several tens of microns under an axial pressure of 100kg without viton constraint.
6. Cell pillar showed a bow of the order of 200 microns in a vertical situation just before diffusion bonding.
7. The global bow of the cell pillar became about 230 microns after diffusion bonding. The bow stays almost in one plane.
8. Cell-to-cell misalignment kept small even after diffusion bonding.
9. Both ends showed the increase of diameter if we assume that the global shape of the cell misalignment is smooth without any kink near ends[24].

14. Summary and discussions

We fabricated DDS3 by stacking on a V-block, transversely constraining by viton plates, transporting to a work several hundred kilometers far, pre-bonding in a vacuum furnace with an applied axial force of 600 kg, diffusion bonding in the same furnace but in a much higher temperature and in a vertical position. Through the above fabrication, we confirmed the following features.

1. Stacking cells on V-block makes cell-to-cell misalignment within a few microns.
2. Ozone -included pure water rinsing seems applicable for all the processes of stacking, pre-bonding and diffusion bonding.
3. Pre-bonding works in a sense that it allows us to obtain a manageable structure through the following diffusion bonding process.
4. Diffusion bonding of cells with 61 mm in diameter and 1.8 m in length in total is possible in a vertical position.
5. Cell-to-cell slippage is kept small through the bonding processes.
6. Steep kinks larger than 1 milliradian /meter does not appear.
7. Large bowing of about hundreds of microns appears but the bowing mainly consists of the lowest order of one-dimensional deformation pattern.
8. There is an indication that the diameter of both ends increased.[24]
9. Vacuum sealing is better than 10^{-8} mbar liter/sec.

We also understand that the following issues are remaining to be improved and/or studied in near future.

1. Cumulative bookshelf phenomenon was observed in the last two cases, DDS3D2 and DDS3. The mechanism and cure should be studied.
2. Mechanism of large bowing should be studied because the amount of bowing is intuitively and strongly preferred to be below 50 microns when considering the tolerance of the straightness of about 10 microns along a structure.
3. The mechanism, the mechanical strength and its reliability of pre-bonding should be studied if we need this technology in future.
4. We have little information on the junction property[25]. The study program should be initiated.
5. Related to item 4, vacuum sealing performance of diffusion bonded junctions should be carefully studied if we rely fully on diffusion bonding in future.
6. Frequency stability through the bonding process should be confirmed. At least the smoothness of the frequencies of the lowest higher mode can be checked, though indirectly, by measuring the phase advance per cell as for the accelerating mode via bead pulling measurement.

Finally we summarize the direction and amount of the bowing in each stage of the bonding process to see globally what happened. Cartoons in Fig. 14.1 are the global views of bowing change through diffusion bonding of the last two structures. With this level of experience, it is not easy to understand the mechanism but we should study based on these experiences in addition to future studies.

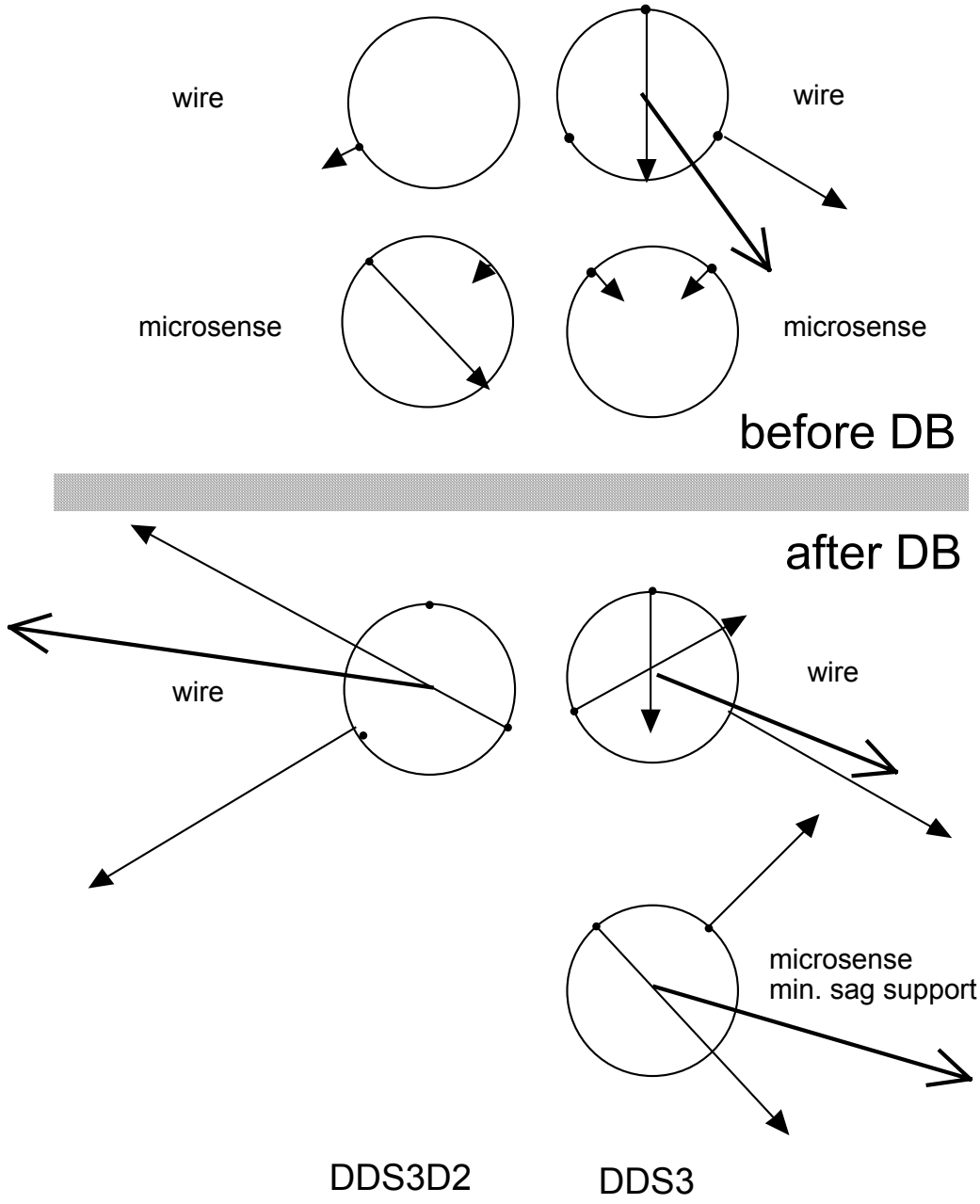

Fig. 14.1 Summary of change of bending pattern due to diffusion bonding of DDS3D2 and DDS3. Thin arrows show the measurements while thick ones show the direction of the global bowing estimated from the measurements. The length of arrows are the amount of bowing. The directions show the direction of the deviation from an axis running through both end cells. Right direction shows X-axis and upward Y-axis as defined in Fig. 8.1.

15. Acknowledgments

At first, the authors would like to greatly appreciate the works by two colleagues who left SLAC by now but contributed a lot in the DDS3 program. Dr. H. Hoag designed the original DDS3 cells in 1996 and fixed a basic design features of DDS3. Dr. R. Pope succeeded the job and contributed much in the process of making assembly drawing to clarify the structure and setting-up the practical schedule for the DDS3.

The authors would like to thank Dr. D. Burke of SLAC to adopt the DDS3 program as a collaborative work between SLAC and KEK. They also thank Drs. J. Wang, J. Rifkin, C. Pearson, R. Ruth and many people of SLAC to support the program. Drs. J. Klingmann and K. van Bibber of LLNL are also greatly acknowledged for their hard work for really producing excellent cells for DDS3.

The authors would thank Director H. Sugawara of KEK, Director M. Kihara of Accelerator Facility and Director K. Kondo of Center for the approval of the program and their continuous encouragements and supports in various stages of the program.

The authors greatly acknowledge Ishikawajima-Harima Heavy Industry, IHI, for supporting the authors and many IHI staff throughout this program. Especially staffs at Kure Work should be greatly acknowledged for their many important comments and helps throughout the bonding stage.

The 'pre-bonding' technology applied for the DDS3 was first proposed by Higashi and tested at Mitsubishi Heavy Industry, MHI. The authors thank MHI for kindly agreeing the technology to be applied for the present activity.

16. References

[1] Design Study Report, KEK Report 97-1.
[2] Zeroth-order Design Report for the Next Linear Collider, SLAC Report 474.
[3] J. Wang et al., "Accelerator Structure R&D for Linear Colliders", PAC99, p3423, New York, 1999.
[4] J. Klingmann et al., "Fabrication of DDS-3, 11.4 GHz Damped-Detuned Structure", PAC99, p777, New York, 1999.
[5] T. Higo et al., "Challenge to a Straight Structure for X-Band Linear Collider", PAC99, p3417, New York, 1999.
[6] R. Jones, "Advanced Damped Detuned Structure Development at SLAC", p548, PAC97, Vancouver, Canada, 1997.
[7] T. Higo et al., "Detuned Accelerating Structure for Linear Collider", APAC98, p166, KEK, Tsukuba, Japan, 1998.
[8] Y. Higashi et al., to be published.
[9] C. Adolphsen et al., "Wakefield and Beam Centering Measurements of a Damped and Detuned X-Band Accelerator Structure", PAC99, p3477, New York, 1999.
[10] Capacitive gap sensor, Model 3401-R02, ADE Technologies, Inc.
[11] Y. Higashi et al., "High-precision machining for X-band Accelerating Structures", to be published in KEK Report.
[12] K. Asano et al, "Elimination Effect of Surface Carbon Contaminations on Field Emission in Superconducting RF Cavities", KEK Preprint 97-126, 1997.
[13] Linear Guide, SR30VZUUC1M + 2280LPM-II, THK Co. LTD.
[14] Ball screw, BTK2806-2.6ZZ+2261LT, THK Co. LTD.
[15] Dynamic Calibrator, HP 5529A, Hewlett Packard Co. LTD.
[16] Three directional Shock Recorder, FIR-302, Yoshida Seiki, co.
[17] "Suntec Foam", made of Polyethylene with independent foam, Asahi Kasei co.
[18] Oxygen absorbing material: "O2 EATER 51-4039-01 Type A-500-50S", Material for absorbing humidity: "Dryer' 94-4024-01 Type C-3849A", both supplied by Iuchi Seieido, Co.
[19] Laser Scanning Gap Meter, LS-5000, Keyence, Co.
[20] H. Tashiro, Materia Japan, vol 35 (1996) 1177.
[21] H. Sakae et al., "Investigation of the drift in the laser correction system", IHI report, 06EI6991, 1998.
[22] 2-axis Photo-electron Autocollimator, NIKON Co.
[23] Private communication, "DDS3 Dummy structure; A study on Structure Bonding (4)", Ishikawajima-Harima Heavy Industry Co. LTD., issued on May 19, 1999.
[24] C. Pearson, presentation in ISG5, SLAC, February, 2000.
[25] H. Tsuchiya, presentation in ISG5, SLAC, February, 2000.

17. Appendix

17.1 Notes on the cell

In the same setup as the surface roughness measurement by ZYGO interferometer system, fairly large amount of pits were observed on the flat surface of many cells, both those made by LLNL and those by IHI. Though they might not affect the bonding performance and electrical characteristics in low power, it should be remembered for the application to a high field operation of the structure in near future. Their typical size is 0.1 micron in depth and 20 microns in diameter of the opening.

Various obstacles were also observed in not only a single place on the flat surface. It seemed that these were sitting on the surface and the size was estimated to be of several microns or even more. Some of them seems not dust. Quality checking of cells should be established taking care of such matters.

17.2 Laser straightness measurement, stability and accuracy

Firstly, the alignment of the stacked cells were measured by running the sensors five times. It took about 1.5 hours. In this run the stability of the laser correction system was checked. The position of the Wallaston prisms for the laser correction were measured as shown in Fig. 17.1. The difference with respect to the first measurement were plotted. The bottom trace and the top one are the second and the last measurement, respectively. Two traces in the middle are 3rd and 4th ones. These traces show a monotonic behavior of the drift. The optical level effect of the mirrors set at the output coupler side was seen in a large drift near the input coupler region. However, not only the mirror angle drift but also some other components are seen. Even if these drifts exist, the correction mechanism by using this laser beam is effective by at least a few microns level.

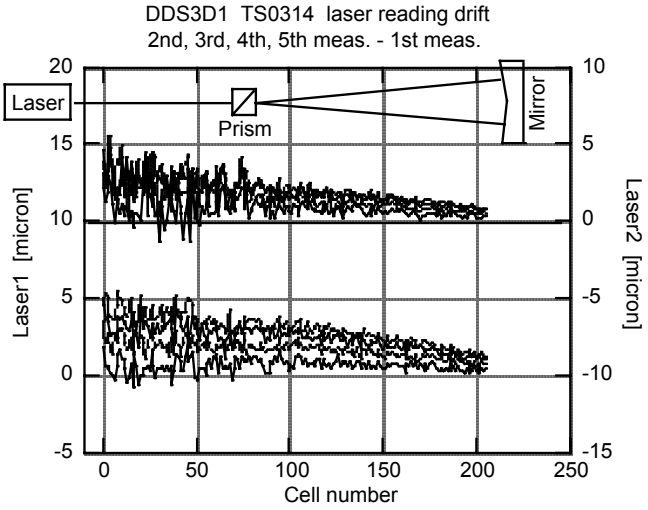

Fig. 17.1 Straightness measurements of the Wallaston prism moving along the V-block were done five times successively. Laser stability can be estimated from these measurements.

17.3 Uniformity of piano wire

Diameter of one of two piano wires with 0.3mm in diameter were measured at the same time as the actual alignment measurement of structure. A typical example is shown in Fig. 17.2.

As shown in the figure, the measurement reading shows the average value larger than the nominal by 9 micron with the scattering with a standard deviation of 3 microns.

There is no systematic deviation as the position of the wire so that we can estimate that the error comes mainly from the wire non-uniformity, meaning that the error due to vibration of wire is much less than 1 micron level.

The total span of deviation is about 20 microns. Then we should consider that the alignment reading error due to the wire diameter scattering is +-5 microns.

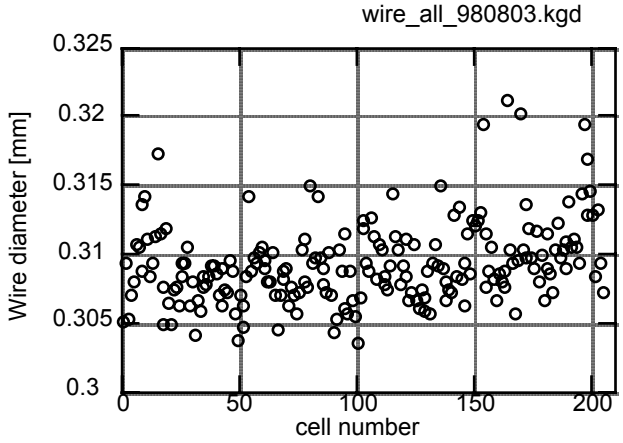

Fig. 17.2 Diameter of one of two wires were measured at the same time with the actual alignment measurement of structure DDS3D2.

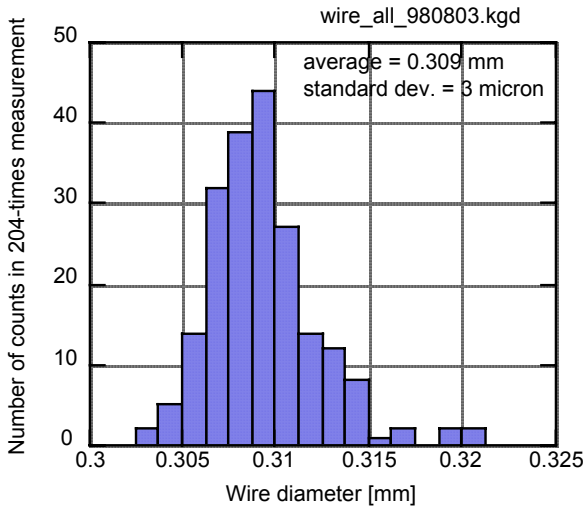

Fig. 17.3 The population of the diameter of the above figure is shown. The standard deviation was 3 microns.

17.4 Estimation of straightness of stretched wire

We use piano wire with 0.3mm diameter. Piano wire is one of the engineering materials with highest strength. It is known that the strength of piano wire shows size effect and the limit of the strength can be the same as whisker crystal. Thinner wire can be used under higher stress, because thin wire has less chance of inhomogeneous deformation in the wire drawing process[20]. However, a position sensitivity of the laser gap meter reduces for the wire with diameter smaller than 0.2mm. Thus, the diameter of the wire was determined such that the laser gap meter functions at a good signal to noise ratio.

Surface of piano wire was inspected by a scanning electron microscope. Some scratches were found along the wire, which might be originated from the roughness of dies for the drawing process. The scratches looked smaller than approximately 1/20 of the diameter of the wire. The amount of the slowly varying outer surface was found much less than the diameter of the wire.

Let us try to estimate a required tension of the wire for keeping straight. We assume that wire is homogeneous without twist. Suppose that a small bump is made on the wire as in Fig. 17.4.

Fig. 17.4 A small bump localized in a region.

The potential energy density due to this bump increases as (1/2) $E\ I\ (y'')^2$ due to the bend and by (1/2) F $(y')^2$ due to a tension, where notations are E : Young's modulus, I : area moment of inertia , and F : the tension respectively. The bump will collapse when the former is smaller than the latter. Using $y' \sim d/l$ and $y'' \sim d/l^2$ for order estimation, we get a relation of

$$l \sim \mathrm{sqrt}(EI / F)$$

This gives a lower limit of the region where the wire can be thought as straight under the tension F being applied.

The tension of the wire was estimated by measuring the frequency of the fundamental vibrational mode of the string. The frequency was about 126Hz, then we calculated the tension F=15kgf. In this calculation, we used the formula of $F=4\ \rho\ A\ f^2\ L^2$, where the density of the wire $\rho = 7.86 \times 10^3$ kg/m^3, the cross sectional area $A = 7.07 \times 10^{-8}$ m^2, the length of the wire L=2.0m and the measured frequency f=126Hz. In the wire, the stress caused by the tension is σ = 2.0 GPa, which is close to the strength of the piano wire with 0.3mm diameter[20].

According to the above equation, we get $l \sim$ 0.24mm. We expect that the wire is straight in the scale larger than l under the applied tension. Since the l is smaller than the diameter of the wire, we expect that the wire is practically straight enough for our measurement.

The top of the wire is connected to a screw for pulling wire to adjust the tension. The current tension adjuster make some angle along the wire at the plate that fixes the stack to the pole. It may cause a bend near the plate when we consider the wire as a thin rod. Assume that a bend of thin rod is determined by the balance of bending moment and tension, the equation is expressed as

$$E\,I\,(d^3y / d\,x^3) - F\,(dy / d\,x) = 0.$$

Solving this equation in x between 0 and L under the boundary conditions of

$$y(0) = 0\ ,\ y'(0) = 0,\ \ y'(L) = \tan\theta,$$

we have the solution

$$y(x) = \tan\theta / \{\alpha \sinh(\alpha L)\}\ \ \{\cosh(\alpha x) - 1\}$$
$$\alpha = \mathrm{Sqrt}\,(F / E\,I)\ \ .$$

The solution varies rapidly in the width of $1/\alpha$ near x=L. It may cause a localized bend of the wire at its end. For example, an estimated deflection is of 0.14mm in a width of 0.24mm when we applied the above result to the wire with 0.3mm diameter, E=2.1 X 10^{11} N/m^2, I=4.03 X 10^{-17} m^4, F=143N and L=2m. This potential error of straightness of the wire can be avoided by improving the tensioning mechanism.

17.5 Checking self-consistency among three wire measurements

It is evident from the relationship between (x,y) and (A,B,C) in section 7 that the average of the readings of three wires, A, B and C, should ideally be zero. This is true in the case that each wire is parallel to the structure with the same distance.

Actually the wire is once pulled and the situation is being kept during the three measurements. Therefore, the relative position between the structure and the wire changes but this change has only linear components as cell position z. Higher components should be the same for the three positions. Then the actual non-straightness of the wire appeared to be the average of three measurements wire-A, wire-B and wire-C.

Thus the straightness of the wire was checked as shown in Fig. 17.5. It was shown that the straightness of the wire was within +-10 microns in the region apart from the end cell by more than 10 cells. The reason why it deviates near the end cell should be studied for the usage of this method in a more precise manner in future.

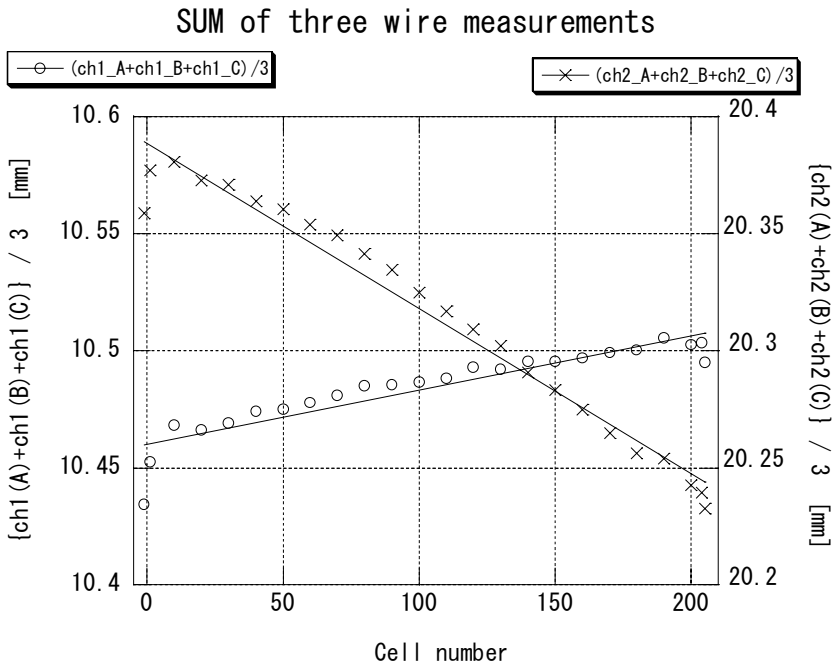

Fig. 17.5 Average value of the measurement for DDS3 with three wire position, wire-A, wire-B and wire-C.